Piston Ring Pack Design Effects on Production Spark Ignition Engine Oil Consumption: A Simulation Analysis

By

Eric B. Senzer

B.S. Mechanical Engineering
University of Miami, 2005

Submitted to the Department of Mechanical Engineering
in Partial Fulfillment of the Requirements for the Degree of

Master of Science in Mechanical Engineering

at the

Massachusetts Institute of Technology

September 2007

Signature of Author_____
Department of Mechanical Engineering
August, 2007

Certified by_____
Tian Tian
Principle Research Scientist, Department of Mechanical Engineering
Thesis Supervisor

Accepted by_____
Lallit Anand
Chairman, Department Committee on Graduate Studies
Department of Mechanical Engineering

(This page was intentionally left blank)

Piston Ring Pack Design Effects on Production Spark Ignition Engine Oil Consumption: A Simulation Analysis

By

Eric Senzer

Submitted to the Department of Mechanical Engineering
in August, 2007 in Partial Fulfillment of the Requirements
for the Degree of Master of Science in Mechanical Engineering

Abstract

One of the most significant contributors to an engine's total oil consumption is the piston-ring-pack. As a result, optimization of the ring pack is becoming more important for engine manufacturers and lubricant suppliers. This leads to current efforts to control the oil transport and flow through the ring pack. Decreasing the amount of oil needed for proper lubrication while minimizing frictional losses are the goals of such research. The hope is to fully understand the mechanisms that govern oil's flow, and then control it. Analytical tools and computer simulation models have been created to assist in predicting the performance of a given ring pack.

This study intended to be an experimental look at the effects of piston-ring-pack design changes on the steady-state and transient oil consumption of a spark ignition engine. Namely, the effects of a V-Cut on the 2nd land, a chamfer on the 3rd land, OCR groove drain holes, and the OCR design were to be examined. However, after some minor measurements, the engine experienced a major malfunction that caused it to cease operation. The focus of the study shifted to a more theoretical, computer simulated concentration of the aforementioned design changes. Different speeds and loads were analyzed along with the notation of some general observations. In the end, the effects of the design modifications on ring dynamics and gas flow were qualified.

The presence of a V-Cut on the 2nd land of the piston had beneficial and adverse effects on the general performance of the ring pack. The added volume decreased the 2nd land pressure enough to avoid 2nd ring radial collapse, but it also caused reverse flutter to occur at lower loads. Using a chamfer on the upper portion of the 3rd land also had mixed results. Stability of the 2nd ring was greatly improved with less radial collapse and an increase in average blowby flow. The performance of the OCR design was primarily dependent on the gap area of the ring and the variation of groove clearances. The OCR groove drain holes were also deemed a necessity.

This research, though theoretical in nature, brings together many ideas that offer solutions to common problems. Radial collapse, reverse flutter, OCR cost, and the use of drainage holes all are part of the attempts to improve the piston-ring-pack performance while driving down cost of production. Future experiments will put the theoretical conclusions to the test with the continuation of the pistons not installed in the engine due to the events previously explained.

Thesis Supervisor:

Tian Tian
Principle Research Scientist, Department of Mechanical Engineering

(This page was intentionally left blank)

Acknowledgments

First and foremost, I'd like to thank my advisor, Dr. Tian Tian for his immeasurable assistance in my research and the guidance he provided throughout both the experiment and my experience as a graduate student thus far. He has been one of my best resources for advice on both academia and life, and for that I will always be grateful. Secondly, Steven Przesmitzki has been one of my closest friends at MIT and in the Boston area, period. I can't count the number of times he's come to my aide when I needed to get the job done or suggested food when he saw I needed a break. After all, food provides fuel for the fire and energy to keep up the good work. Without him, this experiment would have never gotten off the ground, and I wouldn't have enjoyed my experience here at MIT as much as I have.

This project wouldn't have been possible without the support of my sponsors, whose dedication to understanding the mechanisms of oil transport and oil consumption provided more than enough motivation in seeing the project through. These sponsors are members of the Consortium on Lubrication in Internal Combustion Engines at MIT. The consortium's current members include: Volvo AB, Mahle GmBh, Renault SA, and PSA Peugeot Citroen (both for their generous contribution and their parts provision for their donated engine). The representatives from these companies I'd like to thank include: Remi Rabute, Randy Lunsford, Dr. Rolf-Gerhard Fiedler, and Dr. Eduardo Tomanik of Mahle; Bengt Olson and Fredrik Stromstedt from Volvo, and Gabrielle Cavallo of PSA for their input and patience.

Learning is both a process from within and a process that is molded by one's environment. A friend of mine said that I'm not affected by the environment I'm placed in. I beg to differ. The people I met here at the Sloan Automotive Lab have been some of the nicest and most memorable in my life. Such people included: Alex Sappok (my first year mentor, current neighbor, and sailing buddy), Vince Costanzo (who gave me the Pittsburgh outlook on life), Robert J. Scaringe (a fellow Florida boy and cycling/RC car enthusiast like myself), Walter Hoffmann (my German brother), Tiffany Groode (officemate, hostess, and candy provider), Fiona McClure (officemate, Aussie, and always left her desk drawer open for me to partake in some cookies), Nate Anderson (now I know what a Yooper is), Diego Melani (for his Matlab code work), Raymond Phan (a versatile craftsman), Thane DeWitt (always a good source for test cell instrumentation and construction), and finally, Nancy Cook and Janet Maslow for providing an open ear to problems, ideas, and hunger pains.

I'd also like to thank the members of BPΓ, who, without their camaraderie and insight, I would not have had the strength to make a difference. Specifically, Michael Uguccioni, Alfredo Ruiz, Rodolfo Javier Somoza, Luis Oliva, and Maurice Mendes are the ones that stand out the most. Additionally, I'd like to thank my long time friend, Barry Cogen, for providing me a media outlet from which to have some enjoyment during times of stress. Of course, there's my rock, my girlfriend Stacey Queller. Without her good spirits, caring nature, and constant unwavering confidence, I might not be continuing my academic journey in this institution.

Finally, though I'm sure the word has been worn out by now for those reading, I'd like to thank my family. My mother and father, Carol and Marty, for their good judgment and common sense and my brother, David, for listening to me complain about the Mets. It's about time isn't it?

Cambridge, August 2007

(This page was intentionally left blank)

Table of Contents

List of Figures

List of Tables

Chapter 1: Introduction

1.1 Lubrication and Oil Consumption and Their Importance

The piston ring pack (defined as the piston's profile, the liner profile, and the piston rings in their respective grooves) is one of the most critical components of the internal combustion engine. Coupled with the piston itself, the piston ring pack forms a barrier between the combustion chamber and the crank case. Thus, it is imperative that it not only function properly under various operating conditions, but also do so in the most efficient and effective manner possible. The sealing of the combustion chamber from the crankcase is achieved through the movement of the rings within their respective grooves and along the liner. As with all moving parts, sufficient lubrication between rubbing surfaces is paramount in order to minimize friction and wear of the surfaces. This, in turn, increases the longevity of the parts in question and maximizes the life of the engine as a whole. The piston ring pack serves as this lubrication source, providing oil to the grooves and liner during the engine's operation. However, as the old saying goes, "excess within reason." This supply of oil must be controlled because if too much oil is present in certain regions, especially those adjacent to the combustion chamber, there is an unfavorable possibility that the oil will be consumed within the combustion chamber.

The most significant contributor to an engine's total oil consumption is the piston ring pack. As a result, optimization of the ring pack is becoming more important for engine manufacturers and lubricant suppliers, where the decrease in oil consumption signifies an improvement in the overall performance of the engine [1]. Additionally, oil consumption is a considerable source of pollutants. The more unburned/partially burned oil, the higher the hydrocarbon and particulate emissions found in an engine's exhaust stream. This leads to current efforts to control the oil transport and flow through the ring pack and into/out of the combustion chamber. Such efforts involve decreasing the amount of oil needed for proper lubrication while minimizing frictional losses. In doing so, oil consumption and fuel consumption (less friction present) are reduced, decreasing the overall hydrocarbon emissions of the engine (reduced fuel consumption gives a much needed boost to efficiency) [1][2][3]. Unfortunately, the particulates that result from oil transport can also have an adverse affect on oil's flow through the ring pack, changing the oil consumption over time [4]. Furthermore, the additives in the oil contain chemicals that can destroy or decrease the life of exhaust after

treatment systems, such as catalysts in gasoline engines, or particulate traps and NO_x after treatment systems used in diesel systems [5].

As of late, the exact understanding of the processes that cause oil transport are still complex and not well comprehended. Extensive research has been conducted in the past and will be conducted in the future in order to grasp the true reasons behind the paths oil chooses through the ring pack and how to control that flow. At the core of this research is the tug-of-war battle between the ideals of having a sufficient amount of oil supply for proper lubrication and the minimization of oil consumption. As such, most designs in use today are a result of many trial-and-error situations of the past. However, this trial-and-error approach is both timely and more importantly, costly. To remedy these two ills, analytical tools and computer simulation models have been generated in order to assist in predicting the performance of a given piston ring pack. These models utilize many mechanisms present in oil transport (as will be discussed below) in order to give an estimate of the oil consumption for a particular ring pack. The accuracy of the models depends on how well they match experimental findings and the factors they take into account in order to mirror the operation of real world scenarios. Previous research and experiments in oil transport and consumption all attempt to point out significant factors that play a role in the flow of oil through the ring pack.

1.2 Research on Oil Consumption and Oil Transport: Historic Perspective

As stated earlier, the piston ring pack is noted as the most significant contributor to the engine's total oil consumption. As a corollary, since blowby gases can entrain oil when passing through the ring pack, the positive crankcase ventilation (PCV) system also plays a major role in oil consumption. As was found in previous research, the exact contribution of the PCV system to the overall oil consumption varies predominantly with engine load, but does become more significant with higher speeds [6][7]. Research conducted by Froelund[6] shows both the importance of designing an oil separator to be very effective and the effects of the oil separator's performance on oil consumption. The separator's performance is usually measured by the smallest oil droplet it can capture/separate from the PCV stream and thus return it to the sump.

There are different variables of the piston ring pack system that have a notable effect on an engine's oil consumption. First and foremost, the geometry of the piston and rings governs the flow areas through which the oil flows and how it moves through the ring pack [8][9][10].

Additionally, the other side of the flow areas that completes the piston ring pack, namely the liner surface finish [11] and the cylinder bore distortion [12], are equally crucial to oil consumption. Other variables, such as the properties of the oil used [13], the temperatures of the components (liner, piston and rings), and the operating conditions of the engine (speed, load, steady-state, transient behavior) have been examined extensively [7][14][15].

Various studies have been conducted to try and quantify these variables and pinpoint the exact mechanisms that responsible for the oil consumption behavior at a given operating condition. Experiments involving Laser-Induced Fluorescence (LIF) have been used extensively to visually record oil's transport through the piston ring pack system. It is from these experiments that areas of oil accumulation at different operating conditions (engine speed and load) become apparent. With accurate oil film thickness measurements based upon the oil's density (the intensity of the fluorescence), it's possible to get an idea of the amount of oil on the 3^{rd}, 2^{nd}, and top lands as well as how the rings behave (movement within their respective grooves) under the given operating conditions [16][17][18][19][20][21]. To quantify what has been seen from the LIF videos and images, oil consumption measurements have been performed under similar operating conditions with near identical ring packs and engine configurations. In-cylinder measurements, such as land pressures, combustion chamber pressures, and liner temperatures, have been recorded along with the experimental conditions to get a better idea of the type of environment the oil is being exposed to during the trends observed.[14][15]. However, even though extensive tests have been performed, a complete analytical package that fully explains the trends seen in oil transport has yet to be developed.

Though advances have been made in the aforementioned simulations of ring pack dynamics, there still remain many more challenges to address. What has been observed and recorded through experiments leads to the models' accuracy. Gas flows that occur naturally within the ring pack during normal engine operation have been found to transport oil into the combustion chamber. This oil transport can occur in two fashions. First, oil can get entrained or dragged by reverse gas flow from the 2^{nd} land through the top ring gap/groove into the combustion chamber. This occurs when the 2^{nd} land's pressure is greater than that of the combustion chamber at the end of expansion and early exhaust stroke. These effects have been seen in research engines and simulated engine experiments, all with clear windows to view the oil's movements [3][8][9][22][23]. Second, the oil mist that may be present in blowby gasses

can contribute to total oil consumption when the blowby gases are recycled back into the intake manifold [14]. Other observations involve the inertia force present during the piston's constant acceleration and deceleration over the course of the four stroke gasoline cycle. It is believed, and supported, that this inertia can oscillate the rings within their respective grooves, essentially pumping oil into or out of them. In doing so, the oil can make its way to the top ring's upper face. When this occurs, the oil may be flung into the combustion chamber easily by the piston's motion [3][8][9][10][18]. Regarding the liner's role, observed in previous experiments, the evaporation of the oil on the liner has been found to be a considerable portion of the total oil consumption. The oil's evaporation is a function of the oil's composition and the liner temperatures, since both dictate the rate at which the oil can evaporate [7][13][15].

Extensive ring-pack models have been developed and proven at the Sloan Automotive Laboratory at MIT to predict ring dynamics, gas flows, and ring-liner lubrication within the ring pack. Using these analytical models, it is possible to estimate oil transport through the piston ring pack as well as predict the performance of the ring pack on the equally important level of friction [24][25][26][27][28][29][30]. More importantly, these models hypothesize the physical mechanisms that control the oil transport by conferring observations from a 2D LIF one-cylinder research engine [31]. The one-cylinder research engine is derived from the production four-cylinder engine currently used in oil consumption experiments involving a sulfur tracer method. Additionally, in the past, experiments focused on the relative importance of oil consumption sources and their relation to the oil transport within the ring pack as well as the physical environment through which the oil travels (such as the temperature and pressures of the ring pack as noted earlier) [7]. Given that the sources' respective contributions have been further understood, it's imperative that further research examine each source and the improvements that can be made to oil consumption and lubrication in the process. As such, the ring pack itself has been the current focus in this thesis, in attempts to understand the flow characteristics through the rings, grooves, and lands in different operating regimes as well as various changes to the ring pack geometry.

1.3 Oil Consumption Sources in SI Engines

As discussed previously in works by Yilmaz, et.al. [7], five possible oil consumption sources have been suggested to contribute to the total oil consumption of spark ignition engines during the engine's operation. These are depicted in *Figure 1-1* below:

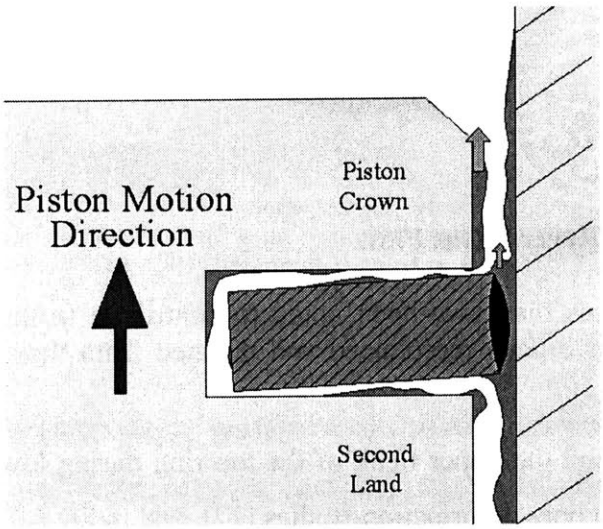

(A) Oil Throw Off

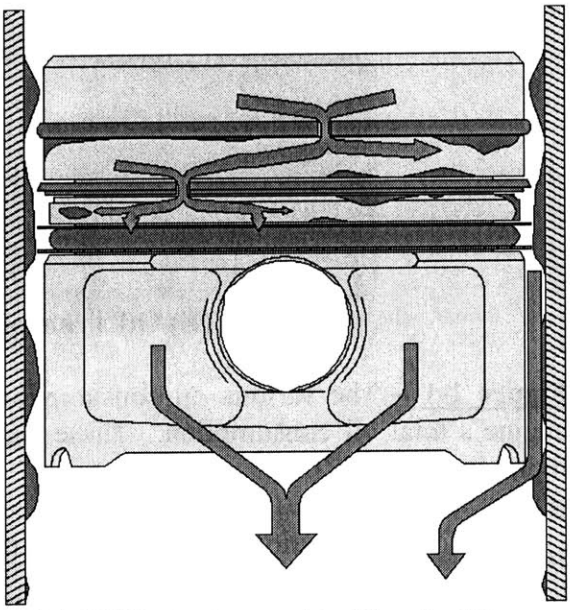

(B) Oil Entrainment in Blowby Flow

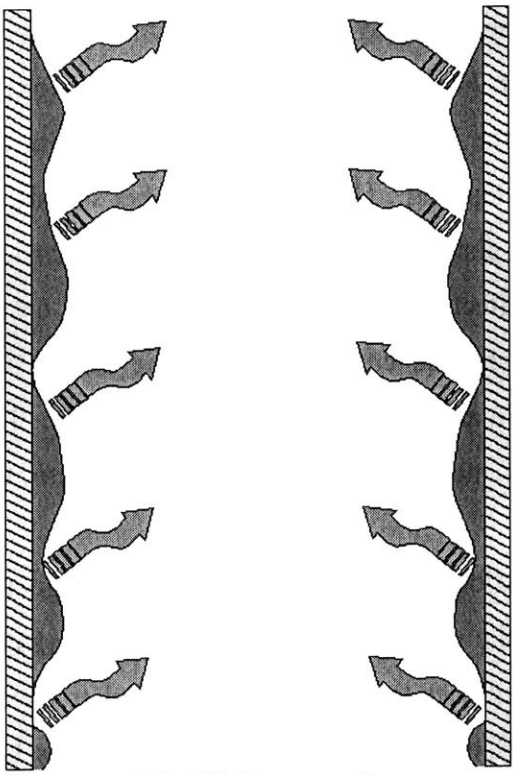

(C) Oil Evaporation

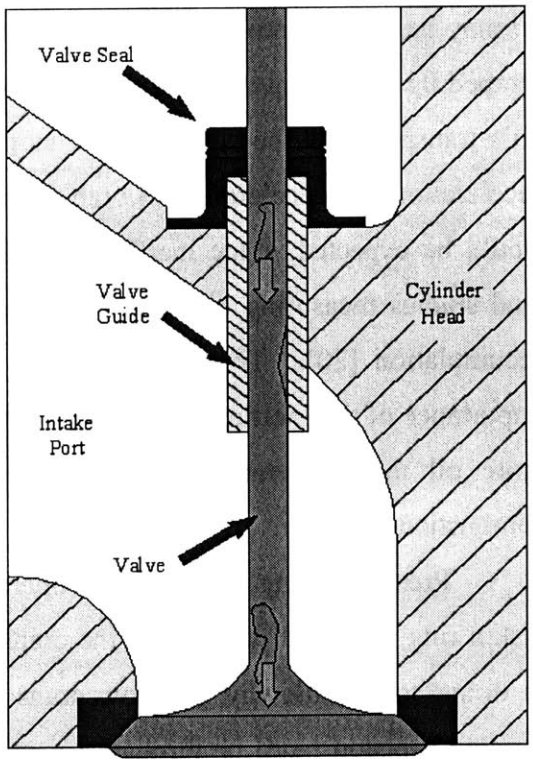

(D) Valve Guide Leakage

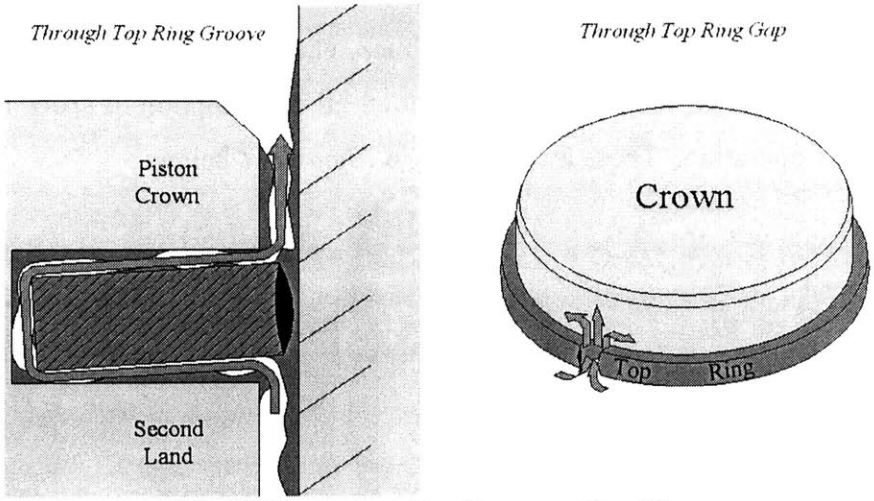

(E) Oil Transport by Reverse Gas Flow

Figure 1-1 – The various oil consumption sources that have been noted to contribute to the engine's total oil consumption. These figures have been reproduced and updated from those found in Yilmaz [7].

Oil accumulation can occur at the crown and the upper flank of the top ring during low load operating conditions. This has been viewed in bore deformation studies [12], and in 2D LIF videos [18]. Once this oil accumulates on the upper flank of the top ring and on the top land, the oil may be thrown into the combustion chamber by either shearing off of the crown or by being scraped up by the top ring. Both scenarios are shown in *Figure 1-1A* above. The reason for the oil's transport into the combustion chamber is due to the inertia forces imparted to it from the acceleration and deceleration of both the piston and the top ring. This occurs at higher speeds, as would be expected, since inertia forces increase with piston/engine speed. Previous transient load studies measuring oil consumption showed the effects low loading conditions had on oil accumulation [20]. The amount of oil accumulated on the crown and top ring affects the importance of the inertia and oil throw-off mechanism in an engine's total oil consumption. The more oil that accumulates, the more prevalent this method is in oil's transport into the combustion chamber.

Present during the engine's operation, combustion gases make their way through the piston ring pack and wind up in the crankcase and intake manifold by way of the PCV system. In doing so, the blowby gas flow drags oil with it, whether through circumferential transport (around a piston land) or through a ring gap/groove (See *Figure 1-1B*) [23]. In previous LIF experiments, it was found that a large amount of the flow is driven by the gas stream's search for

the ring gap since it is the path of least resistance when compared to the ring grooves. Additionally, many videos showed oil flowing through the grooves. Oil mist was created in some cases by oil flowing into these passages (gap and grooves) with a reasonable amount of driving force from the gas flow [16]. This entrained oil mist winds up in the intake manifold, and thus has become the subject of studies with regards to its contribution to the engine's total oil consumption. Previous experiments carried out involving different engines have concluded that this oil consumption source varies from engine to engine, as well as the oil separator used in the valve cover of the cylinder head [6]. However, oil consumption values follow closely to that of blowby, having a greater dependence on engine load rather than speed (oil consumption due to entrainment increased with increasing engine load) [14]. *Figure 1-2* shows how blowby gases drag oil as depicted in *Figure 1-1B*.

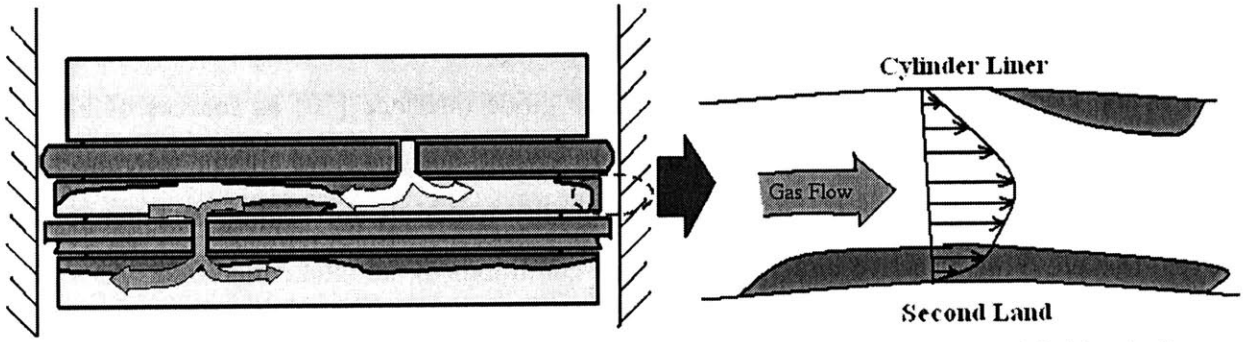

Figure 1-2 - Schematic of how gas flows through the rings gaps and enters the third land. In doing so, oil is dragged by the gas flow, especially throughout the 2nd land.

In addition to oil entrainment into the intake manifold charge, oil that's present on hot surfaces can evaporate and be lost in the combustion chamber (*Figure 1-1C*). As observed in previous experiments, liner evaporation seems to be the main contributor to total oil evaporation of the ring pack system. Oil evaporation's contribution to the total oil consumption of the engine increases drastically with loading conditions. As one would expect, increasing the loading conditions increases the thermal conditions of the engine components that the oil is exposed to [14][15]. Other experiments have noted the oil's composition as a factor in its evaporation and the effects loading conditions and liner temperature have on the oil tested. They go on to state that the oil evaporation could have a major role in the engine's total oil consumption [13][32]. Liner finish plays a role in the oil evaporation process, since the number of valleys or crevices in the surface can serve as reservoirs for oil, evaporating from the thermal heating caused by

combustion or high loading [11]. To confer with experimental results, a number of models have been created that show oil evaporation's dependence on both the oil's composition (volatility and viscosity) and the component temperatures that make contact with the oil (in experiments, the higher the oil temperature and the surface temperatures making contact with the oil, the higher the oil evaporation and oil consumption) [29][33]. Unfortunately, there still remain some uncertainties in predicting the evaporation rate of the oil and its contribution to the engine's oil consumption. Only qualitative hypotheses have been made with regards to evaporation's contribution based on temperatures and oil composition.

In earlier designs of SI engines, when the intake manifold pressure dropped to low loading conditions (considerably below atmospheric), oil in the cylinder head traveled through the valve guides into the intake port of the head (See *Figure 1-1D*) and thus into the combustion chamber during the intake valve's opening. Studies have confirmed previous valve seal designs that performed poorly at high speed and high intake vacuum (low loading conditions) [34] as well as the clearance of the valve stem and valve guide interface [10] as sources of high oil consumption in older designs. However, modern engine designs have tighter tolerances and positive valve stem seals (made out of higher quality materials for sealing and temperature fluxes) that are more effective under high vacuum conditions in the intake manifold. As a result of these improvements, oil consumption via the valve guide into the intake port has been regarded as a negligible contribution to the engine's total oil consumption [7][14].

Finally, a major contributor to oil consumption is oil's transport through the ring pack system and into the combustion chamber [1]. Specifically, the accumulation of oil in the upper piston-ring-liner system that gets driven into the combustion chamber by reverse gas flow is the part of oil transport that contributes to oil's consumption. The physical conditions that cause this reverse gas flow have been documented in numerous experiments. During low load operation, LIF videos show oil accumulation on the second land and its channeling towards the top/crown land through the top ring gap and groove as pressure builds in the 2nd land (See *Figure 1-1E*). In most cases, oil enters the groove as a liquid, but when driven through the gap, it exits as a mist due to the high flow velocities. The dependence on which route to take, groove or gap, depends on the path of least resistance and how well the top ring is sealing, specifically, how well it's sitting in its respective groove during axial motion. Also noticed is the significant rise in oil consumption due to the alignment of the top and 2nd ring gaps, providing an easy channel for gas

flow [17][18][23]. The pressure effect of the 2nd land has been shown in studies that increased 2nd land volumes, either by piston design [3] or liner surface finish [11], resulting in a reduction in 2nd land pressure and reverse blowby gas flow (and, consequently, the oil consumption) of the given engine [4][22]. Reverse gas flow becomes a more prevalent problem during transient loading operations, especially going from low load to high load operating conditions after the oil accumulation in the upper section of the piston ring pack gets consumed in the combustion chamber [20].

Combined, the above oil consumption sources contribute to an engine's total oil consumption during its operation. With the exception of leakage through the valve guide, these oil transport and consumption mechanisms can be controlled by the proper design of the piston-ring-liner assembly system. Along with friction, the amount of oil consumption produced by a given piston ring pack design is an excellent measure of that design's performance. However, other factors, such as the engine's design, the engine's operating regime, and the properties of the oil, affect the oil's transport through the piston ring pack. In doing so, one or more transport mechanisms may dominate over the others in their contribution to the total oil consumption. Therefore, a piston ring pack design becomes more engine and mechanism specific, and, as such, should be designed to control the dominating oil consumption source.

The prediction of oil consumption is driven by the understanding of the aforementioned mechanisms that govern oil's transport through the piston ring pack to the combustion chamber, and the amount of oil that accumulates in the volumes of the piston ring pack (ring grooves, piston lands, etc.). The transport of oil can be carried out by gas flow dragging it, inertia forces imparted to the oil by the piston and ring's movement, and by the relative movement of the rings relative to the piston and liner as well as the piston relative to the liner. This relative motion varies the volume that the oil occupies, and thus imparts a pumping action to the oil, forcing it to evacuate or fill certain regions, depending upon the movement. Oil on the piston lands is moved by gas flow or by the piston's inertial force. Oil residing in the ring grooves is also driven by the shear flow from gases as well as the pumping motion of the rings when they move axially within their respective grooves. The shearing of the oil, as stated earlier, can create an oil mist that flows with the gas easily, whether into the combustion chamber or back into the crankcase. The ring-liner interface also serves as a regime for oil transport as noted earlier and governs the

lubrication of the ring pack. *Figure 1-3* below depicts these forces and flow regions in greater detail, showing how oil can transport through the piston-ring-liner system.

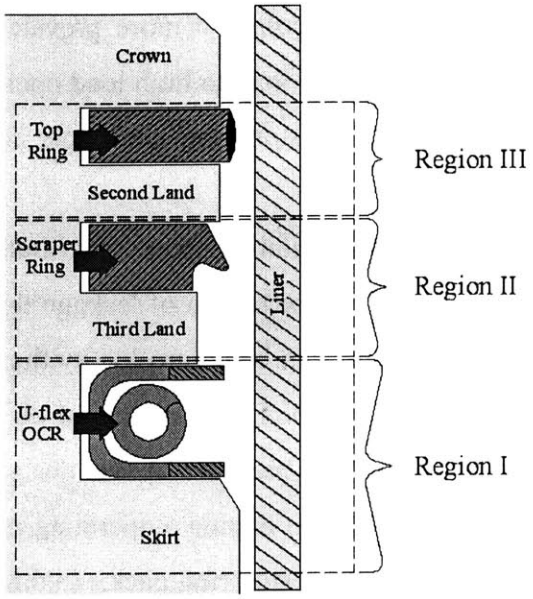

(A)

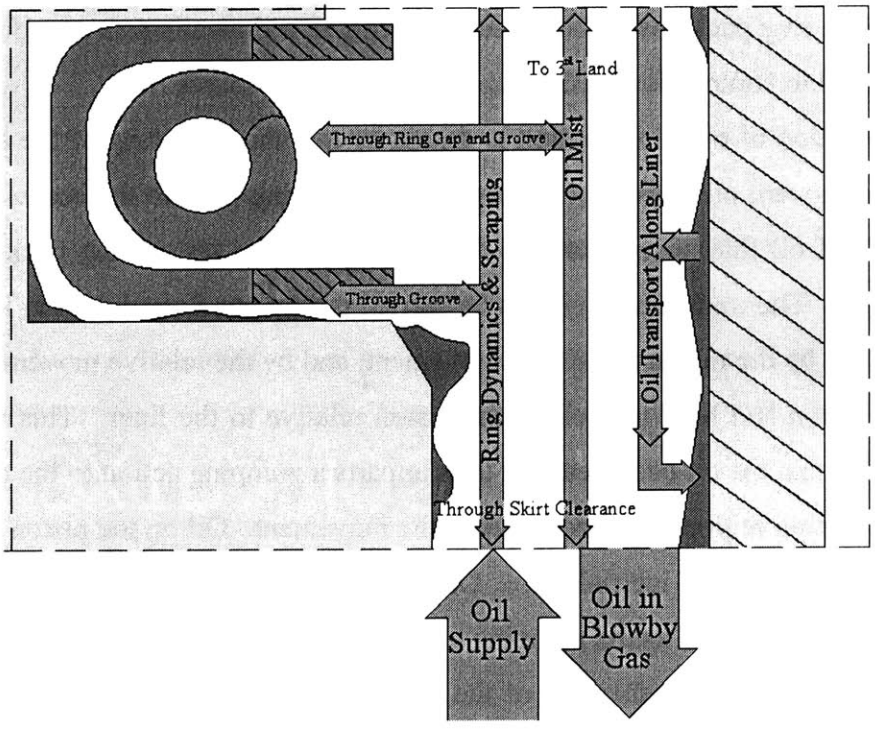

(B)

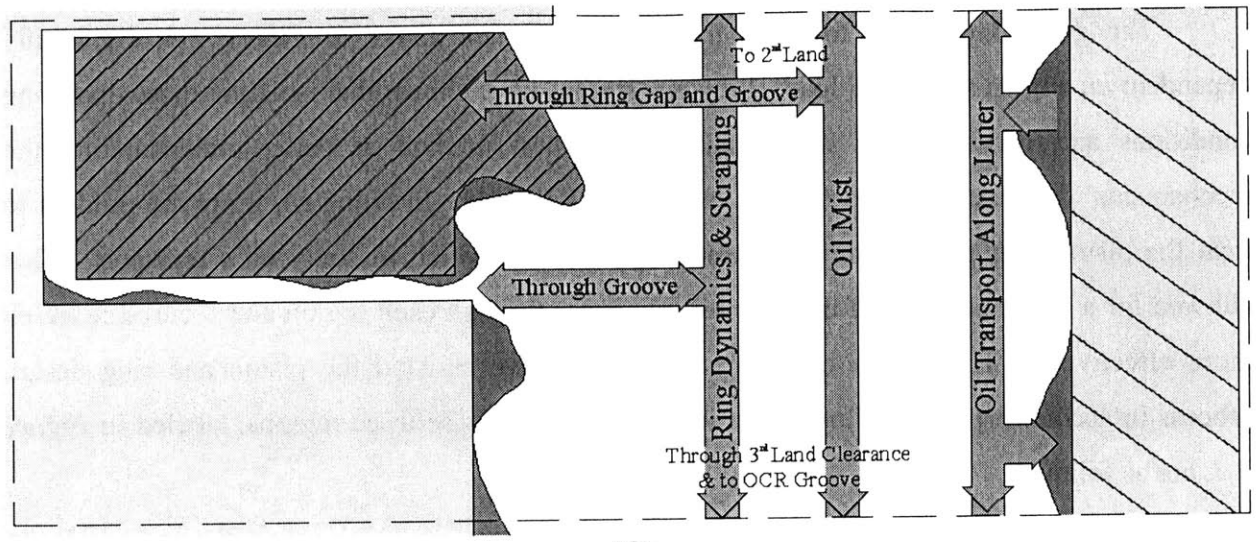

(C)

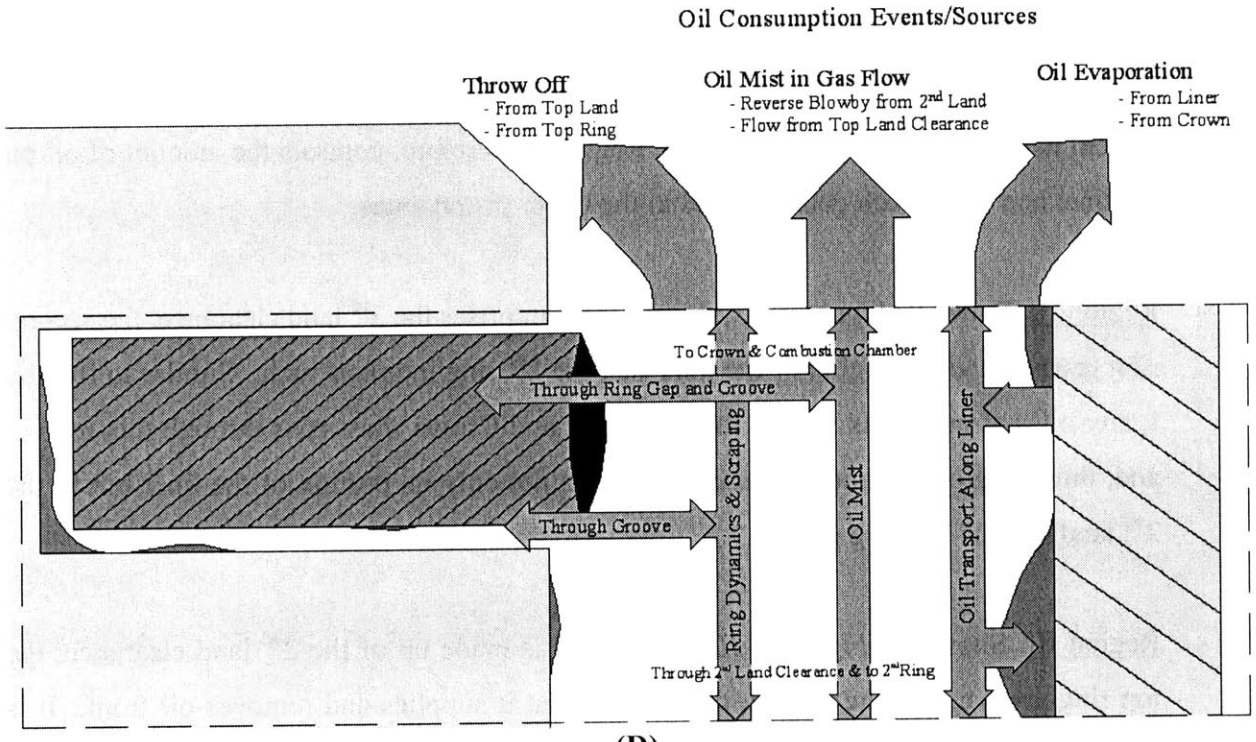

(D)

Figure 1-3 – Diagram depicting the transport of oil through the different regions of the piston ring pack system and the volumes in those regions that channel the flow. All show the ways that oil can be transported through the ring pack. **(A)** Shows how the piston-ring-liner system is divided into its respective regions. **(B)** Shows Region I, including the skirt and OCR and how the oil gets supplied to the ring pack. **(C)** Shows Region II, including the 3rd Land and the Napier/Scraper Ring. **(D)** Shows Region III, including the Crown, Top Ring, and how the oil that reaches the crown gets consumed. Similar figures have been found in [7], [17], and [21].

The governing forces for oil's transport, as shown above in *Figure 1-3*, are highly dependent on engine speed and load. Previous studies have shown that isolating these operating conditions and varying them individually is the best method at better understanding the mechanisms' dependence on these two variables [7][17][31]. In doing so, it proved prudent to treat the piston ring pack as three separate regions from which to study oil's transport. This allowed for a better analysis of how the oil transports through each region and focused research more effectively. The results of such experiments have assisted the piston and ring design process in accounting for the flows seen in each region. These three regions, labeled in *Figure 1-3*, are as follows:

- Region I: Shown in *Figure 1-3B*, this region is composed of the upper piston skirt clearance, the oil control ring (OCR) groove, and the portion of the liner that the OCR comes in contact with. Since any oil that is going to be supplied to the piston-ring-liner system has to pass through this region, Region I, therefore, controls the amount of oil on the liner and how much gets supplied to the upper piston areas.

- Region II: Shown in *Figure 1-3C*, this region comprises the 3rd land clearance, the second ring groove, and the region of the liner that the 2nd ring interacts with. Similar to Region I, any oil that makes its way to the Top Ring and Crown must pass through this region, and, thus, Region II controls the oil supply to not only its portion of the liner but to the 2nd land and the top ring groove.

- Region III: Shown in *Figure 1-3D*, Region III is made up of the 2nd land clearance, the top ring groove, and the portion of the liner that it supplies and removes oil from. It is here that direct oil consumption occurs, since any oil that passes through this region may go into the Top Land clearance and thus be consumed. Any oil that is removed from this region and reaches the crown, either by reverse blowby gas flow, being pumped out of the groove, or thrown off due to inertia, is typically considered lost and unrecoverable (consumed). Since this region reaches the uppermost part of the piston stroke, it determines the amount of oil left on the liner during its descent (down stroke). In doing so, the amount of oil that gets lost due to evaporation and the amount that gets recovered

due to scraping is purely a result of this region's performance. Finally, oil may be recovered and sent down to the previous two regions by way of entrainment due to blowby gas flow through the ring gap and groove.

By dividing the piston ring pack into three regions, it becomes easier to understand oil's transport into the combustion chamber. In doing so, each region's contribution to oil's overall transport into the combustion chamber becomes apparent, leading to improvements on the piston ring pack design in each of the respective regions in order to control oil flow and lubrication. As such, the design changes in each area become an important aspect of oil consumption study.

1.4 Ring Pack Design Effects

The first function of the piston rings is to seal the combustion chamber from the crankcase, especially under high combustion gas pressures and the gas pressures on the various lands. The rings move up and down axially within their respective grooves without failure. This is primarily due to the presence of oil between the ring and groove interface, assisting in this sliding motion. It is, therefore, important to control this oil and keep it from being burned within the combustion chamber, amongst other places, while still providing sufficient lubrication for the rings in their grooves and along the liner. Like all design processes, something that is desirable can't always be attained due to the surfacing of another problem if implemented. Thus, there are pros and cons to certain design considerations, especially when considering the piston ring pack as discussed below. Of course, any ring pack design is engine specific (noted earlier), fairing better or worse when used in a different engine design.

Starting from Region III with the crown land and working down the piston ring pack to the skirt, the design aspects of the piston ring pack are discussed with regards to oil transport and recommendations from previous research. For example, LIF videos taken at the Sloan Automotive Laboratory, show that oil flow across the piston's lands depends on speed, while oil transport through the grooves can be controlled/restricted by good ring and groove geometry design. Further, there are competing flows at work for oil's transport – blowby gases dragging the oil back down to the crankcase and inertia drawing it up to the combustion chamber [17]. From those same LIF videos, oil has been shown to flow on the lands in both the axial and circumferential direction. The axial flow being caused by the piston's alternating motion inertia,

and the circumferential flow from the dragging of blowby gases around the piston lands from one gap to the other. As will be explained later, the ring's axial movement can pump oil into and out of the grooves to and from the piston lands. This couples with the already present gas flows through the piston lands [16].

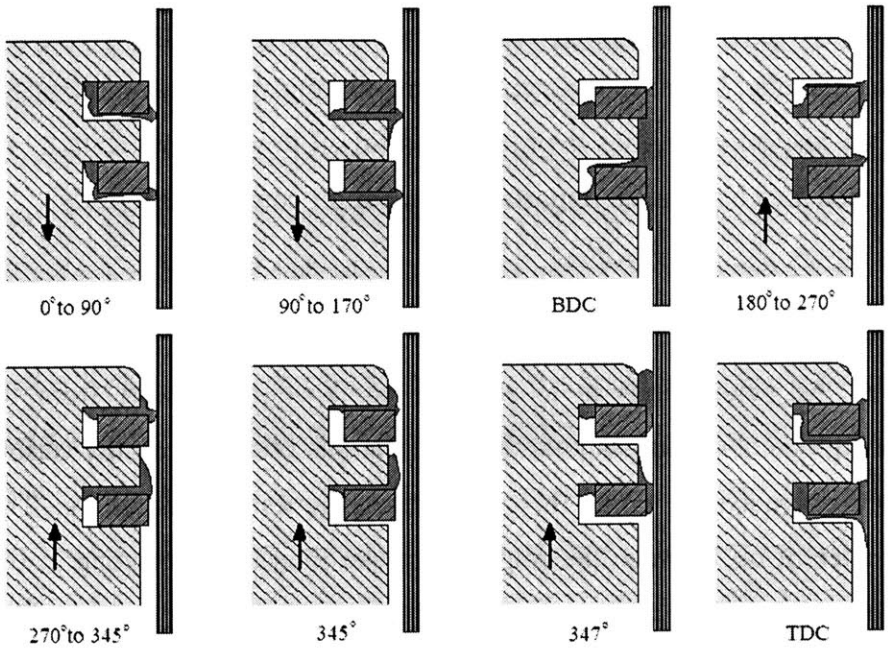

Figure 1-4 – The rings' movement within their grooves, independent of the piston's direction at certain points in the cycle, can cause oil pumping from the grooves to their respective lands and, consequently, the combustion chamber. (Redrawn from Ref [10]).

Examined more closely, and discussed here for a better understanding of ring motion described later on, the two methods of oil pumping through the ring pack are axial and lateral movement. Axial oil pumping occurs when, due to inertia, the rings move up and down axially in their respective grooves. On the up stroke, the rings are pushed to the lower surface of the groove in the first part of the stroke, allowing oil to enter the groove and remain on the upper surface. Due to the piston's deceleration, the rings move to the opposite side of the groove. On the down stroke, the rings switch sides to the top, pumping some of the oil out of the groove and into the lands and liner. *Figure 1-4* shows how this works.

During normal engine operation, combustion causes pressure variations through the ring pack that play a role on the axial inertia movement of the rings. This will be discussed later on. So, the ring groove clearance is necessary to allow gas to pass freely to the back of the ring in a small flow, but too big a clearance will cause radial collapse and no seal will occur. Axial clearances are very controlled due to this pumping effect. Groove clearances are on the order of 0.0016"-0.0032". Lateral oil pumping into the groove comes from the piston's tilting action.

The lateral ring motion varies with piston to liner clearance, where there's a reduction in ring pack efficiency with increasing clearance. The lateral ring oil pumping rate is affected by ring groove geometry: a keystone groove pumps more than a rectangular groove because, when the rings push into the groove, the decrease in volume of the groove is more rapid with the keystone than with the rectangular profile [10].

1.4.1 Region III Design Considerations: Crown Land, Top Ring, and Second Land

Region III doesn't have a direct effect on lubrication, but contributes significantly to oil consumption for reasons stated earlier (evaporation, throw-off, etc.) [21]. In previous experiments from Yilmaz, oil transport under low load conditions was found to be the dominant oil consumption source over evaporation and blowby gas entrainment. This is attributed to a combination of low blowby flow and the increase of oil accumulation on the upper piston regime (Region III) [14]. This was observed during transient loading operations in both LIF and production engine oil consumption research. Under low load operation, oil transport to the upper piston area was heightened by low blowby flow rates to the crankcase; the oil accumulated on the piston lands and grooves. When ramping to full load operation, the oil accumulated on the lands and rings decreased significantly, indicating that the top ring may have lost its sealing ability and fluttered in its groove. Top ring flutter will be explained shortly, but now it's suffice to say that the top ring's flutter assisted the reverse gas flow through the grooves, entraining the oil accumulated from low load, and drove it into the combustion chamber [20].

1.4.1.1 Crown Land Design

For emissions purposes, the crown land should be minimized in order to decrease the crevice volume of the combustion chamber [2]. This is especially important in diesel engines from an emissions standpoint. Furthermore, the larger crevice volume can become a source of hard carbon buildup, facilitating oil up-scraping on the liner or heating up the oil on the liner to evaporate it. Both would lead to higher oil consumption. A smaller crown land can quickly seat the top ring and give a more desirable pressure distribution throughout the ring pack. This would increase the top ring's radial pressure at the start of the down stroke, decreasing oil consumption. However, the height of the crown is limited by temperature control and heat transfer through the piston from combustion. Insufficient heat transfer can cause micro-welding of the top ring to the

groove, usually of the bottom flank to the bottom of the groove, which occurs during full load operation when the greatest gas temperature and pressure are present from combustion. For reasons that are beyond obvious, the occurrence of micro-welding is undesirable [10].

As observed through LIF operation, oil can reach the crown land through the top ring groove during oil accumulation on the 2nd land or through top ring up-scraping at high engine speed and low load [18]. More methods of oil transport to the crown land are discussed below.

1.4.1.2 Top Ring Design

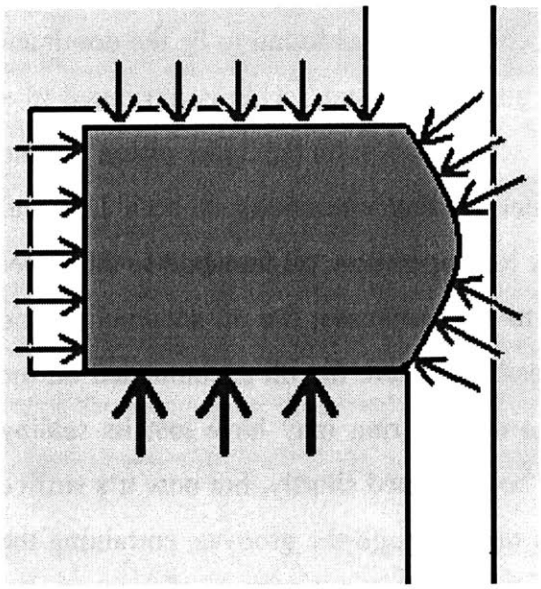

Figure 1-5 - Forces acting on the top ring at a given point in time. The bottom arrows are from the piston's force on the top ring due to inertia. Note that depending upon time in the cycle studied, this normal force from the piston can be either on the top or bottom flank, based upon the inertia of the ring. The other arrows, in clockwise order starting from the left hand side, are the top ring groove pressure forces pushing the top ring radially outward, the top ring groove and combustion chamber pressure forces on the top flank, and finally, a combination of combustion chamber pressure forces (above the barrel's line of symmetry), 2nd land pressure forces (below the barrel's line of symmetry), and, depending on the ring's position, the normal force of the liner.

The primary purpose of the top ring is to seal the combustion chamber. Oil that passes through the top ring gets thrown into the combustion chamber due to the inertia on the top ring causing lift-off. Top ring lift-off occurs during the end of the compression and early part of the expansion strokes, throwing oil into the combustion chamber (See *Figure 1-4* above). Aside from throw-off, pressure buildup below the top ring can carry oil into the combustion chamber through the ring groove and gap. The ring groove flow area is affected not only by the ring's position, but by the piston tilt varying the clearance between the ring and groove. In doing so, larger flow areas are created for oil or blowby gas, depending on the stroke [35]. Additionally, the ring/liner lubrication along the circumference of the rings varies greatly due to piston tilt, ring twist, and bore distortion. The piston's tilt varies the degree of scraping of oil by the top

ring between the thrust and anti-thrust side in both the up and down direction [28]. *Figure 1-5* shows the various pressures present on the Top Ring at any one point in time in the cycle.

Thus, it's important to minimize the top ring gap in order to minimize the amount of combustion gases that can flow past the top ring. Previous research shows that a flow restriction decreases oil flow and, thus, oil consumption [22]. This leads to a geometric design problem when the top ring heats up and expands. During the ring's design, this temperature variation and the tolerances present are considered. Typical values of the top ring gap size are on the order of 0.3mm $^{+}/_{-}$ 0.1mm. The top ring's gap and inertia (a function of the piston speed) play a major role in oil consumption and blowby. The gap influences 2nd land pressure and, thus, the motion of the second ring within its groove. As will be discussed later, a change in the 2nd land volume has similar effects. Both changes influence blowby [3][9]. It should be noted that ring rotation, where the rings spin in the circumferential direction within their respective grooves, can grossly affect gas flow patterns, oil transport, and blowby flow. The top and 2nd rings rotate independently of each other in an arbitrary fashion. In doing so, the gaps may become aligned and thus provide a direct channel through which oil can flow in a short period of time [23].

At top dead center (TDC), the top ring experiences its most severe lubrication region, where it can become "dry"; that is, it's starved of oil. If the ring becomes oil starved, friction becomes more important since the oil film thickness between compression rings (the top two rings) and the liner shouldn't be too thin [9]. Oil starvation is due to a lack of a direct supply of oil from the oil control ring (OCR) to the liner (as seen in Region I above) since at TDC, the Top Ring isn't in a region where the OCR has previously been, therefore no oil is supplied. However, on the down stroke, compression rings are lubricated by a thicker film than on the upstrokes [1]. *Figure 1-6* below shows how the top ring can become oil starved. Notice this neglects oil's transport through Regions II and III, where oil can bridge to the liner and make its way up to the top ring groove. Additionally, if the ring twists within its groove such that its ID is touching the top of the groove, the OD bearing surface can wear significantly, causing scuffing and increased oil consumption without sufficient lubrication [9].

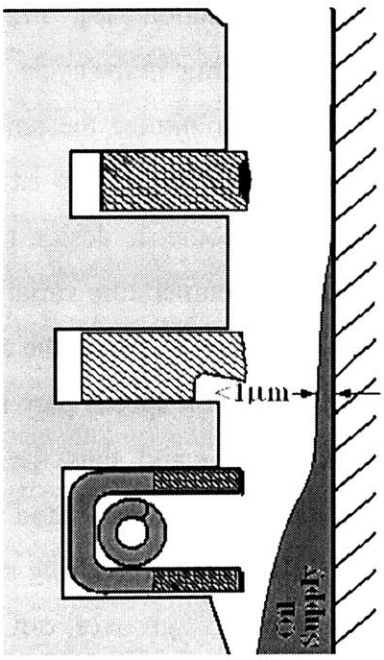

Figure 1-6 – Schematic of how the top ring region can become oil starved at TDC and how the OCR supplies most, if not all, of the oil to the ring pack. Not drawn to scale.

The current trend is towards a thinner top ring and groove, since the ring's conformability (how well the ring meshes with the liner's surface – how well it seals) to the liner is enhanced with a reduction in ring thickness. Increased conformability reduces oil consumption without increasing frictional losses [12]. This conformability is desirable for other reasons in addition to proper sealing. Uniform circumferential contact between the ring and the liner can also reduce the oil throw-off since higher bore distortion creates bore depressions. These bore depression fill with oil and when the rings rotate, they can scrape off a larger amount of oil from these valleys. The basic design of a top ring can be seen in Region III of *Figure 1-3D* above. Namely, the top ring is rectangular with a barrel-face and a molybdenum coating. The barrel-face is good for gas sealing and oil control (generates hydrodynamic lift) while molybdenum has superior scuff resistance and is tolerant of hot spots present from bore distortion. Unfortunately, if the coating wears away, the top ring doesn't seal as well, and thus the gap may widen, creating undesirable results. There are typically three types of top ring designs, though only two are used extensively. These are, non-twist, positive twist, and negative twist top rings. Non- and positive twist are used for blowby control and, as will be explained shortly, while negative twist rings are rarely used (*Figure 1-7* shows these top rings) [10].

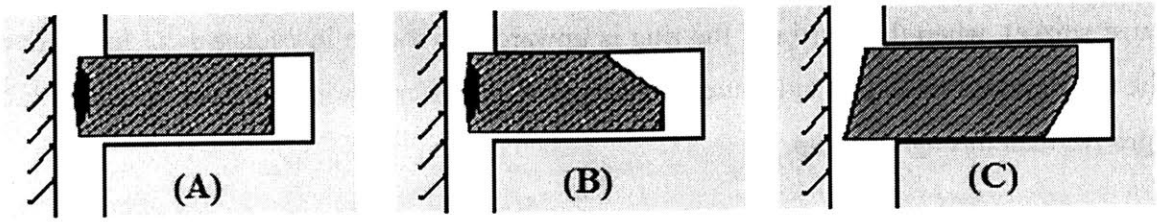

Figure 1-7 – Three types of top rings: **(A)** Barrel-faced no twist rectangular ring, **(B)** barrel-faced positive twist ring, and less commonly used, if at all, **(C)** taper-faced negative twist ring.

The top ring's movement within its groove is a strong function of the operating conditions of the engine and the design of the ring. The ring oscillates inside the groove several times within a portion of a cycle. This will occur with or without gas flow and gas pressure fluctuation; it just needs inertia induced by the piston's motion. Ring flutter is driven mainly by the competition of the difference in gas pressures and the inertial forces. These forces have a major effect on gas and oil flow. Ring flutter follows these steps. First, the ring goes to one side of the groove due to a change in the direction of net force acting on the ring (pressures, inertia, etc.). Second, gas flows to the evacuated region in the groove, changing the land pressures. Finally, the land pressure change causes the net force on the ring to reverse and the ring moves back to the other side. Ring flutter occurs when the land pressures and inertia forces holding the ring to its groove are ineffective versus gas pressure. *Figure 1-8B* shows how flutter occurs and its result.

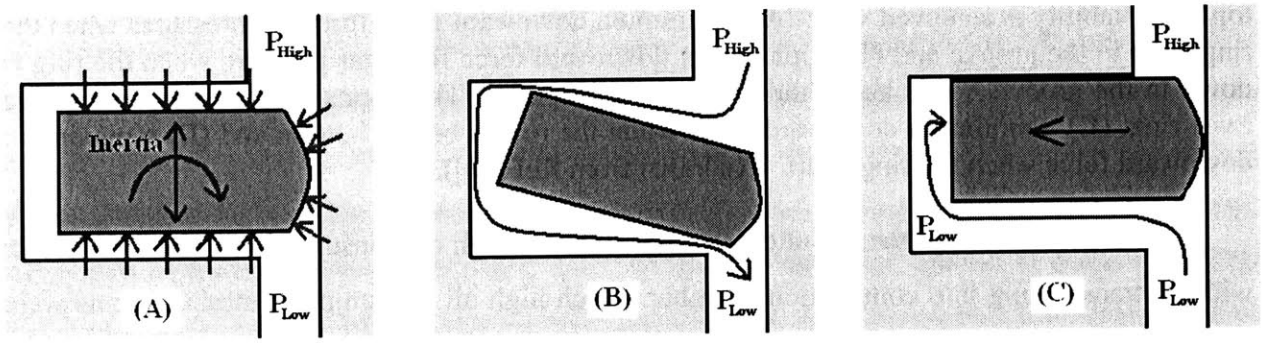

Figure 1-8 – **(A)** The forces present on the top ring at any one point in time during the four stroke cycle as discussed in *Figure 1-5*. **(B)** The position of the top ring and the visual occurrence/cause of flutter. **(C)** The position of the top ring and the conditions that case radial collapse.

The cause for this ineffectiveness is the relative angle between the ring and the groove. *Figure 1-9* shows the effects of the top ring relative angle on its stability within the groove. Reverse flutter can take place late in the compression stroke or late in the expansion stroke (early

exhaust stroke), when the inertia of the ring is upwards, as shown in *Figure 1-9*. In either case, as the top ring loses stability and flutters in the groove, it offers a much greater flow rate through the groove than through the gap.

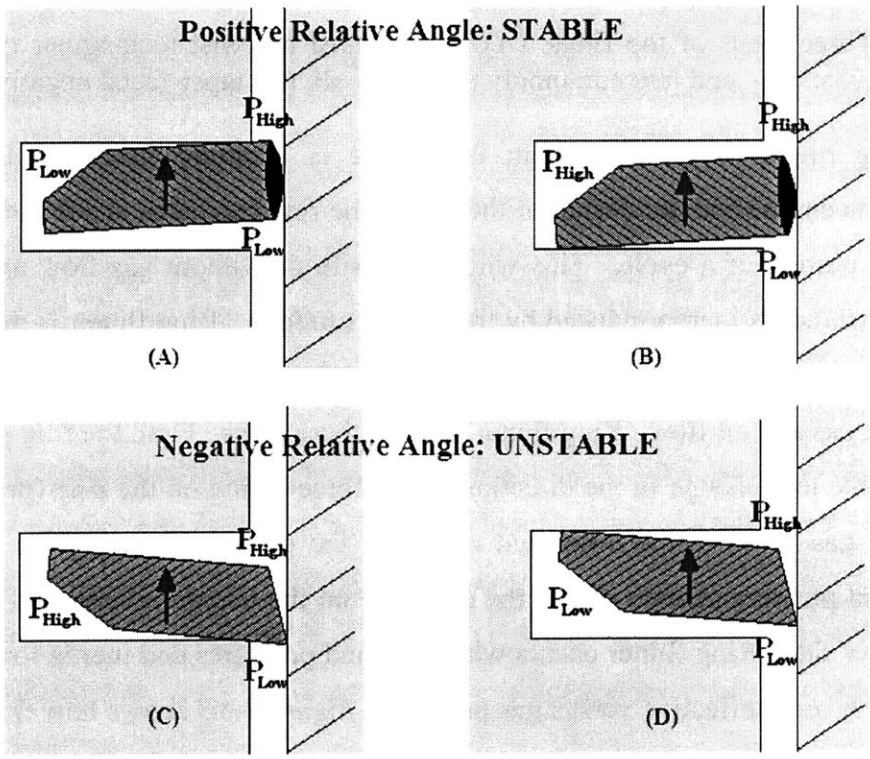

Figure 1-9 – The red arrows represent the inertia of the ring, and show that for a positive twist top ring, stability is achieved with: **(A)** a minimum downward force from gas pressures when the ring is up in the groove and **(B)** a maximum downward force from gas pressure when the ring is down in the groove. This keeps the ring seated properly. The opposite is true for a negative twist ring: **(C)** a minimum downward force when the ring is on the bottom and **(D)** a maximum downward force when the ring is up. (Redrawn from Ref [26]).

It is thought that reverse flutter is responsible for high oil consumption in load transients with oil transporting into combustion chamber. Such high oil consumption measurements were seen and recorded by Yilmaz, et al [20] when going from low to high load caused large amounts of oil to be consumed. Entraining the oil accumulated during the low load conditions, the reverse gas flows through the groove during flutter and drives the oil into the combustion chamber. To counteract top ring flutter, the top ring must be designed with a static positive ring-groove relative angle and other means of reducing the ring's dynamic twist during operation. Torsional stiffness is the key to controlling flutter – 1) the top ring needs more static positive twist for softer materials (too positive of an angle causes radial collapse as will be explained

next) and 2) axially thicker rings are more stable due to higher mass and inertial forces [26]. Thus, this presents a design problem in that the top and 2nd rings need the least possible mass but biggest moment of inertia to minimize both wear and oil consumption problems from the dynamic twist [9]. *Figure 1-8A&B* above as well as *Figure 1-10B* below show how the positive static twist assists in the top ring's proper sealing.

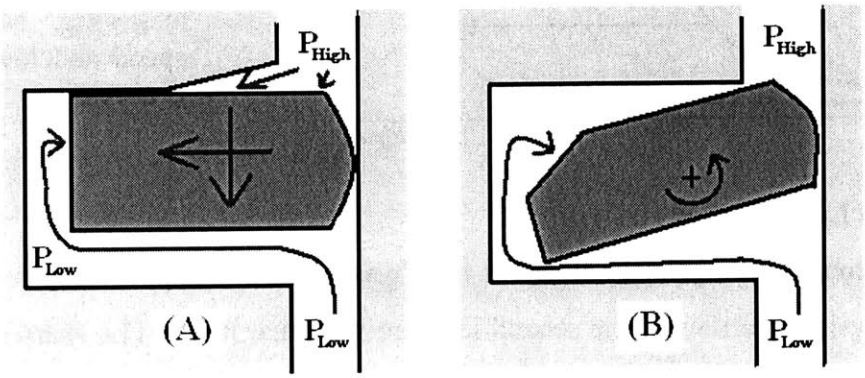

Figure 1-10 – **(A)** The use of a chamfer in the crown to prevent radial collapse by making use of the high pressures present. **(B)** The use of a chamfer in the top ring in order to impart a net positive twist to the ring and prevent opening a channel from high to low pressure, increasing blowby.

Top ring radial collapse occurs if the top ring's static positive twist is too large (past a critical limit). When the ring seals the gas flow path through the upper part of the groove, making contact with the OD corner of the upper side of the groove, radial collapse occurs. The ring's radial collapse pushes the ring inward due to gases acting on the running surface with the liner, causing a direct gas leakage through the ring-liner interface, impacting blowby and oil transport. Radial collapse is more likely to occur for a 2nd ring with a positive twist (Napier or tapered face) for the reason of more of the running surface being exposed to higher pressures. Even good positive static twist top rings have radial collapse at high speeds and low loads in SI engines. Radial collapse occurs in a wider operating regime in SI engines with a larger top ring axial height. In the end, however, it's a trade off between flutter and collapse when dealing with the top ring's design [26]. *Figure1-8C* shows a top ring's radial collapse while *Figure 1-10A* depicts one design solution to prevent such an event. *Figure 1-11* illustrates the effects of the design changes of *Figure 1-10* on the blowby of an engine.

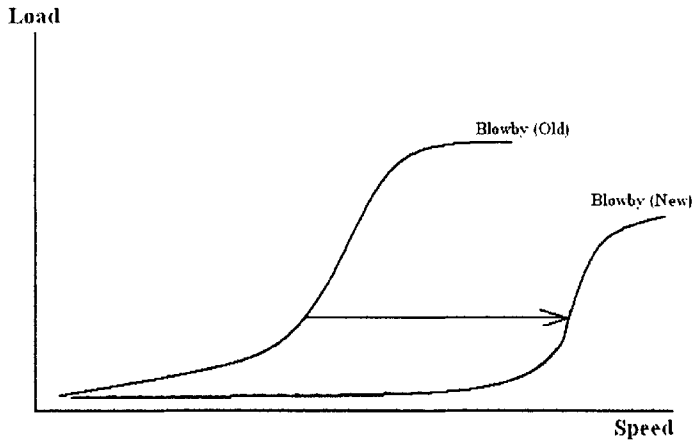

Figure 1-11 – Blowby increases with speed and load. With the addition of crown and top ring chamfers depicted in *Figure 1-10*, this graph is shifted out as the top ring becomes more effective at sealing. Note that at high speed and low load, blowby is excessive.

1.4.1.3 Second Land Design

The second land's primary function is to give top ring support. Concentrating on this function, the design qualities of the second land are such that it has: 1) a sharp edge on the top ring groove's bottom surface and 2) a region of larger volume to accumulate gas. The second design necessity is most effective when such a groove in the land increases the volume percent greatly (only when the top and 2nd rings are close together). The sharp edge and oil accumulator reduce oil consumption and blowby. The oil accumulator's purpose is to minimize the pressure buildup between the top and 2nd rings. Studies show that the longer it takes for the pressure to build up, the longer the top ring remains on the bottom of the groove, properly sealing and performing its job. In doing so, blowby and oil consumption are reduced. If there's an improper balance however, the 2nd ring can flutter and cause deterioration in oil control [10]. Thus, in experiments by Yoshida, the oil consumption can be reduced by decreasing the 2nd land pressure, making the 2nd ring lift off at a higher speed. If the 2nd land pressure is high enough to make the top ring lift off during the expansion stroke, combustion gas that flowed into the 2nd land through the gaps and grooves is blown up into the combustion chamber, dragging oil along with it. This results in an increase in oil consumption [3].

The behavior of the oil in the 2nd land, according to LIF videos, is highly sensitive to the ring gap locations of both the top ring and 2nd ring. The oil in the second land is influenced by both the axial and circumferential flows discussed earlier. Inertia forces are dominant at high engine speeds, creating a large amount of oil accumulation on the land and causing top ring up-scraping leading to increased oil consumption in the process. However, at low speeds and load, the top ring's down-scraping was the major source for oil accumulation on the 2nd land. This oil

accumulation on the land can, as stated earlier, be transported to the crown land as a liquid through the top ring groove, or as a mist through the top ring gap; while some gets to the 3rd land through the 2nd ring gap and/or groove [18]. Thus, the main design objective of the 2nd land is to keep the gas pressure below the top ring at a minimum, and to decrease the inertia effects from causing high oil consumption. However, too low of a pressure can cause 2nd ring flutter. Designs that are currently used to accomplish these goals are the use of a V-cut/groove in the 2nd land to act as both an inertia reservoir for oil and to increase the volume of the 2nd land without compromising the sealing qualities of the top ring. The increased volume helps decrease the 2nd land pressure. But, this increased volume stores more oil and can become ineffective at high loads due to the high gas flows found in that region. The high flow rates coupled with more oil increase overall oil consumption. Another design option is to minimize the clearance of the 2nd land for better sealing of the top ring. This minimization is limited by the secondary motion of the piston and the accompanying increase in 2nd land pressure.

1.4.2 Region II Design Considerations: Second Ring and Third Land

The main objective of Region II, as noted earlier, is to control oil supply to the top ring groove, and to provide adequate lubrication and oil supply to Region III.

1.4.2.1 Second Ring

Typical 2nd rings of SI engines are made of cast iron and, in the past, had a negative static twist for effective oil control. The current trend has been towards the use of a Napier/Scraper ring that has a rectangular base shape. *Figure 1-12* shows the contrasting designs of these two rings. In either case, the purpose is to seal the lower outer periphery and upper inner side of the 2nd ring groove. In doing so, the ring scrapes oil from the liner during the piston down-stroke, and, since the lower outer edge is sealed, prevents the oil from going into the groove and up around the ring during the piston's upstroke. Both types of rings have a taper face to prevent top edge contact due to a negative dynamic twist. Because of negative twist, blowby is higher, but the design has proven better for oil consumption/control. Taper faced rings in tests had better oil control than rectangular rings when dealing with inertia force at high speeds because they held oil in a better position, down in the 3rd land. The Napier ring has the additional feature of a hook that can act as an oil reservoir during high inertia (high speed) conditions, as well as a positive

static twist to assist at these higher speeds [10]. This oil accumulation in the Napier ring has been viewed in LIF videos, where the ring scrapes the oil off the liner onto the 3rd land. Additionally, this same hook was shown to release oil onto the liner due to inertia during the early part of the piston's upstroke [16].

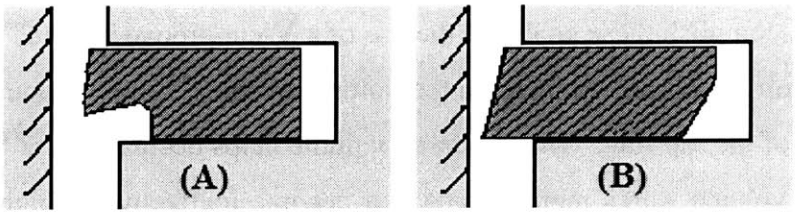

Figure 1-12 – Two design choices used for a 2nd ring: **(A)** a Napier/Scraper ring, used most commonly in modern designs, and **(B)** a ring with negative static twist.

Analogous to the top ring, oil can be dragged through the 2nd ring gap by blowby gases, entering the gap as a liquid and leaving as a mist. This oil is supplied by the 3rd land, whose origin is from the inertia flow through the OCR gaps [16]. This entrainment of oil in blowby gases to the 3rd land, and hopefully to the crankcase, can be enhanced by lowering the 2nd land pressure with a larger 2nd ring gap (this would assist Region III's efficiency as noted earlier) or by inducing 2nd ring flutter. However, in doing so (both a larger ring gap and inducing flutter), regions where reverse blowby gas flow is dominant, such as at high speed and closed throttle, should be avoided since the ring pack can become flooded with oil. This oil can travel to the combustion chamber at a higher rate and, thus, increase the engine's oil consumption [17].

Designing the 2nd ring for flutter usually has little effect on blowby, but any effect it has would increase blowby and, thus, decrease oil consumption. Flutter releases the 2nd land gas to the 3rd land, decreasing 2nd land pressure and assisting in blowby flow from Region III. Additionally, flutter can inhibit oil flow from the 3rd land to the 2nd ring groove, driving oil from the 2nd land and 2nd ring groove down to the 3rd land. In summation, the ring's flutter assists in driving oil away from the combustion chamber. Use of a negative static twist design helps induce flutter, since 2nd land pressure rises more slowly and has a lower magnitude than cylinder pressure, thus negating any use of dynamic twist. If flutter doesn't occur, this 2nd ring design can pump oil out of the groove and into the 2nd land, especially at high speeds due to high inertia forces. These high forces increase dynamic twist and, thus, the pumping action similar to what was seen for the top ring. Due to an SI engine's wide range of speeds and loads, the use of negative static twist scraper rings has decreased giving way to the favorable Napier ring, which has a positive static twist to control this oil pumping into and out of the groove [26]

Much like the top ring, the 2nd ring can also experience radial collapse, where contact from the 2nd ring to the liner is lost and oil film pressure goes to zero. The radial collapse causes gas to flow to the 3rd land through the ring-liner interface while also increasing the oil film thickness on the liner. Once on the 3rd land, the gases can flow into the 2nd ring groove, dragging oil with it. Thus, radial collapse adversely effects blowby and oil consumption. The increased blowby can heat up the tapered face of the 2nd ring and cause scuffing [36]. As with the top ring, proper design of the 2nd ring can control its radial collapse. Two things needed for ring collapse are: 1) that the ring stays on top and 2) that the upper land gas pressure is sufficiently high. For the 2nd ring, the gap size or clearance below it (increase 3rd land volume) would reduce the land pressure difference between the 2nd and 3rd lands (note that the Napier ring has a greater gap size than a normal taper face ring due to its hook). These changes should be done with caution – gap size affects blowby and oil transport under conditions when the ring doesn't collapse and piston clearance for the 3rd land below the ring has limits due to oil control and ring support [26].

Another method in controlling 2nd ring radial collapse is to force the ring down before it collapses by adding a chamfer at the OD corner on the upper side of the groove so more of the upper flank of the ring gets exposed to higher upper land pressures (similar to that seen in *Figure 1-10A*). This creates negligible volume change to the upper land as long as the chamfer's height is small, creating little effect on the ring pack's performance during other operating conditions when the ring doesn't collapse. This chamfer depth needs to be increased with increasing operating speed. Since 2nd ring collapse occurs in the mid speed range, a chamfer on the upper corner of 2nd ring groove can eliminate collapse (chamfer size on order of ~1mm). This can be done for top rings as well, with minimal crevice volume increase [26].

1.4.2.2 Third Land

Traditionally, the 3rd land is cut back to create an oil accumulation region above the OCR. This helps to improve oil consumption but causes an increase in blowby. It improves oil consumption by lowering the pressure above the OCR, increasing the time that the OCR is in contact with the top of the groove. This position is ideal for oil scraping done by the 2nd ring to accumulate oil. The accumulated oil would get drained once the OCR leaves the upper part of the groove. The addition of a 3rd land chamfer, shown in *Figure 1-13*, to the lower part of the 2nd ring groove also assists in oil accumulation [10].

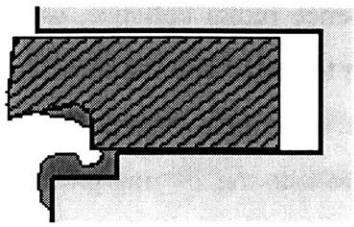

Figure 1-13 – The use of a Napier Ring coupled with a 3rd land chamfer provide areas for oil to accumulate due to the increased volume.

The mechanisms that fill up the 3rd land with oil employ inertia and are thus speed dependent, the higher the speed, the earlier the effects. A greater engine load will delay the start of these transport mechanisms and reduce their magnitude while the opposite is true for low engine load. The use of a Napier ring with a 3rd land chamfer is good for temporary oil storage when compared to the effects of a negative static twist scraper second ring. As stated earlier, the combination of the Napier ring's hook and the 3rd land chamfer create a "buffer region" to prevent oil from coming up due to the upward force of inertia. In piston reversal, this region serves to throw the oil back down towards the OCR [21]. However, if too much oil accumulates, bridging occurs. Bridging is where oil touches both the piston and liner at the same time, exchanging oil from the piston to the liner. Higher engine speeds increase the amount of oil on the 3rd land, while higher loads decrease it. Therefore, the most bridging occurs at high speed, low load. Bridging is good for lubrication and wear for the upper two rings, but doesn't transfer oil to the upper regions of the piston during the down stroke. It increases oil consumption when it occurs near TDC (late-compression, early-expansion strokes) because the top ring can scrape the extra oil present on the liner into the combustion chamber later in the cycle [19].

1.4.3 Region I Design Considerations: Oil Control Ring and Skirt

The OCR controls the liner oil film thickness for lubrication of the top ring running surface. It has to meter the oil to the top two rings while scraping excess oil off the liner. Additionally, it supplies oil to Region II [21]. The purpose of the skirt is two-fold. First, it takes up the brunt of the secondary side force imparted by the connecting rod/piston pin. Secondly, it helps guide the piston within the cylinder. There are two main ways that oil gets supplied to the ring pack during normal operation. The conventional, and cheaper, method involves oil splashing from the crankcase onto the skirt. The dry sump method involves injecting oil up towards the piston ring pack. Current models of the piston skirt and secondary motion are under

development at the Sloan Auto Lab at MIT in attempts to understand the skirt deformation and the oil film thickness changes that are caused by the skirt's interaction with the liner.

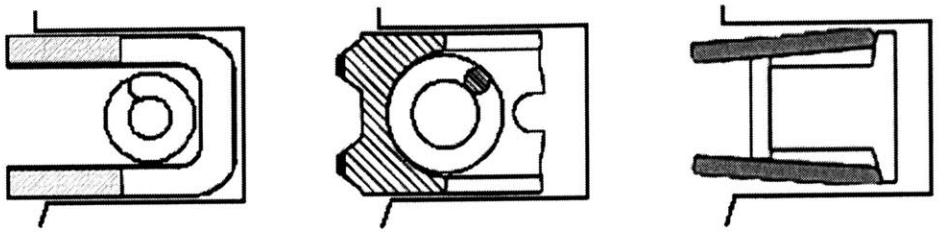

Figure 1-14 – The three types of oil control rings currently used in production engines: **(A)** U-flex, **(B)** 2-piece, and **(C)** 3-piece.

Traditionally, there have been three different designs for the OCR. These are listed in order of increasing cost: 3-piece, 2-piece, and U-Flex. *Figure 1-14* shows these three OCRs. The two-piece OCR releases a large amount of oil at one location on the piston circumference (near its gap) while the U-Flex gaps release a small quantity of oil at about 50 evenly spaced locations around the circumference of the 3rd land, giving a better oil distribution [21]. Typically, a small oil ring height (a small ring contact area) is preferred because its contact with the liner is less affected by piston tilt as well as showing a decrease in liner-running surface contact (less friction). Hence, in the designs of all the aforementioned OCRs, the contact area is composed of thin sections. As stated earlier with regards to the top ring, the thinner axial height allows it to follow the bore's surface more effectively. Nevertheless, the piston's secondary motion does influence the effectiveness of the OCR's scraping of oil off the liner. Unlike the top two rings, the OCR isn't gas loaded, so everything in the groove is oil. Drainage holes in the back of the groove assist in emptying the pools of oil that have accumulated in the groove to the back of the piston and into the crankcase [10]. The OCR's geometry determines the oil supply to the 3rd land and to the part of the liner between the OCR and the 2nd ring, where the 3rd land can bridge [17].

The OCR experiences a higher unit pressure on its face profile when compared to the top two rings because its face profile contact area is far less than that of the top two rings, therefore the OCR is typically stiffer than the other two. That is, the OCR has high ring tension. As a result, coupled with high unit pressure on the face and low 3rd land pressure, the OCR never experiences radial collapse. However, the OCR can flutter within its groove, causing large quantities of oil to flow towards the top two rings, especially during light load and transient

loading conditions [35]. It flutters when the 3rd land pressure pushes the OCR down during the late part of the compression stroke and part of the expansion stroke. The flutter is due to the fact that pressure can't build up below on the skirt or inside the groove due to its large volume and use of drain holes to the crankcase. The 3rd land pressure drops quickly when the OCR is pushed down and an upward force from inertia and friction can bring the OCR up again [26].

Figure 1-15 summarizes some of these design recommendations along with current approximate dimensions for some of the key components previously discussed.

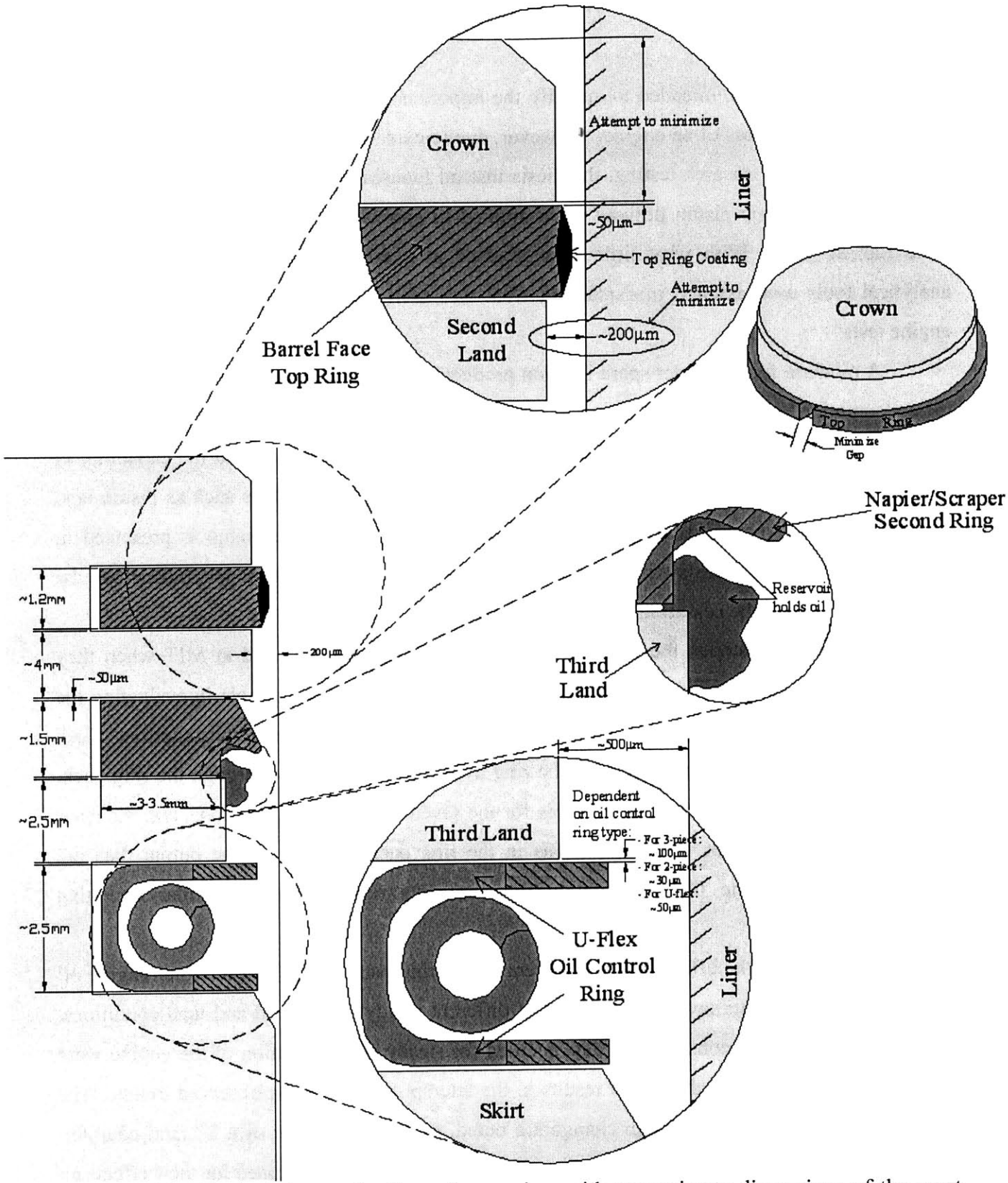

Figure 1-15 - Typical ring pack of gasoline engine, with approximate dimensions of the most modern design used in current spark ignition engines. Not drawn to scale.

1.5 Project Direction

This thesis work intended to quantify the importance of piston ring pack designs on the oil consumption sources of an engine. However, due to extenuating circumstances that involved the delay of further research testing, the thesis instead focuses on the theoretical and analytical aspects of those same piston designs when applied to current models developed at the Sloan Auto Lab at MIT. With what little data obtained at steady state operating conditions, the analytical tools used assisted in explaining what was seen in the experimental data from the engine tests.

A modern, four-cylinder spark ignition production engine was used to originally measure oil consumption with prototype pistons. An extensive diagnostic system was developed and implemented by Yilmaz, [7], to measure the engine's oil consumption. It had the capability to simultaneously measure oil consumption, blowby, and in-cylinder variables such as piston land pressures, cylinder pressure, and liner temperatures. The experimental setup is presented in *Chapter 2*, though this thesis will rely more heavily upon the analytical models rather than the data accrued prior to the cessation of engine operation.

Chapter 3 illustrates the results of the simulation codes developed at MIT when they were applied to the piston ring packs to be tested. The models were valuable in evaluating the driving forces for oil's transport through the ring pack and its subsequent consumption. Such information given by the programs show the ring dynamics, the gas flow through the ring pack, the different operating pressures in the cycle for the given steady state conditions, and the mass flow rates of the gases at various locations in the ring pack system. These output data are coupled with real time oil consumption measurements recorded under similar operating conditions.

In *Chapter 4*, the effects of the different piston ring pack designs on the total engine oil consumption is characterized and quantified at different steady state speed and load conditions. Where possible, the oil consumption data accrued for steady state operation of the engine were analyzed and compared to the model results in the attempt to explain the observed trends. The effects of a 2nd Land V-Cut design change are noted, as well as the use of a 3rd land chamfer. Additionally, the use of three different types of oil control rings are discussed for their effects on oil consumption as well as the effect of the OCR groove drain holes. Recommendations are

made for future research to be conducted once the engine is repaired. Future real time oil consumption measurements, for both steady state and transient conditions are in order to complete the picture of the oil transport discussed in this thesis.

Chapter 5 draws together some basic conclusions from the results presented in *Chapters 3* and *4*.

(This page was intentionally left blank)

Chapter 2: Experimental Setup

2.1 Experimental Objectives

As with all experiments conducted, a clear and concise format that follows both the scientific method and logic must be undertaken. The choices made regarding to equipment and test methods are critical in performing a successful experiment with meaningful results. This section present the experimental methodology.

As described earlier in *Section 1.3*, oil transport through the piston ring pack system is governed by a number of sources, namely the presence of oil on the ring-liner interface, ring pack dynamics, and gas flow through the system. All of these sources of oil transport, and, consequently, oil consumption, vary based upon engine operating conditions and, more importantly, ring pack and piston design. In order for these governing forces to be predicted using computer models developed at MIT (see *Section 3*), a list of physical parameters of normal engine operation are required. These parameters include in-cylinder pressure traces, land pressure traces, the geometry of the ring pack, and liner temperature at varying locations. The importance of the liner temperature and its effect on oil consumption and oil evaporation has been discussed previously in [7].

Oil consumption variation for identical engine designs at the same operating conditions is most likely caused by the variations in oil transport inside the piston-ring-pack. Therefore, in order to fully understand the aforementioned mechanisms of oil consumption, it is imperative that real-time oil consumption measurements are conducted simultaneously with measurements of the physical parameters mentioned earlier that play a major role in oil transport. Fortunately, a robust measurement system for acquiring such data was previously constructed and thoroughly tested for plausibility and repeatability. This system fulfilled the requirements of the following experimental objectives:

1) Real-time oil consumption during engine operation
2) Blowby measurements
3) Measurements of physical in-cylinder parameters affected by ring-pack design, including:

- Land and cylinder pressures
- Cylinder liner temperature

Once fulfilled, these experimental objectives will give a better understanding of the role of ring pack design on oil transport and the mechanisms governing oil consumption. It is from these results that comparisons are made to the aforementioned computer simulations, providing a more concrete basis to make such conclusions of the mechanisms and factors affecting oil transport. Unfortunately, the system built and described below is currently not operational due to a malfunction that occurred during data acquisition. As such, conclusions will be limited and the data actually gathered is far less than originally anticipated.

2.2 Experiment Equipment

2.2.1 Test Engine: Type and Modification

The central piece of equipment, without which there would be no experiment, was the test engine. The motor was a typical four-cylinder production spark ignition engine with many modern design features, such as 16 valves and port fuel injection, but lacked some of the more advanced subsystems present in engines today, such as variable valve timing or cam phasing. The properties of this engine are displayed in *Table 2-1* below:

Engine Manufacturer	Peugeot Société Anonyme (PSA)
Production Year	1997
Engine Code & Type	Code: XU10J4R/L; Type: RFV
Fuel Delivery	Port Fuel Injection
Ignition Type	Spark Ignition
Boost Type	Naturally Aspirated
Number of Valves	16
Number of Cylinders	4
Displacement	2.01L
Bore	86.25mm
Stroke	86.00mm
Maximum Power	97.4kW @ 5500RPM
Maximum Torque	180N-m @ 4200RPM
Compression Ratio	10.4:1

Table 2-1 - Test engine characteristics courtesy of Peugeot Société Anonyme (PSA). Ref. [7] and [37]

Prior to the current experiment, the test engine was modified and fitted with various measuring instruments and control devices in order to better govern the engine's operating

conditions and measure the effects of the changing physical parameters on oil consumption. Since this is a production engine, the engine's factory computer, which controls the numerous sensors that monitor the engine autonomously, was left unmodified in order to ensure operation as close to production specifications as possible.

The cylinder head was modified to fit pressure transducers in the third and fourth cylinder, though cylinder pressure traces were only taken in the third cylinder in order to better correlate the in-cylinder pressure and land pressures measured with those generated from the computer models. Additionally, the engine block and liner of the third cylinder were machined to allow the installation of pressure transducers, thermocouples, and silica windows for optical access to the piston-liner interface for oil film thickness measurements. However, during the course of the experiment, only the liner pressure transducers and thermocouples were used for measurement. These in-cylinder measuring devices penetrated the water jacket that surrounded the cylinder liner. The problems and precautionary steps that arose with their use were addressed previously by Yilmaz, et al. [7], and did not present a problem during the course of the experiment, operating as planned and desired.

As was executed in previous experiments with the current engine, the thermostat was removed in order to control the coolant temperature of the engine externally. In place of a radiator, a large (approximately 30L capacity) coolant tank was used to both store the coolant and act as a source of flow into the engine much like a radiator. In place of the radiator fins and fan that are normally present to cool the coolant prior to reentry into the engine, a shell-and-tube heat exchanger was used (See *Table B-1* for heat exchanger specifications). The cooling fluid was city water pumped into the feed line at a pressure of approximately 60psi, and its flow rate was controlled by a regulating valve that could be adjusted to the desired temperature (this can be done by adjusting the spring valve's adjustment screw) (See *Table B-2*). The heat capacity of the additional coolant slowed the engine's thermal response to changes in the operating conditions, which is important in the control of liner temperature and, consequently, oil evaporation.

In addition to coolant temperature control, the oil and inlet fuel temperature were also regulated. The inlet fuel was fed through a single-pass cross flow heat exchanger with city water again as the cooling fluid, keeping the fuel in most operating conditions at a temperature less than or equal to 35°C (it reached this temperature during high load and speed operations that

generated excessive heat from the engine). The oil was cooled using a shell-and-tube heat exchanger much like the coolant system, but on a much smaller scale (See *Table B-3*). The oil pan was modified to accommodate this external cooling system, where fittings were previously made in order to pump oil into and out of the sump using an external pump driven by an electric motor connected to a solenoid (See *Appendix B*). The temperature controlled solenoid monitored the pressurized oil temperature (the oil that was pumped up the engine from the pan due to the chain driven oil pump) and grounded the motor to complete the circuit when the pressurized oil temperature exceeded a pre-set value (for the experiment, this value was kept at approximately 95°C). The heat exchanger pump would pump the oil from the sump into the heat exchanger where city water cooled the oil and then back into the pan. This oil cooling system minimized the effects of viscosity changes on oil consumption, prevented oil thermal decomposition and, consequently, prolonged the life of the engine. *Appendix A* gives the layout for the entire experimental setup and better illustrates this system.

2.2.2 Components for Measuring Oil Consumption

2.2.2.1 Different Methods for Measuring Oil Consumption

Typical oil consumption rates of modern passenger car engines are on the order of 10 $^{g}/_{hr}$. In the past, this small amount was a problem to researchers in the automotive industry attempting to monitor the oil consumption of an engine. Presently, however, a number of new methods exist for monitoring the minute oil consumption of an engine, the most popular being those that are real-time (the delay, if any, between the reading and the actual oil consumption is small). This competes against an older method of weighing the amount of oil present before and after running (in some cases, the amount can be weighed continuously during the experiment), requiring hours of operation to get an appreciable amount. Interference from fuel dilution and combustion by-products entering the oil due to blowby make less desirable when compared to more accurate real-time methods.

Real-time oil consumption measuring techniques currently involve using a tracer or mass spectrometry to analyze the exhaust gasses during operation. Two tracer systems are currently employed: radioactive and sulfur. The radioactive tracer system measures oil consumption by adding radioactive tracers (typically tritium) into the oil and measuring the concentration of the tracer in the exhaust gases. The measurement times of these methods are on the order of several

minutes (not hours as seen with weighing the amount of oil in the engine), but the handling of the radioactive material requires special equipment and procedures.

The other tracer technique mentioned earlier is the sulfur trace method, where sulfur acts as the tracer in the oil rather than radioactive material. This requires the use of high sulfur oil and low sulfur fuel such that, when the composition of the exhaust gas is analyzed, the concentration of sulfur present will be from the contribution of oil being consumed. Researchers in the automotive industry have successfully demonstrated the capability of the sulfur tracer technique to measure oil consumption during steady state and transient operating conditions [6][7][14][15][20][35]. Due to the system's extensive use in the industry, as well as previously with the current engine setup, the sulfur tracer system was implemented on the test engine to measure engine oil consumption. The specific requirements of the oil and fuel properties necessary to apply the sulfur tracer technique are described in *Sections 2.2.2.2* and *2.2.2.3*, respectively.

2.2.2.2 High Sulfur Oil

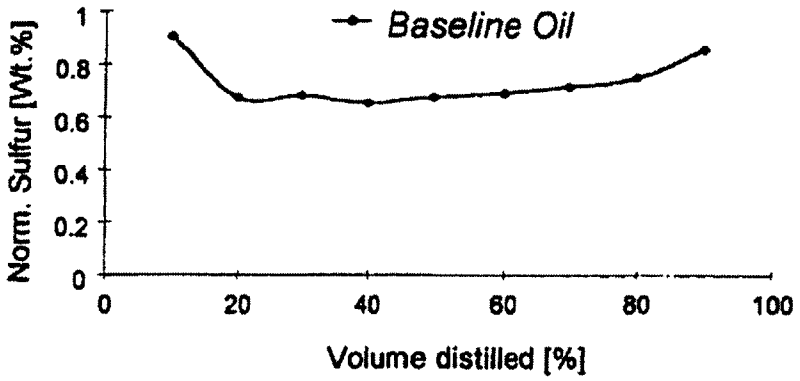

Figure 2-1 – Sulfur content present in the baseline oil during distillation according to both ASTM D5236 and ASTM D 4294 standard tests. (Source – Lubrizol Corporation, reprinted from [7])

Due to past research conducted by [7], oil with a sulfur concentration of 1.5% [wt.] was used. As was previously deduced and noted, since oil transport into the combustion chamber is in liquid and vapor form (evaporated oil), a consistent sulfur concentration in the oil is required throughout the oil distillation curve in order to assume that the consumed oil (in liquid and vapor form) in the exhaust has the same concentration of sulfur as in the original oil. For this reason,

oil created by Lubrizol Corp. was used throughout the experiment in order to better compare the results to previous research. The relevant oil properties of the Lubrizol oil are shown in *Figure 2-1* and *Table 2-2*.

High-Sulfur Baseline (Mineral) Oil Properties		Test Method
SAE Viscosity Grade	10W-30	
Sulfur [wt. %]	1.51	ASTM D 1552
Volatility: GCD % off @ 371° C	11.6	
Noack	16.8	ASTM D 5800
Kinematic Viscosity @ 100° C [mm²/s]	10.77	ASTM D 445
HTHS viscosity [cP]	3.04	ASTM D 4683

Table 2-2 – Properties of baseline oil used throughout the experiment. Created and provided by Lubrizol Corporation. (Source – Lubrizol Corp. Mineral Oil Data Sheet, and redrawn from [7])

2.2.2.3 Low Sulfur Fuel

As stated earlier, the sulfur trace method analyzes the amount of sulfur present in the exhaust gasses. Therefore, to properly measure the amount of oil consumed, it is imperative that other sources of sulfur are minimized or, better still, eliminated. There are two other sources of sulfur that could alter the amount of sulfur present in the exhaust gas: air and fuel. As will be noted later, air contributes little sulfur, if at all, to the combustion products. However, most common gasoline that is purchased at the pump has a sulfur concentration high enough to create erroneous results when the exhaust stream is analyzed. To negate this effect, a special blend of low-sulfur research gasoline was created by and purchased from Chevron Phillips Chemical Company LP that contained a sulfur concentration below 2 ppm [wt.]. Similar to previous research by Yilmaz [7], this fuel provided little to no contribution to the sulfur levels in the exhaust and, as was found later on in the experiment, was a much cheaper alternative to other low-sulfur fuels such as pure grade isooctane. *Table 2-3* below depicts the properties of one of the drums of the gasoline used, while a more detailed example of a data sheet is provided in *Appendix C*.

Low-Sulfur Gasoline Properties		Test Method
Specific Gravity 60/60	0.7397	ASTM D 4052
API Gravity	59.8	ASTM D 1250
Sulfur [ppm, wt.]	0.9	ASTM D 5453
Reid Vapor Pressure [psi]	8.3	ASTM D 5191
Hydrogen [wt. %]	13.9	ASTM D 5291
Carbon [wt. %]	86.1	ASTM D 5291
Research Octane Number	90.4	ASTM D 2699
Motor Octane Number	84.6	ASTM D 2700

Table 2-3 - Properties of one drum of low-sulfur gasoline used in the experiment. Created and provided by Chevron Phillips Chemical Company LP. (Source – Chevron Phillips Chemical Company No-Sulfur Gasoline Certificate of Analysis Sheet)

Each drum delivered had a different concentration of sulfur, hydrogen, and carbon, which were all corrected for in the data acquisition program as will be explained in *Sections 2.2.2.7* and *2.2.2.8*. In total, approximately 8 drums of gasoline were to be used over the course of the experiment. All fell within the requirements of having low sulfur concentration ($\leq$2ppm) and a Reid vapor pressure between 7.0-9.0 psi (similar to that of commercially available gasoline).

2.2.2.4 Exhaust Sampling System

To properly measure the oil consumption, as stated previously, the sulfur trace method requires sampling of the exhaust gases of the engine. This was the first phase in the oil consumption measurement process, with the other phases being, in natural chronological progression, the SO_2 Analyzer and the computer data acquisition system. As stated earlier, *Appendix A* provides a clear layout of all the components discussed here.

There were two main components of the exhaust sampling system: the sample runners and the common sample rail. The sample runners were a set of four stainless steel (Grade 314, $^1/_4$" OD, 0.175" ID) tubing that are connected to taps in the exhaust manifold, one sample runner per tap and one tap per exhaust runner. It's important to note that the taps were placed close enough to the exhaust ports so as to obtain a representative sample of the undiluted exhaust stream. Placed to far away, and the sample's individual composition will mix with the composition of the other exhaust runners due to pressure fluctuations inherent to the exhaust manifold. Placed too close, and the tap runs the risk of creating a stress concentration near the manifold-cylinder head interface, causing a crack to develop in the runner due to vibrations of the engine. This would dilute the sample, giving erroneous readings. For each runner, a needle valve was installed to allow individual sampling of the cylinders. All four sample runners coalesce to a junction where they funnel into the common sample rail. It is this tube, also cut

from stainless steel (Grade 314, $^1/_4$" OD, 0.175" ID) tubing, that carries the test exhaust stream to the analyzer for measurement retrieval. Since the oil consumption measurement of individual cylinders was made possible, the sample runners and common sample rail were made short enough to prevent real-time measurement delay, but long enough to be connected to the analyzer in its safe position and dampen out pressure oscillations that would occur due to individual cylinder cycles. In total, the test exhaust stream would have to travel approximately 6 feet from tap to analyzer entrance.

Stainless steel (Grade 314) was chosen for sample runners for two reasons: 1) exceptional corrosion resistance to both sulfur/SO_2 (a byproduct of combustion with sulfur present); and 2) though Teflon has better corrosion properties when exposed to sulfur/SO_2, stainless steel is able to withstand the high temperatures of spark ignition exhaust gases as well as maintain its physical and chemical properties at the elevated temperatures needed to prevent sulfur/SO_2 condensation. This leads to an important variable in the design of the sampling system: the runner and line temperature. The hot exhaust gases, along with the particulates present in the stream, come in contact with the cold wall of the sampling system. If the temperature of the wall is low enough, the particulates may accumulate and clog the sample line (a phenomenon known as thermophoresis), or the sulfur/SO_2, along with other unburned hydrocarbons, can condense and not be detected by the analyzer. Either situation, or a combination of both, would give flawed and inconsistent values for the oil consumption measurement. To prevent this, as was done in past experiments, copper dust impregnated fiberglass tape (also known as copper header wrap) by Cool It Thermo Tec was placed around the sample runners, while rope heater (*Table B-6*), was wrapped around the common sample rail underneath a layer of the aforementioned copper header wrap. The fiberglass helped insulate the walls of the tubing to prevent any condensation and thermophoresis, while the addition of a rope heater ensured that the exhaust gases entered the analyzer at an elevated temperature to prevent any condensation and dilution whatsoever. Over the course of the experiment, the common sample rail internal gas temperature (and therefore, the inner wall temperature of the tube) was maintained at approximately 300°C.

2.2.2.5 SO_2 Analyzer

Once the exhaust stream entered the sampling system, the gases were then drawn into the second phase of the measurement process, the Antek® Sulfur-Analyzer (Model R6000 SE),

where the sulfur concentration in the exhaust gas sample is detected. *Figure C-3* illustrates the components of the analyzer in detail as given by Antek® Instruments, Inc. in their service manual. The instrument was designed as a flow through analyzer, outputting a continuously varying signal as the sample stream through it, giving a real-time value. Additionally, because it is a flow-through analyzer, volumetric flow rate is important; variations in such would cause variations in the output measurement value.

As can be seen in *Figure C-3*, the sample gas is pulled the first pyrotube by a bellows pump. This furnace will assist in the conditioning of the sample stream by combusting any particulates in the gas prior to entering the second pyrotube. Both the first and second furnace operate at a temperature of about 1000°C to properly catalyze the process needed. Some of the sulfur in the first furnace may be converted to SO_2, so the bellows pump is heated to approximately 120°C to minimize the retention of SO_2 by the cold stainless steel within the pump. After the pump, the stream's flow is regulated to remain constant by a fixed restriction transfer tube and a back pressure regulator. The restrictor tube carries a set amount of flow while the back pressure regulator vents excess gas from the stream. It was important that throughout the experiment that the back pressure regulator was kept at a value of about 7psi. In combination, these two provide a constant flow rate of sample gas to the second pyrotube. Oxygen is fed into the second furnace to convert the sample's constituents that weren't converted in the first furnace. Sulfur is converted to SO_2, nitrogen into NO, and any hydrocarbons into CO_2 and water. The water is removed from the stream by two membrane dryers prior to the addition of ozone. The ozone converts the NO to NO_2 to eliminate the interference of NO in the sulfur analysis. According to the manual, approximately 100ppm of NO is detected as 1ppm of SO_2. The stream then enters the sulfur fluorescence chamber where UV light is emitted, causing the SO_2 to emit light. This light is then picked up by the photomultiplier (PM) tube. The PM tube converts the intensity of this radiation into a voltage value that is linearly proportional to the concentration of SO_2 in the stream. This value is displayed on a detector interface module. The linear relationship is found through calibration, where a zero gas is fed through the sample line (usually ambient air) a zero point and a span gas of known SO_2 concentration is fed in as the upper bound (usually adjusted to a value of 10V). Thus the machine was calibrated prior to every daily run in order to adjust the linearity for the day's current ambient conditions [40].

2.2.2.6 Air Flow Meter and Lambda Meter

The third phase involves data acquisition. This first involves recording the voltage value obtained in phase two from the analyzer and the air and fuel flow rates into the engine. The air flow rate was measured with the use of a laminar flow element. This element provides a region through which the air must flow on its course to the intake manifold. This laminar flow region is calibrated by the manufacture (Meriam Instrument) to correspond to a calibration curve that is dependent on the pressure drop across the region and the temperature of the air stream. Both of these variables are used to create correction factors from the standard conditions that the element was calibrated in (namely 70°F and 29.92"Hg = 760mmHG). More specifications are shown in *Table B-7*. These values were sent to the LabView data acquisition system for processing in order to give an air flow rate. The calculations for the LabView code are reprinted below for clarity and were taken from [39]. The input flow rate from the flow element must be corrected based upon differences due to temperature, pressure, and viscosity variation. First, the air temperature and viscosity correction factor and the pressure correction factor:

$$TVCF = 0.00002T_{air}^2 - 0.007T_{air} + 1.1368 \qquad \textbf{(2.1)}$$

$$PCF = \frac{P_{flow}}{760} \qquad \textbf{(2.2)}$$

where T_{air} is the inlet air temperature to the flow element in units of Celsius and P_{flow} is the atmospheric pressure, and consequently the inlet air pressure, at the time of the experiment in units of mmHg. The value of P_{flow} was updated daily with the aid of a Mercury filled barometer in order to get accurate measurement readings and to account for atmospheric changes that would occur due to local temperature and weather conditions. Given the correction factors above, the standard volumetric flow rate in units of ft^3/min is given by *Equation 2.3*:

$$Q_{a,STD} = TVCF \cdot PCF \cdot Q_a \qquad \textbf{(2.3)}$$

where Q_a is the volumetric flow rate as read by the laminar flow element into the data acquisition system and $Q_{a,STD}$ is the standard volumetric flow rate as defined by the given conditions of 70°F and 1atm. Given that the density of air at the standard conditions mentioned is $\rho_{a,STD}$ = 1.19978062733 $^{g}/_{L}$, we get the following two equations:

$$Q_{a,LPS} = \frac{28.316846592\text{L}}{1ft^3} \cdot \frac{1\text{min}}{60\text{sec}} \cdot Q_{a,STD} \qquad \textbf{(2.4)}$$

$$\dot{m}_a = \rho_{a,STD} \cdot Q_{a,LPS} \qquad (2.5)$$

where $Q_{a,LPS}$ is the volumetric flow rate or air in units of $^{L}/_{s}$, while $\dot{m}_a$ is the air mass flow rate in units of $^{g}/_{s}$.

A lambda meter was used in conjunction with the air flow rate to calculate the fuel flow rate. The lambda meter reads the output voltage from an oxygen/UEGO sensor located in the exhaust and gives a corresponding air/fuel ratio value relative to the stoichiometric air/fuel ratio. The calculation of lambda and the stoichiometric air/fuel ratio is given by *Equations 2.6* and *2.8*, respectively.

$$\lambda = \frac{(A/F)_{actual}}{(A/F)_{st}} \quad (2.6) \qquad (A/F)_{actual} = \frac{\dot{m}_a}{\dot{m}_f} \quad (2.7) \qquad (A/F)_{st} = \frac{138.24768(1+0.25y)}{12.011+1.008y} \quad (2.8)$$

where $(A/F)_{st}$ is the stoichiometric air/fuel ratio, $(A/F)_{actual}$ is the actual air/fuel ratio, λ is given by the Lambda Meter, $\dot{m}_a$ is the mass flow rate of air into the engine, $\dot{m}_f$ is the mass flow rate of fuel injected into the engine, and y is the hydrogen to carbon ratio of the fuel on a wt% basis [2]. Using the air flow rate calculated from *Equation 2.5*, *Equations 2.6-2.8* above, and the HCR ratio given by the fuel's data sheet, the fuel flow rate was calculated using *Equation 2.9*.

$$\dot{m}_f = \frac{\dot{m}_a}{(A/F)_{actual}} = \frac{\dot{m}_a}{\lambda(A/F)_{st}} = \frac{\dot{m}_a(12.011+1.008y)}{138.24768\lambda(1+0.25y)} \qquad (2.9)$$

2.2.2.7 LabView Data Acquisition System

As shown in *Appendix A*, the final step of the oil consumption measurement process is the data acquisition system. This system uses a typical desktop computer with a DAQ-MX PCI card and LabView Version 7.1 installed in order to acquire the data and record it, respectively. A data acquisition program was written in LabView to record raw data, calculate and record the oil consumption rate in two forms ($^{g}/_{hr}$ and $^{\mu g}/_{cyl\text{-}cycle}$ as described below), calculate and record the corrected air and blowby volumetric flow rate, and display the aforementioned items in LabView's front control panel during the engine's operation. These other parameters include approximately 15 different temperature readings, five different pressure values, the engine speed, the lambda meter reading, the amount of fuel consumed, the value of the sulfur analyzer's voltage output, three different flow rates, a saving control setup, and six different input values

that are essential to the oil consumption calculation process as described below. Since the real-time oil consumption was visually displayed, the program was a good indicator for the validity of the test, providing warning if any of the equipment needed to be recalibrated or if intervention was needed during the experiment. This improved the speed at which data was accrued over the course of the experiment. The program alerted the operator to the engine's impending self-destruction during a test run; soon after which the engine failed and is currently inoperable.

When transient testing became a central issue to ring pack performance in the normal driving cycle of an automobile engine, the original program was modified to not only record the aforementioned information, but also to control the intake manifold pressure and the speed of the engine. This was advantageous for two reasons: 1) each oil consumption data run (typically lasting 30 minutes) soon became automated, providing consistency in terms of intake manifold pressure, speed, and the amount of time held at each operating condition; 2) with the addition of a user interface that required the input for manifold pressure and/or speed, throttle hystersis, throttle movement speed, and the duration held at each operating point, the change to a different transient was made possible in a matter of seconds as well as the effects of transient variation on oil consumption. Thus, transient variation over the course of a run was made more efficient and consistent, isolating the ring pack's effect on oil transport.

Both LabView control panels, steady state and transient, can be found in *Appendix E*, along with their accompanying code. It's important to note that due to the limited number of output channels from the LabView SCXI breakout box, the updated program could only operate speed transients or load transients for a given test period. This is noted by the tabbed variations shown and the different case conditions of the program code. In the end, this was more valuable as a safety precaution than a nuisance due to the sensitivity of the system to changes in operation.

2.2.2.8 Oil Consumption Formula

The core of the LabView program described above is the oil consumption formula used in the calculation of the ring pack's performance under various operating conditions. The equations derived make use of the measured SO_2 concentration in the exhaust, the airflow rate, the lambda value, the hydrogen to carbon ratio (HCR or y as defined earlier) of the fuel, and the mass fractions of sulfur in the oil, fuel, air and the span gas used in calibration. The assumptions made when deriving the formula are described below.

First, the amount of sulfur from the oil consumed by the engine can be calculated with the use of mass conservation in *Equation 2.10* below:

$$\dot{m}_{S,Oil} = \dot{m}_{S,WetExhaust} - \dot{m}_{S,Fuel} - \dot{m}_{S,Air} \quad \textbf{(2.10)}$$

where $\dot{m}_{S,Oil}$, $\dot{m}_{S,WetExhaust}$, $\dot{m}_{S,Fuel}$, and $\dot{m}_{S,Air}$ are the mass flow rates of sulfur in the oil, wet exhaust gas, fuel, and air, respectively. Since the sulfur content of air is on the order of 10ppb, it was assumed during the experiment that $\dot{m}_{S,Air} = 0$, and:

$$\dot{m}_{S,Oil} = \dot{m}_{Oil} \bullet W_{S,Oil} \quad \textbf{(2.11)} \qquad \dot{m}_{S,Fuel} = \dot{m}_{Fuel} \bullet W_{S,Fuel} \quad \textbf{(2.12)}$$

$$\dot{m}_{S,WetExhaust} = \dot{m}_{WetExhaust} \bullet W_{S,WetExhaust} \quad \textbf{(2.13)}$$

where $W_{S,Oil}$, $W_{S,Fuel}$, $W_{S,WetExhaust}$ and are the mass fractions of sulfur in the oil, fuel, and wet exhaust, respectively. Likewise, $\dot{m}_{Oil}$, $\dot{m}_{Fuel}$, $\dot{m}_{WetExhaust}$ are the mass flow rates of the oil, fuel, and wet exhaust, respectively. Substituting *Equations 2.11-13* into *Equation 2.10* above gives:

$$\dot{m}_{Oil} = \frac{1}{W_{S,Oil}}(\dot{m}_{WetExhaust} W_{S,WetExhaust} - \dot{m}_{Fuel} W_{S,Fuel}) \quad \textbf{(2.14)}$$

Now, given *Equation 2.9*, relating the air mass flow rate to the fuel mass flow rate, and mass conservation, we get:

$$\dot{m}_{WetExhaust} = \dot{m}_{Air} + \dot{m}_{Fuel} + \dot{m}_{Oil} \approx \dot{m}_{Air} + \dot{m}_{Fuel} = \dot{m}_{Air}\left(1 + \frac{1}{\lambda(A/F)_{st}}\right) \quad \textbf{(2.15)}$$

where it is assumed that the mass flow rate of the oil is small compared to the mass flow rate of both the air and fuel. The mass fraction of sulfur in the wet exhaust can be given as:

$$W_{S,WetExhaust} = X_{S,WetExhaust} \bullet \frac{M_S}{M_{WetExhaust}} \quad \textbf{(2.16)}$$

where $X_{S,WetExhaust}$ is the molar concentration of sulfur in the wet exhaust gas, and M_S and $M_{WetExhaust}$ are the molecular weights of sulfur (given as $32^{g}/_{mol}$) and the wet exhaust gas, respectively. Since the Antek analyzer converts all the sulfur in the exhaust gas into SO_2 and removes all of the water in the stream, we get:

$$X_{S,WetExhaust} = X_{SO_2,WetExhaust} \quad \textbf{(2.17)} \qquad X_{SO_2,WetExhaust} = X_{SO_2,DryExhaust} \bullet (1 - X_{H_2O}) \quad \textbf{(2.18)}$$

where $X_{SO_2,WetExhaust}$ and $X_{SO_2,DryExhaust}$ are the molar concentrations of SO_2 in the wet and dry exhaust gas, respectively, while X_{H_2O} is the molar concentration of water in the exhaust gas.

Thus substituting *Equations 2.15-18* into *Equation 2.14*, gives the following oil consumption formula below:

$$\dot{m}_{Oil} = \frac{\dot{m}_{Air}}{W_{S,Oil} \bullet \lambda \bullet (A/F)_{st}} \left[\left(\left\{ \lambda (A/F)_{st} + 1 \right\} \bullet \frac{M_S}{M_{WetExhaust}} \bullet X_{SO_2,DryExhaust} \bullet \{1 - X_{H_2O}\} \right) - W_{S,Fuel} \right] \quad \textbf{(2.19)}$$

To calculate the molecular weight of the wet exhaust gas and its molar fraction of water present, ideal, complete combustion is assumed and the water present in ambient air as well as lesser constituents are ignored. Therefore, the two cases for the calculations based solely on the relative air/fuel ratio, λ, are:

Case 1 (λ<1):

$$CH_y + \lambda\left(1+\frac{y}{4}\right)(O_2 + 3.773N_2) \rightarrow \lambda CO_2 + \frac{y}{2}\lambda H_2O + 3.773\lambda\left(1+\frac{y}{4}\right)N_2 + (1-\lambda)CH_y \quad \textbf{(2.20a)}$$

$$M_{WetExhaust} = \frac{\lambda M_{CO_2} + \frac{y}{2}\lambda M_{H_2O} + 3.773\lambda\left(1+\frac{y}{4}\right)M_{N_2} + (1-\lambda)M_{CH_y}}{1+\lambda(3.773+1.44325y)} \quad \textbf{(2.21a)}$$

$$X_{H_2O} = \frac{\frac{y}{2}\lambda}{1+\lambda(3.773+1.44325y)} \quad \textbf{(2.22a)}$$

Case 2 (λ>1):

$$CH_y + \lambda\left(1+\frac{y}{4}\right)(O_2 + 3.773N_2) \rightarrow CO_2 + \frac{y}{2}H_2O + 3.773\lambda\left(1+\frac{y}{4}\right)N_2 + (\lambda-1)\left(1+\frac{y}{4}\right)O_2 \quad \textbf{(2.20b)}$$

$$M_{WetExhaust} = \frac{M_{CO_2} + \frac{y}{2}M_{H_2O} + 3.773\lambda\left(1+\frac{y}{4}\right)M_{N_2} + (\lambda-1)\left(1+\frac{y}{4}\right)M_{O_2}}{\frac{y}{4} + 4.773\lambda\left(1+\frac{y}{4}\right)} \quad \textbf{(2.21b)}$$

$$X_{H_2O} = \frac{\frac{y}{2}}{\frac{y}{4} + 4.773\lambda\left(1+\frac{y}{4}\right)} \quad \textbf{(2.22b)}$$

where M_{CO_2}, M_{H_2O}, M_{N_2}, and M_{O_2} are the molecular weights of CO_2, H_2O, N_2, and O_2, respectively, and y was defined earlier in *Section 2.2.2.6* as the hydrogen to carbon ratio of the

fuel. The last step in the oil consumption calculation process involves acquiring the value of $X_{SO_2,DryExhaust}$ with the aid of the Antek analyzer and the following equation below:

$$X_{SO_2,DryExhaust} = X_{SO_2,Span} \frac{V_{Measured}}{V_{Span}} \tag{2.23}$$

where $X_{SO_2,Span}$ is the molar concentration of SO_2 in the span gas used to calibrate the machine, V_{Span} is the voltage reading from the analyzer for the aforementioned span gas concentration, and $V_{Measured}$ is the voltage reading from the analyzer for the current SO_2 concentration in the exhaust stream passing through.

2.2.3 Blowby

Blowby is defined as the leakage of combustion gases through the ring pack system, consisting of the piston-ring-liner interface, into the crankcase. Blowby gases are composed of burned and unburned combustion gases, and lubricating oil. Blowby gases are generally fed into the intake manifold by a positive crankcase ventilation (PCV) system to prevent their emission into the atmosphere. However, as was discussed in [7], it was imperative that the blowby gases did not affect the readings of the analyzer by adding to the amount of oil present in the combustion chamber, and, hence, the exhaust gases. This was accomplished by routing the blowby gases from the PCV system through a blowby flow meter and into the exhaust trench. The blowby meter was based on the Von Kármán-vortex shedding principle. Its details are summarized in *Table 2-4* below. The results of Yilmaz's work noted that the influence of blowby on oil consumption is minimal, though its effects are still noticeable: blowby recirculation increased the oil consumption readings slightly when compared with non-recirculation. The end result: oil entrainment from blowby gas flow has negligible impact on oil consumption.

Blowby Meter	
Manufacturer	ECM
Model No.	BB100
Output (Linearised)	0-5V (Rate); 0.5-4.5V (Total)
Flow Rate Range	4-150LPM (0.15-0.54CFM)
Flow Total	1000L (Total), 100.0ft^3 (Total)
Accuracy	1% of reading
Repeatability	0.5% of reading

Table 2-4 – Blowby flow meter that was to be used for the experiment.

Blowby is a pulsating flow where there are periods of flow reversal, though the average flow rate is out of the crankcase. This oscillating flow is mainly caused by volume changes in the crankcase due to the kinematics of the crankshaft. The volume displaced by a descending piston corresponds to the swept volume of an ascending piston only when they are traveling in opposite directions. However, at mid stroke, the total crankcase volume is decreased to a minimum. *Figure 2-2* below shows the estimated volume fluctuation for the test engine during one engine cycle (four strokes). The average volume inside the crankcase is on the order of several liters, with the variation of the crankcase volume decreasing on the order of 0.1L during one stroke. This variation generates pressure fluctuations and high gas flows inside the crankcase. These pressure waves may generate flow pulsations in the ventilation system, creating flow values that can be higher than the actual average blowby flow. The flow pulsation frequency is twice the frequency of the crankshaft and, therefore, dependent on engine speed.

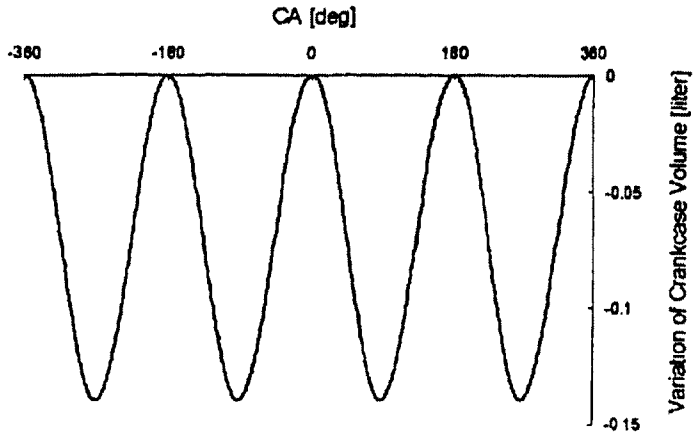

Figure 2-2: Variation of the crankcase volume during one engine cycle. Reprinted from [7].

The blowby meter was setup to measure flows only in one direction. If the meter were installed without any modifications into the blowby flow path, the flow meter may indicate higher flow rates than actual due to these flow reversals. To remedy this problem, a system was installed upstream of the meter that had two purposes: 1) to dampen the flow fluctuations to the meter; 2) to allow the expansion of the gases to precipitate out any water present. It was found that, after a full day of testing, water left in the blowby meter would condense out. This water, in liquid form, would cause the meter to give erroneous readings the next time the engine was run if the meter wasn't drained prior to testing. As compared with previous tests done by Yilmaz, this dampening/water-separation system proved more than adequate for this application.

For ease of comparison to other data and validity of the ring pack's performance, the value given by the blowby meter was converted to the volume flow rate at STP – 0°C and 1atm (1013.25mbar). To accomplish this, correction factors were created similar to those used for the air mass flow rate described earlier in *Section 2.2.2.6*. These equations are:

$$TVCF_{Blowby} = \left[0.00002T_{Blowby}^2 - 0.007T_{Blowby} + 1.1368\right] \bullet \left[\frac{273.15}{294.2611111}\right] \quad \textbf{(2.24)}$$

$$PCF_{Blowby} = \frac{P_{Blowby}}{1013.25} \quad \textbf{(2.25)}$$

$$Q_{STP,Blowby} = Q_{Blowby} \bullet PCF_{Blowby} \bullet TVCF_{Blowby} \quad \textbf{(2.26)}$$

$$\dot{m}_{STP,Blowby} = Q_{STP,Blowby} \bullet \frac{\rho_{Air,STP}}{60} \quad \textbf{(2.27)}$$

where Q_{Blowby} and $Q_{STP,Blowby}$ are the actual and standard volumetric flow rates of the blowby gases in $^{L}/_{min}$ and specific $^{L}/_{min}$, respectively. $TVCF_{Blowby}$ and PCF_{Blowby} are the temperature and viscosity correction factor and pressure correction factor, respectively. T_{Blowby} is the temperature of the entering blowby gases in °C while P_{Blowby} is the blowby gas pressure in units of mbar. Finally, $\dot{m}_{STP,Blowby}$ and $\rho_{Air,STP}$ are the air flow rate (in units of $^{g}/_{s}$) and density of air (defined for the experiment as $1.29228367^{g}/_{L}$) at STP, respectively.

2.2.4 In-Cylinder Measurements

The third cylinder (as measured by distance from the dyno) of the engine was modified in order to record the previously discussed in-cylinder measurements. Pressure transducers, thermocouple probes, and an LIF system were installed to accomplish these tasks. In previous experiments, LIF was used extensively. However, with the aid of the PSA sapphire window research engine (currently be operated by Przesmitzki [19]), this was unnecessary, and abandoned for the duration of the experiment. Piezoelectric pressure transducers were positioned along critical positions on the cylinder liner in order to give land pressure traces, while a pressure transducer was mounted in the cylinder head in order to provide cylinder pressure traces. Thermocouples were installed along the cylinder liner to measure liner temperature at two different positions. These variables proved to be valuable inputs for the computer simulations. This setup was installed previously by [7], the reasoning behind their placement mainly being accessibility to the test conductor: the LIF windows for cooler

temperatures and ease of access (on the Anti-thrust side, near the intake manifold), while the land pressure transducers and thermocouples were set and left to stand alone to provide data on the thrust-side (near the exhaust manifold). *Figure 2-3* below illustrates the positioning of these measurement probes in the third cylinder.

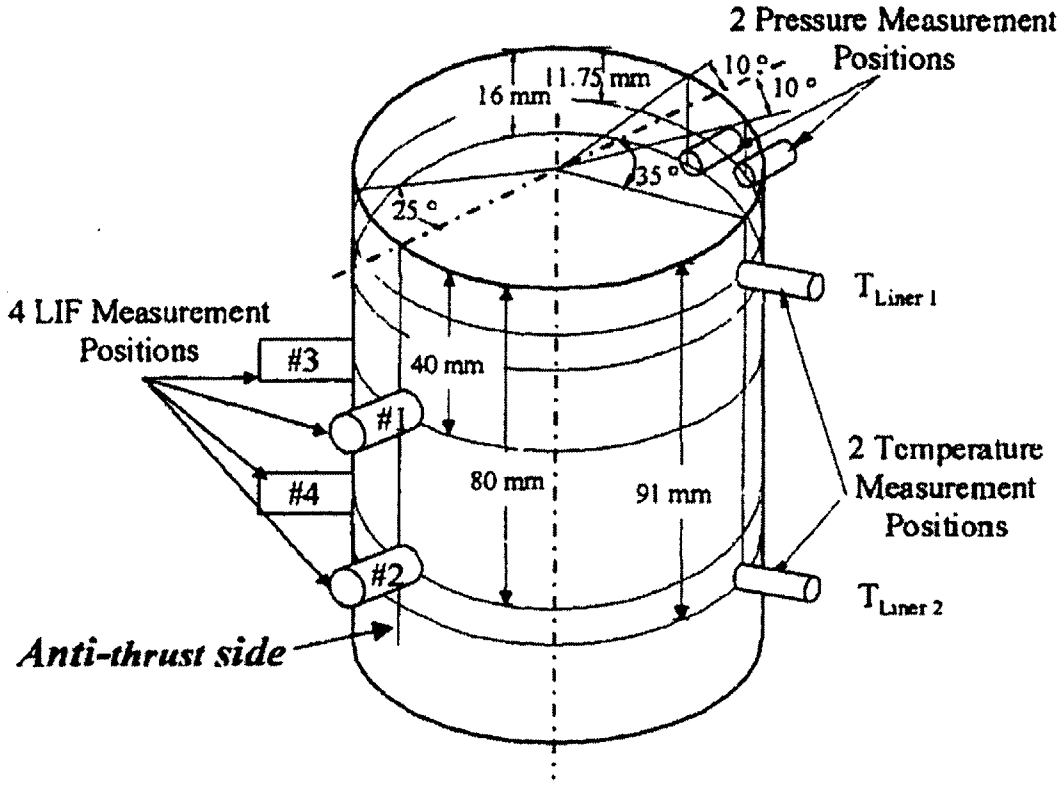

Figure 2-3: Measurement locations of in-cylinder variables in the third cylinder (as measured from the dyno). Reprinted from [7].

2.2.4.1 Cylinder and Land Pressure Measurements

The cylinder head of the engine was machined by the previous researcher to have the capability to measure cylinder pressure traces in two cylinders (cylinders 3 and 4), however only one cylinder was measured during the experiment (as stated, cylinder 3). The third-cylinder pressure measurements were taken using a water-cooled piezoelectric transducer (*Table B-10*). Additionally, the liner and engine block were previously machined at two critical locations in order to place pressure transducers that would measure inter-ring pressures. These locations ensured the measurement of inter-ring pressures for the longest possible crank angle period. One transducer is located just above the top dead center (TDC) position of the second (Napier) ring to

measure second land pressures during the period between the compression and expansion strokes when the piston reverses its direction of motion. Looking at *Figure 2-3* above, this pressure transducer was located 11.75mm below the surface of the piston crown at TDC. The other transducer was positioned lower on the liner. The axial difference between the two transducers was larger than the height of the 2nd land on the pistons used in the cylinder during the experiment.

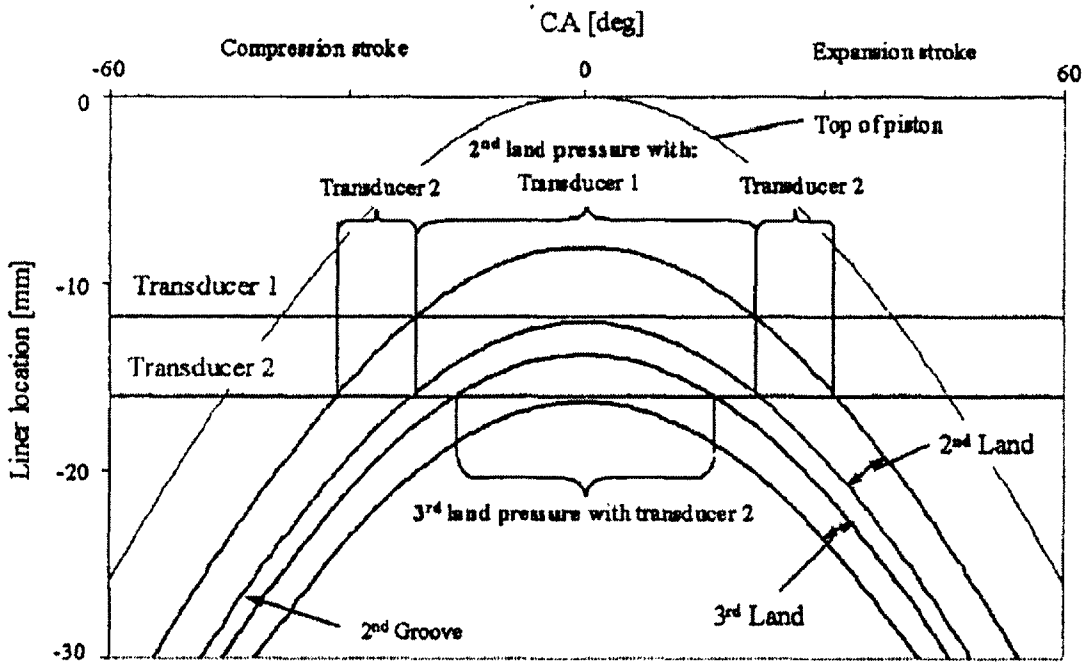

Figure 2-4 - Axial positions along the liner of different piston regions as a function of crank angle. Reprinted from [7].

This transducer arrangement allowed for the measurement of the second land pressure by the lower transducer for periods just before and after the upper transducer was exposed to the second land. During the period when the upper transducer was exposed to the second land, the lower transducer provided third land pressure measurements. Therefore, the combination of both pressure transducers provided second land and third land pressures for a period of 62°CA and 32°CA, respectively. *Figure 2-4* above depicts the axial positions of both pressure transducers on the liner and the instantaneous position of different piston regions as a function of crank angle during late compression and early exhaust strokes. The instantaneous positions of the piston regions during the exhaust and intake strokes are identical to the compression and expansion strokes, respectively.

To hold both of the pressure transducers into the engine block and seal the coolant passage from leaking both into the cylinder and out of the engine, an adapter was designed as shown by the schematic in *Figure 2-5* below. All of the measurements given are in units of millimeters.

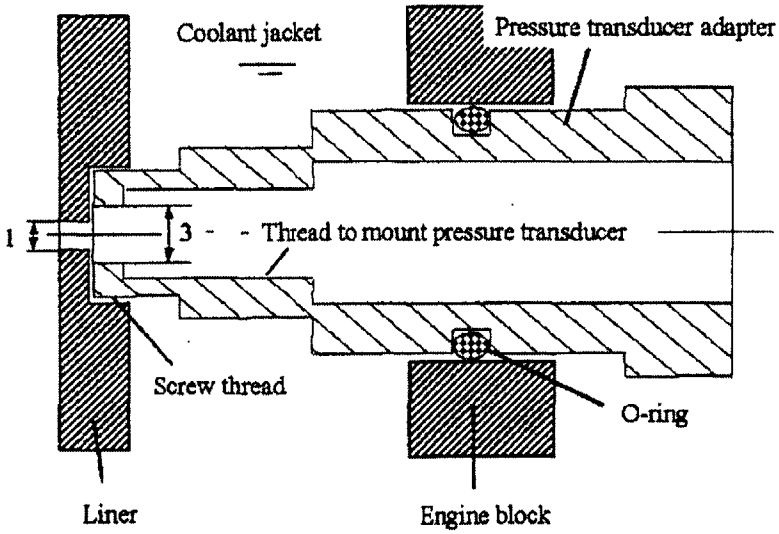

Figure 2-5 - Side view schematic of engine with mounted pressure transducer adapter. Reprinted from [7].

As was noted in previous experiments, the holes in the liner and the adapter increase the clearance volume between the liner and piston, which may alter land pressures and gas flow in the ring pack from ideal conditions. However, this additional volume was found to be negligible, since its greatest impact on the land clearance volumes was only a 3% increase.

2.2.4.2 Liner Temperature Measurements

The cylinder liner temperature is believed to influence oil evaporation and thus oil consumption, and hence is an important parameter to measure during testing and to use for the oil transport models developed at MIT. However, the liner temperature varies with engine operating condition and according to location along the liner. Therefore, as accomplished previously by Yilmaz, the liner and engine block were machined to install two fine tip transition joint thermocouples into the liner to measure the local liner temperature. The ports that thermocouples were inserted into were blind holes that placed the thermocouples within less than 1mm of the combustion side of the liner. That is, the temperature measurements accrued for their respective liner positions were nearly equal to that of the actual liner surface. The

thermocouples were located at the TDC position of the scraper/Napier ring and at the bottom dead center (BDC) position of the top ring (see *Figure 2-3* above).

2.2.5 Computer Simulations of Oil Transport

Since the engine malfunctioned, the focus of the paper switched from that of real time oil consumption behavior effects from different piston-ring pack designs to computer simulations of these designs. The computer simulations would provide insight into the type of mechanisms and the relative amounts of oil consumption that would be present with the different configurations. With the aid of RINGPACK-OC, a program developed here at the Sloan Automotive Laboratory at MIT [24][26], the ring dynamics and the gas flows through the passages considered in the piston-ring-liner system were predicted for the various ring packs to be tested. The model required a number inputs in order to run properly and effectively. These were the in-cylinder pressure trace (provided by Steve Przesmitzki), the viscosity properties of the oil (these were given earlier in *Table 2-2*), the geometry of the piston-ring-liner system, and the temperatures of both the piston and liner at various points for each operating condition analyzed (the calculations for such were previously done by Benoist Thirouard).

As will be noted later on in *Section 2.3.3*, there was some variation in the piston geometries as well as the rings themselves between the testing operations to be executed. As such, it was important to have a different data inputs for each, both in terms of the volumes present for gas flow through rings and piston as well as the different rings between the older and prototype designs. These design changes will be made clearer later on. For now, it is suffice to say that the model inputs were changed in order to better fit the piston to be tested.

2.3 Experimental Conditions

2.3.1 Engine Start-Up Procedure

It was found during the initial days of testing that, in order to assume proper engine operation and in order to make the data recording process more robust, a start-up procedure needed to be prepared, tested, and proven reliable. Such a procedure was created and proved valuable for a number of reasons. First, the hot exhaust gases produced by the procedure assisted in heating up the UEGO sensor to allow the closed loop running of the engine with its original control module. The internal heaters that normally would heat up the sensor were

malfunctioning due to what was thought to be a faulty transistor in the ECU. Finding another ECU was deemed not an option since the model is old and obtaining NOS (new old stock) was difficult at best. Repairing it was considered timely and risky, for fear of damaging other operating parts were seen as a greater risk than trying to repair what was broken. Thus, this heater issue previously required extensive running of the engine at an operating point in order to achieve stoichiometric operation for proper oil consumption measurement. Secondly, the higher speed and combustion temperatures assisted in heating up the oil and coolant to an operating temperature desirable for running the experiment. As a result of the large amount of oil and coolant present in the engine, heating them to a steady-state temperature was extensive, especially due to their high heat capacity. Once both the UEGO and oil/coolant were at elevated temperatures, testing throughout the day could be facilitated without waiting as long to reach steady state operating temperature at a given operating test condition.

The steps undertaken at the start of every test day are described here, with their respective approximate times noted where appropriate. The first crucial step is, of course, starting the engine. Following startup, the engine was run at 2500RPM and the throttle slowly opened to wide-open-throttle to increase the exhaust gas temperature quickly. This would hasten the heating of the UEGO sensor. Typically the opening of the throttle would take on the order of one minute to ease the engine into the operating condition, especially since the engine and fluids were still cold (room temperature). Next, the engine was run until it was operating at stoichiometric. Typically this would take anywhere from three to five minutes after the engine was running at wide-open throttle. The limiting factor here is the time taken for the exhaust gases to get hot enough to heat the UEGO and ensure proper operation. Next, the oil temperature control switch/solenoid was set to a value above 212°F (100°C) so that the oil would reach that temperature prior to the activation of the oil pump to cool off the oil in the pan. This high temperature, typically around 220°F, would ensure the evaporation of any water that may have condensed in the crank as a result of blowby gases from the testing of the previous day. When the switch was activated twice, that is oil was pumped through a heat exchanger on two separate occasions, it was deemed that the engine oil had reached a high enough temperature for an extended duration that would ensure the proper evaporation of any residual water, as well as to allow the tester to shut down the engine without fear of much loss over a period of 2 minutes for refueling. Typically, this oil temperature stabilization took on the order of fifteen minutes.

Once the fuel tank was refilled, the engine was restarted and set to the desired operating point, namely the speed and load for the specific test. Once the operating conditions were specified, and with the engine running at stoichiometric, the aforementioned oil control switch was set to approximately 200-210°F. Again, the switch was activated twice before the specific cylinder sample line valve was opened in order to flush the SO_2 analyzer with the exhaust stream and start reading a signal from the detector. It's important to note that prior to the initial starting of the engine, the analyzer was turned on and run under the conditions specified previously in *Section 2.2.2.5*. During the initial warming of the oil at 2500RPM, the analyzer was calibrated. With that being said, the signal generated by the detector was watched along with both the coolant and oil temperature in order to determine when steady-state (less than a 10% change in the overall value for each variable) was achieved. When steady-state operation was realized, data accruement began. From the initial starting of the engine to the actual point of initial data accruement, the approximate startup time was 45 minutes.

2.3.2 Engine Operating Conditions

The primary objective of this study was to investigate the physical characteristics of the ring pack that effect oil consumption under a wide range of different engine operating conditions. These conditions included engine speed, engine load (as dictated by intake manifold pressure), and the changes that occur when either of those variables are changed drastically during the engine's operation. Transient operating condition changes would complement the engine's steady state operation in order to give a more complete picture of the mechanisms of oil transport through the piston ring pack. The test engine was operated between 1500RPM and 3500RPM with loads varying from low (~300mbar) to high (~1bar). For both steady state and transient operation, the startup procedure described above was conducted religiously at the beginning of each testing day and prior to each data run in order to ensure consistency and confer previous results. Unfortunately, the days these were carried out were numbered for the engine.

2.3.2.1 Steady-State Engine Operation

The engine was run at steady-state operating conditions (constant speed and load) in order to understand the ring pack's performance with regards to oil consumption, blowby, and the aforementioned in-cylinder variables. Steady-state oil consumption maps were generated at

five different speeds (1500-3500RPM in 500RPM intervals) and three different loads (350mbar, 650mbar, and 950mbar). The load was measured (low, medium, and high) in reference to the intake manifold pressure at near wide-open throttle. The intake manifold pressure at wide-open throttle ranged from 950mbar to 1bar, therefore, for consistency, 950mbar was chosen as 100%, or full, load for all the speeds examined. Likewise, 350mbar was chosen since it was the lowest load ensuring stable steady-state engine operation for all speeds. Consequently, 650mbar was chosen as the midway load between the two extremes of stable steady-state operation. The intake manifold pressure, and thus the throttle position, was held constant with the aid of a stepper motor and stepper motor controller. Switches were installed to operate lights that signaled the position at which the throttle was fully closed and wide open. These switches also grounded the stepper motor controller in order to kill power to and cease movement of the stepper motor. For all operating conditions, in-cylinder measurements were made in order to assist in the oil consumption analysis and of oil transport through the different ring pack designs tested. *Table 2-5* below shows the fifteen different operating conditions that were to be analyzed for the steady-state experiments run.

Speed	Load
1500RPM	350mbar
	650mbar
	950mbar
2000RPM	350mbar
	650mbar
	950mbar
2500RPM	350mbar
	650mbar
	950mbar
3000RPM	350mbar
	650mbar
	950mbar
3500RPM	350mbar
	650mbar
	950mbar

Table 2-5 – The fifteen operating conditions examined during the steady state experiments.

Each steady-state operating condition was recorded for twenty minutes. This length of time ensured a good view of the oil consumption variation over time. Since data was taken every tenth of a second, the number of data points gathered in twenty minutes provided a more than adequate value for the steady-state oil consumption at a given operating condition. Additionally,

20 minutes was sufficient to view any variation of the oil consumption from a single cylinder to prove that the engine's real-time oil consumption really was steady/constant.

To filter out the noise inherent in the pulsating flows of the cylinder exhaust taps and the natural signal from the analyzer, a rolling average was used in post data processing for creating oil consumption figures. *Equation 2.28* describes how this works, where $(s_i)_{i=1}^{N}$ is the raw data signal series, $(d_j)_{j=1}^{N-n+1}$ is filtered data signal series, n is the number of points being averaged at one point in time, and N is the number of data points gathered (12000 for steady state):

$$d_j = \frac{1}{n}\sum_{k=j}^{j+n-1} s_k \qquad \textbf{(2.28)}$$

For the experiment, n was given a value of 10 in order to filter out most noise and oscillations, but not negate any trends that would occur during operation. Once the data was filtered, the steady state oil consumption was calculated using a Riemann sum method (area under the curve) to get the average of a discrete function as described by *Equation 2.29* below:

$$\dot{m}_{SS} = \frac{1}{T}\sum_{i=2}^{T/\Delta t - n+1} \frac{1}{2}(d_i + d_{i-1})\Delta t \qquad \textbf{(2.29)}$$

where Δt = 0.1sec, T = 1200sec, and $\dot{m}_{SS}$ is the average steady state oil consumption value in units of $^{g}/_{\text{hr-cyl}}$ or $^{\mu g}/_{\text{cyl-cycle}}$ depending on value of d_i.

2.3.2.2 Engine Transients

In real world operation, the engine doesn't solely run at steady state conditions but, rather, is usually in a transient state. This is where an engine's true performance is tested and established. Thus, in order to simulate real driving conditions, an extensive analysis of oil consumption behavior during engine load and speed transients was conducted with the intention of providing insight into oil transport and the factors affecting such. During these transients, the engine load was to be changed from the initial steady state operating condition by opening or closing the throttle to the next operating condition. As noted earlier, a stepper motor controller was used to operate the engine throttle. For load transients, the engine was held at a constant speed while the load was changed in a matter of a second. For speed transients, the engine was held at a constant load while the dynamometer was adjusted during operation. For each experimental run, the initial steady state condition was recorded for five minutes prior to the

condition change. For the sake of consistency, the new operating condition was held for five minutes as well. In total, for a given thirty minute transient test run, each operating condition considered for the current experimental run was analyzed for a total of three five-minute intervals, each interval separated by a five-minute interval of the other operating condition. *Table 2-6* shows the load and speed transient testing that was conducted.

Speed	Transient Load Operation
1500RPM	350mbar→950mbar
	350mbar→650mbar
	650mbar→950mbar
2500RPM	350mbar→950mbar
	350mbar→650mbar
	650mbar→950mbar
3500RPM	350mbar→950mbar
	350mbar→650mbar
	650mbar→950mbar

Load	Transient Speed Operation
350mbar	1500RPM→2500RPM
	1500RPM→3500RPM
	2500RPM→3500RPM
650mbar	1500RPM→2500RPM
	1500RPM→3500RPM
	2500RPM→3500RPM
950mbar	1500RPM→2500RPM
	1500RPM→3500RPM
	2500RPM→3500RPM

Table 2-6 – Load and speed transients investigated for the experiment.

2.3.3 Ring-pack Designs Tested

The steady state and transient operations were performed on an individual cylinder basis with the aid of exhaust taps, as illustrated in *Appendix A*, for a total of four times per engine configuration. In total, there were three different engine configurations to be tested prior to the engine's malfunction as shown by *Table 2-7* below:

	Engine Rebuild Number		
Cylinder #	**Build 1**	**Build 2**	**Build 3**
1	A	B	D
2	B	D	E
3	C1	C2	C3
4	D	E	A

Table 2-7 – Engine testing configuration, with pistons designated by their respective letters. The numbers of the cylinders start such that cylinder 1 is closest to the dynamometer.

Each cylinder for each engine configuration had a different ring pack design. The piston-ring pack designs tested are given below in *Figures 2-6* and *2-7*. Pistons A, B, D, and E were experimental pistons with thinner ring grooves versus the original factory installed pistons along with experimental rings. Piston C's design was a variation of the original manufacturer piston design, along with the different numbers signifying changes to the oil control ring between ring

pack configurations. The difference between Piston C's profile and that of original design from the manufacturer of the PSA engine is the addition of a V-Cut to the second land. The original manufacturer design was used as a baseline in previous experiments conducted by Yilmaz. It is from these results that comparisons were to be made with regards to piston-ring pack designs.

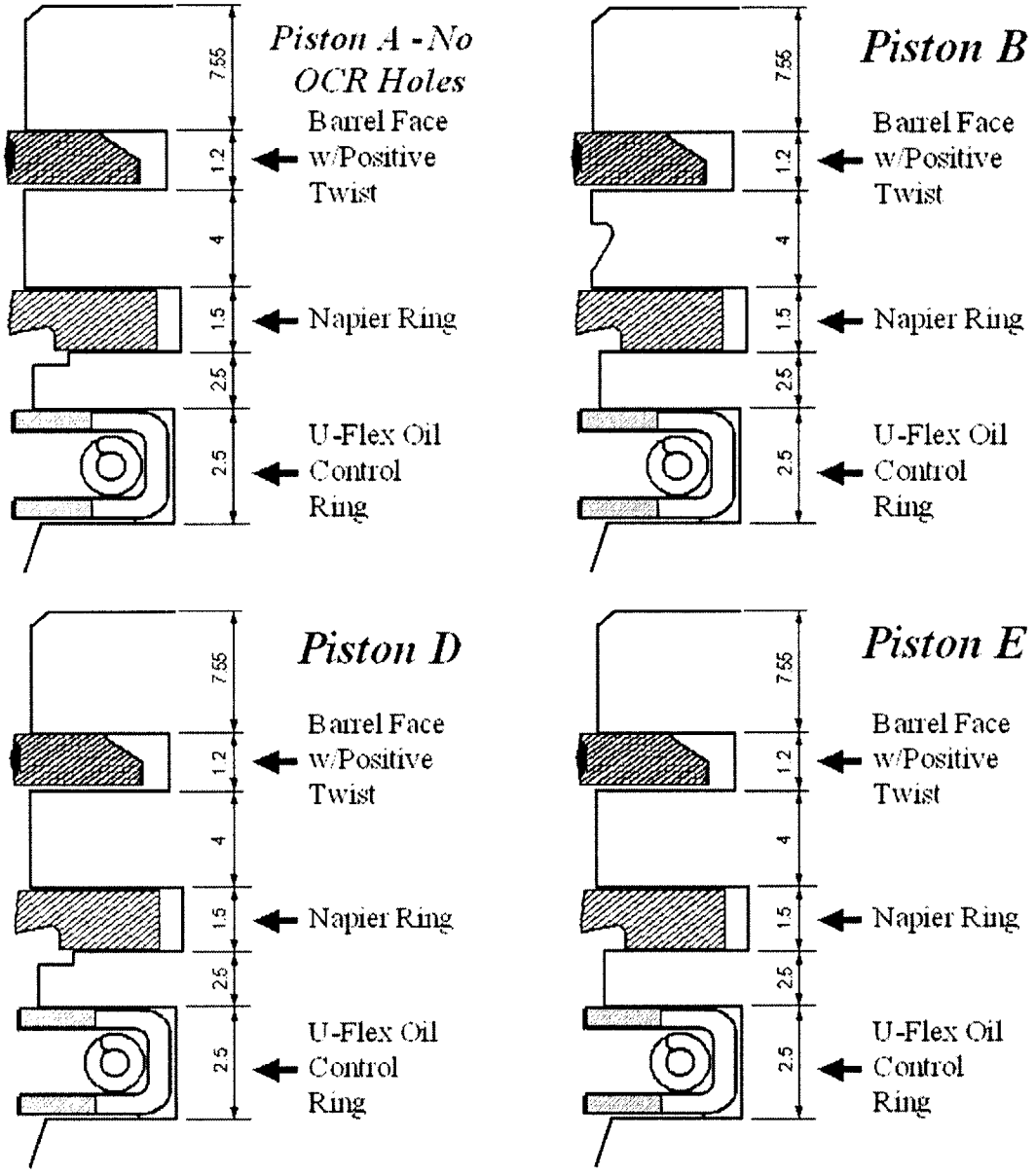

Figure 2-6 – Experimental piston designs with narrower ring grooves when compared to the original piston designs in *Figure 2-7* below. The piston rings were of the same design for all four pistons. All dimensions are in millimeters. The pistons were created by Mahle, while the rings were provided by A Perfect Circle. Not drawn to scale.

Comparison of Piston D to Piston E highlights the effects of the chamfer on the third land as seen on Piston D. Likewise, comparing Piston B to Piston E gives the importance, or lack thereof, of the presence of a V-Cut on the 2nd Land. And, finally, the comparison of Piston D to Piston A would show the consequences of the omission of holes in the oil control ring groove. Combined, these would give a better understanding of the mechanisms of oil consumption and oil transport through the piston-liner-ring pack interface. Additionally, when comparing Pistons C1, C2, and C3 to one another, the significance of the oil control ring design would become apparent. This is especially beneficial from a cost perspective, where the U-flex OCR costs more to produce than the two-piece ring, which in turns costs more than the three-piece ring.

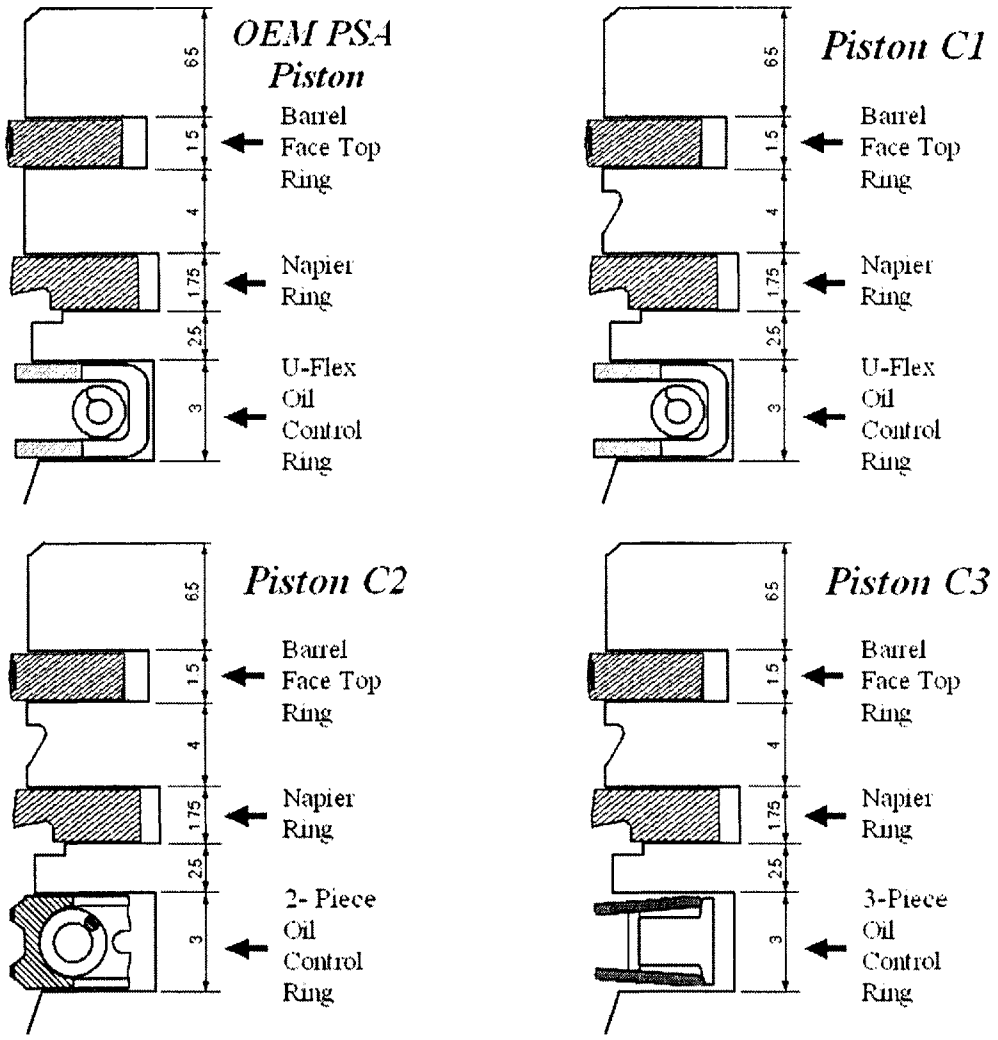

Figure 2-7 – Original piston design specifications from the manufacturer, with the addition of a V-Cut on the 2nd land for Pistons C1, C2, and C3. The top two piston rings were of the same design for all cases, while the OCR was changed where noted. Like before, all dimensions are in millimeters. The pistons were created by Mahle, while the rings were provided by A Perfect Circle and Citroen. Not drawn to scale.

The Piston C ring-pack consisted of a rectangular top ring with a barrel-faced running surface, a taper-faced Napier scraper ring, and the choice of a U-flex, two-piece, or a three-piece oil control ring as shown above. This ring pack was chosen due to their previous use with [7]. Similarly, Pistons A, B, D, and E all used a barrel-faced top ring with a positive static twist, a taper-faced Napier scraper ring, and a U-flex oil control ring, all with narrower axial thicknesses than those of the original design for the PSA engine. The positive twist top ring was chosen for reasons discussed in *Section 1.4.1.2*, while the other two rings were chosen due to their use in the original piston design for the engine.

(This page was intentionally left blank)

Chapter 3: Oil Consumption and Ring Dynamics of the Experimental Piston-Ring-Packs

3.1 Oil Consumption Influences and Ring Pack Performance

As has been discussed extensively, there are a number of factors that affect the oil consumption characteristics and values of a specific piston-ring-pack in a spark-ignition internal combustion engine. Due to the variation in the normal operating conditions of a production engine, it is imperative that an extensive study not only examine the full range of operation, but simulate the actual driving conditions that an engine would be exposed to. The engine's speed and load are the main physical variables that define a given operating point. Taken individually, the speed and load affect the ring dynamics, and thus the gas flow, in differing ways.

The load plays a number of roles in the ring dynamics of the engine. First, when going from a low load of around 300mbar (closed throttle) intake manifold pressure to about 1 bar (wide open throttle), the peak pressures within the cylinder increase by as much as 6 times, depending upon the engine's speed. As such, the pressures that are present on the crown, 2nd, and 3rd lands all increase accordingly. The increase in pressure drives the flow at higher rates, both in the axial and circumferential direction within the piston-ring-pack. The added pressure also affects the dynamic twist of the rings, changing the direction/paths of gas flow through the various regions listed earlier in *Section 1.3*. Additionally, an increase in pressure and gas flow accompanies an increase in peak temperatures. This affects the physical state of the gas, the viscosity of the oil, and the extent of expansion of all parts of the system. In sum, the engine's load is a major player in oil transport, ring dynamics, and thus oil consumption. Its teammate is the engine's speed.

The oscillating motion of the piston, due to the operating speed, has a number of effects on the mechanics of the system. First, the inertia of the piston can cause throw-off of the oil on the crown land and/or the top ring into the combustion chamber to be consumed. Additionally, as was discussed in *Section 1.4*, the inertia imparted to the rings can either conflict with or heighten the pressure forces acting on the rings. An increase in the speed gives way to an increase in peak pressures and temperatures and a decrease in residence time. Thus the physical properties that normally define a state, namely pressure and temperature, are closely bound to the engine speed. Finally, friction is directly proportional to engine speed. As such, the more an

engine is operated at higher speeds, the face profile of the rings can grossly change over time. This has an impact on the ring-pack's performance in both sealing properly and the gases in the flow paths.

The above is a brief summary of the reasons for studying the effects of speed and load on oil consumption and why they are interrelated to the ring pack designs tested. Any modification to the ring pack will have a different effect on traditional trends, specifically in oil consumption, found for a given ring pack and engine. This gives way to the use of analytical/theoretical tools with the hopes of better understanding these effects. Coupling the computer models with the actual data results assisted previous experiments in quantifying the importance of some of the many mechanisms that affect oil consumption [7].

3.2 The Use of Computer Models and The Associated Uncertainty

Though numerous computer models have been developed to shorten testing time and experimental research requirements, there still remains voids to be filled in the understanding of oil transport and the performance of a piston-ring-pack system. Advances have been made to account for temperature variation, different ring and piston geometries, and to take other inputs such as the known cylinder pressure trace, bore expansion, the rings' face profiles, the wear profiles of the rings within their grooves, and the friction between the rings and liner. Still, as complex as these models have become, they still fall victim to the uncertainties that plague research. These deviations from actual measurements are to be expected during the development phase of a new product. The cost benefits from research, development time reduction as well as production time reduction, and prototype testing more than outweigh the deviations from the actual ring pack performance. This is due to the fact that the discrepancies are minor, and the analytical tools still give an idea as to the rings' movement within the system.

The uncertainties that couple with the analytical tools, those that would cause the results to be different from those seen in experiments, are hard to eliminate and can only be minimized through improved tolerances and quality control and, in Catch-22 fashion, through extensive tests. The variations that exist with the dimensions of rings, the piston, the engine bore, etc., are one source of error. Additionally, the difficulty to predict oil flow through passages remains a problem in some instances when dealing with the combination of circumferential and axial flow. Such phenomena as ring rotation and preferential movement are still hard to predict. The wear

patterns chosen may not be exactly what occur after a number of hours of use, while the bore expansion data may not take into account anisotropic behavior of the cylinder as well as the exact honing specifications of the liner. At best, these unknowns may cancel out each other as far as oil transport and ring effects are concerned. However, they do provide a source for a butterfly effect, where one discrepancy may cause a chain reaction that soon changes flow patterns and the exact ring dynamic and movement within the groove. As such, there still remains the ideal that temperature distribution is, in some cases, circumferentially independent. The models used within this study are still, in many ways, two-dimensional in that they don't consider discrepancies that exist in the localized temperature distribution around the circumference at a given axial height.

That being said, the experiment was halted due to an engine malfunction, as has been mentioned numerous times previously, and, as such, limited data results have been attained for the real time oil consumption of the piston-ring-packs tested. However, a preliminary analysis can still be made in order to compare what was seen from the test runs conducted and what the analytical models would predict.

3.3 Oil Consumption Variation: Ring-Pack Design, Engine Speed and Engine Load Effects

3.3.1 Steady-State Operation

Prior to the cessation of experimental operation, the engine provided some valuable data that veers away from the norm in some instances from conventional oil consumption measurements (i.e. – oil consumption increasing with increasing speed and load). It serves prudent to provide the contour maps of such data below, and to discuss what is occurring and the cause of such trends later on in *Chapter 4*. In some instances, oil consumption does increase steadily, or, more conservatively speaking, generally with speed and load. However, as will be shown and explained below, in other cases, this was far from true. In short, very erratic behavior was viewed for the piston-ring-pack designs that were able to be tested.

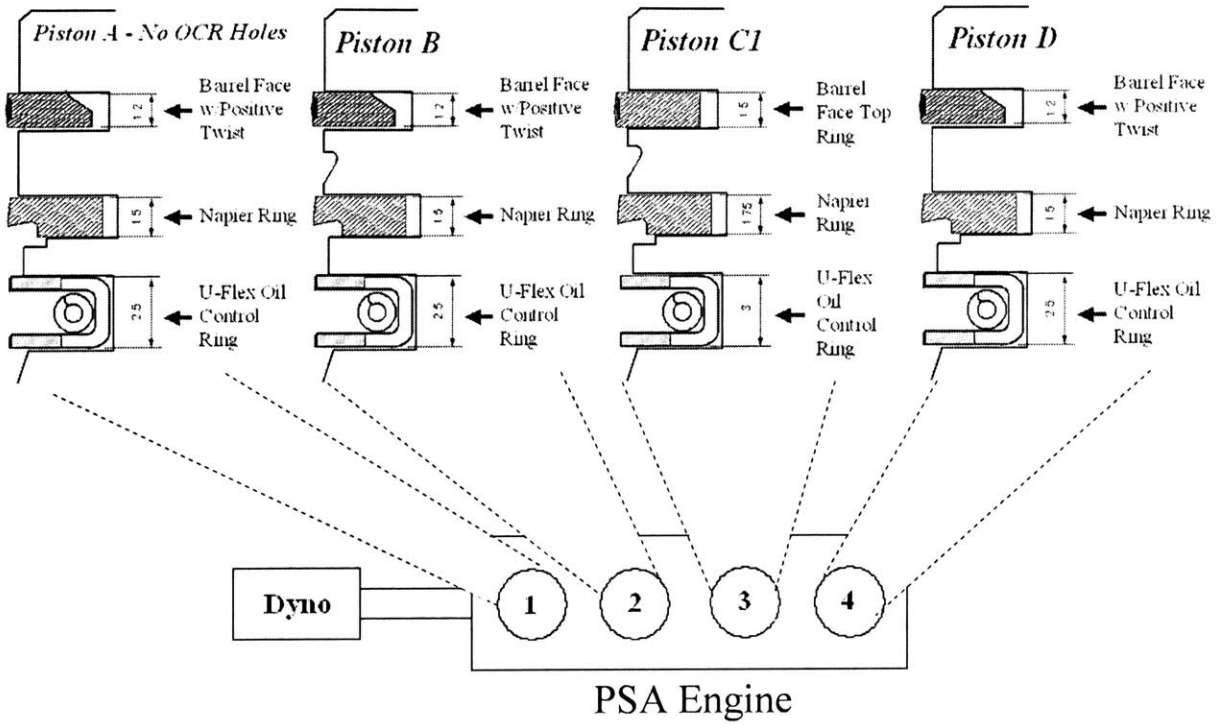

Figure 3-1 – Build configuration at the time of the engine's failure. This is Build 1 from *Table 2-7*. Numbering scheme for the cylinders is opposite that of industry.

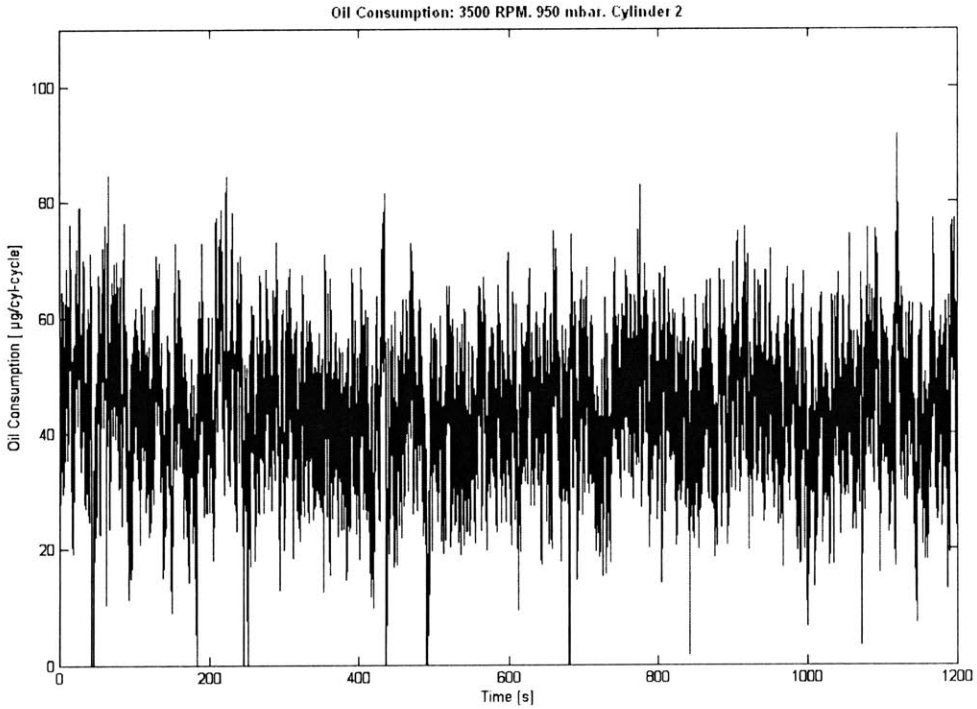

Figure 3-2 – An example of the oil consumption signal from Piston B filtered as described in *Section 2.3.2.1* over the span of 20 minutes at the operating condition specified in the title. As stated earlier, the oscillations from the pressure waves within the exhaust runner are picked up by the analyzer.

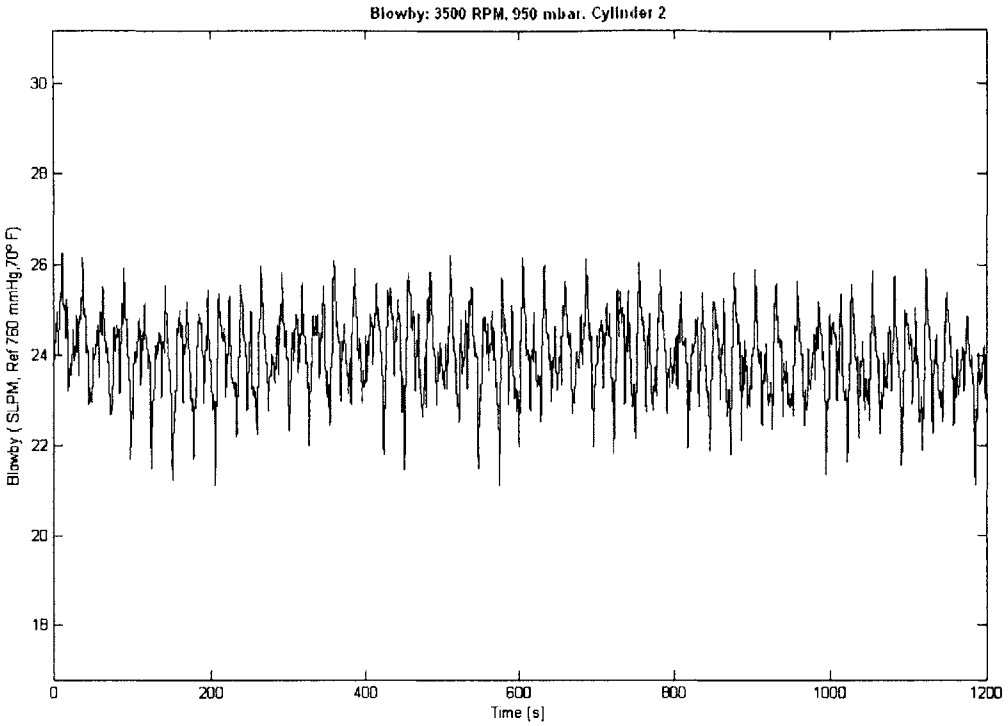

Figure 3-3 – An example of the blowby signal from Piston B filtered as described in *Section 2.3.2.1* over the span of 20 minutes at the operating condition specified in the title. It should be noted that this blowby measurement was measured for the engine as a whole rather than for individual cylinders.

Figure 3-1 illustrates the layout of the engine during Build 1 as described in *Table 2-7*. As can be seen from the build, there are four different piston-ring-pack designs that are being analyzed individually, with their accompanying drawings reprinted from *Section 2.3.3* in order to save the trouble of referring back to previous pages. Explained and detailed earlier, each cylinder was analyzed and produced a data set very similar to the examples shown in *Figures 3-2* and *3-3*. *Figure 3-2* is the real-time steady-state oil consumption trace at the labeled operating condition while *Figure 3-3* is its accompanying blowby trace. Both have undergone the signal conditioning described in *Chapter 2* (namely *Equation 2.28*), to filter out the inherent noise in the system. *Figures 3-4* to *3-7* were created from such raw data, above, using *Equation 2.29*. While previous research conducted by Yilmaz recorded the oil consumed on a cycle basis for the engine as a whole, the nature of these experiments saw fit to calculate such consumption on a per cylinder per cycle basis.

Though the research testing was cut short due to the mishap mentioned numerous times already, Piston Λ (features of no OCR groove drain holes and a chamfer on the third land) was already exhibiting strange behavior at all loads drawn. At the speeds recorded, the low loading

condition had the highest oil consumption in general at all speeds (with the exception at 2500RPM though the difference is small). The low load's recorded oil consumption peaked at 2000RPM. In a mirror-like fashion, the mid load operation had a valley at 2000RPM. The high load (950mbar) exhibit typical behavior, increasing with increasing speed. Though the number of data points is limited, some preliminary analysis can be made, which will be further explored in *Chapter 4*. First, the lack of drainage holes in the OCR groove has a peculiar and, in some cases, an adverse effect on oil consumption. Secondly, the presence of a chamfer on the 3rd land plays a role in the amount of oil that would be present on the 3rd land and consequently for the OCR groove. Finally, increasing the speed affects the trends of oil consumption values recorded.

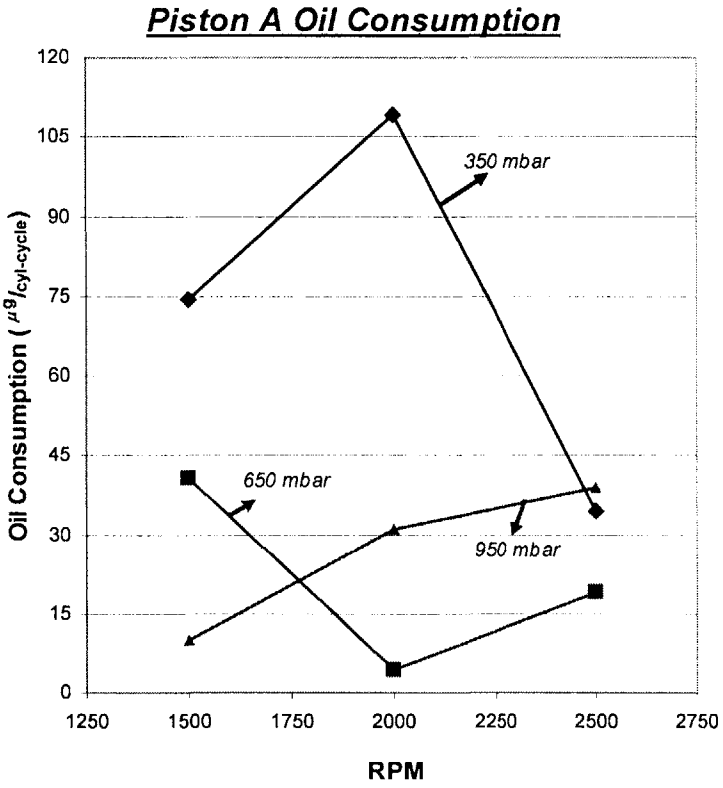

Figure 3-4 – Piston A steady-state oil consumption values with loads marked. As shown in *Figure 3-1* above, this piston was tested in designated Cylinder 1 prior to engine cessation.

Figure 3-5 illustrates Piston B's behavior for the load and speed points listed. Piston B's design feature is a V-Cut on the 2nd land. The first thing that's noticeable is that in general, at a constant load, the oil consumption increases with speed. This holds true for the low and mid load, however at 950mbar, the trend is not as apparent. Though there is a marked increase from 1500 to 3000RPM, the oil consumption drops immensely at 3500RPM. Additionally, for most of the operating speeds, the low load condition produced a higher oil consumption rate than the mid load condition, however high load operation was the highest over all speeds. At a glance, it

seems the added area in the 2nd land from the V-Cut affects the gas flow (as would be expected), especially at high loads (recall that high loads cause high gas velocities throughout the piston ring pack).

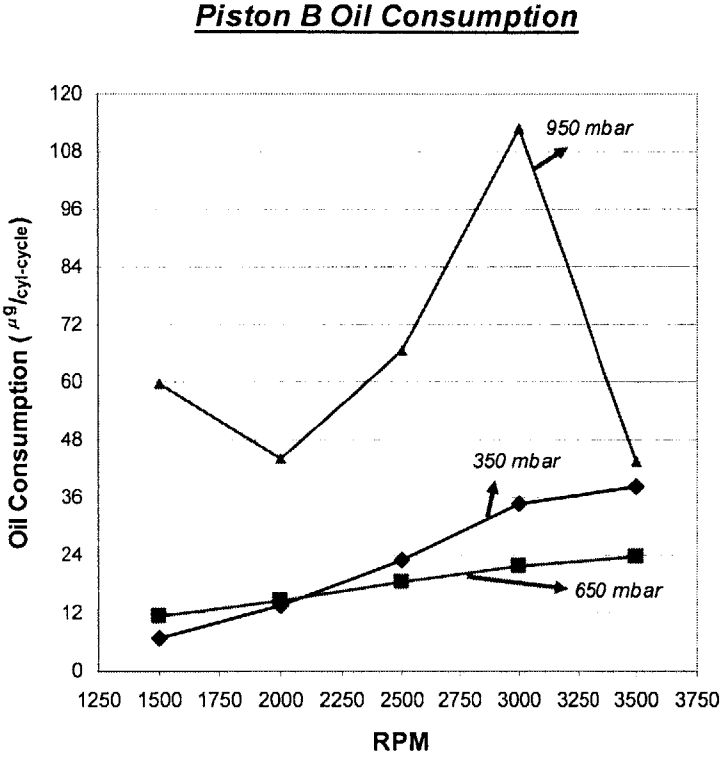

Figure 3-5 – Piston B steady-state oil consumption values with loads marked. As shown in *Figure 3-1* above, this piston was tested in designated Cylinder 2 prior to engine cessation

Piston C1, whose oil consumption readings are given in *Figure 3-6*, has the original dimensions of the engine's factory installed pistons, except it has the addition of a V-Cut on the 2nd land. The ring set is also the same as that tested by Yilmaz in [7]. We see that with the exception of 2000RPM, the oil consumption at 950mbar is the highest of the three loadings, generally increasing with speeds (with the exception at 3500RPM). Likewise, the 650mbar loading conditions increased overall with speed, having values less than those of 350mbar for speeds less than 2500RPM, and being higher for 3000RPM and up. The low loading condition exhibited no consistent trend whatsoever, increasing and decreasing at various speeds in an erratic fashion, much like what was seen for Piston A.

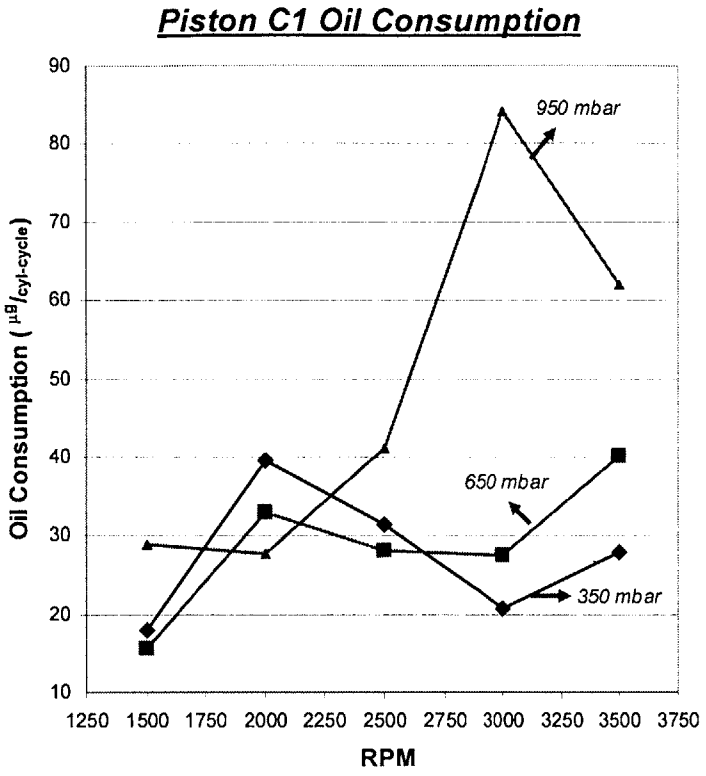

Figure 3-6 – Piston C1 steady-state oil consumption values with loads marked. As shown in *Figure 3-1* above, this piston was tested in designated Cylinder 3 prior to engine cessation.

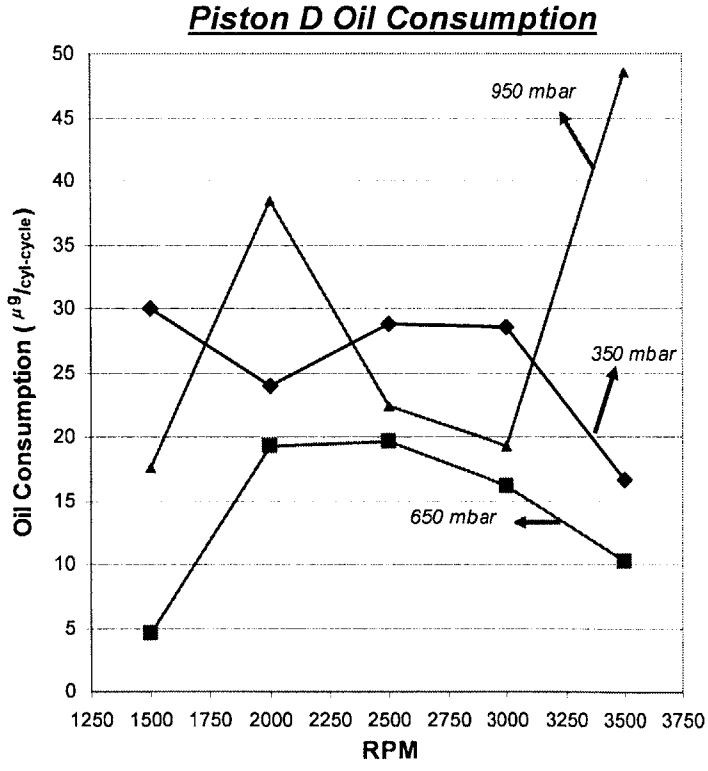

Figure 3-7 – Piston D steady-state oil consumption values with loads marked. As shown in *Figure 3-1* above, this piston was tested in designated Cylinder 4 prior to engine cessation.

Oil consumption readings for Piston D, whose design is the same as that of Piston A, except with OCR groove drain holes present, are illustrated in *Figure 3-7*. Like Piston A, D exhibits erratic behavior for all loads, with no apparent trend that stands out. For high loading, the amount of oil consumed increases, then decreases to a local minimum at 3000RPM, only to rise again at 3500RPM. Similarly to Piston A, the oil consumption readings were, in general, higher at the low load than the other loads, except for the rare cases as viewed by the high load values shown. Overall, however, the mid load operating regime was the lowest for all of the speeds tested.

It's important to note that most of the values given from the testing were on par or higher than typical values of oil consumption at similar operating conditions. In most cases, on a per cylinder basis, the measurements recorded here were quite different, both in trends and in amounts when compared to [7]. The exact reason for this has yet to be determined, though will be understood more fully once the engine has been rebuilt for future research. However, the blowby values during the recording of the piston designs tested were normal and showed no sign of a ring pack error or malfunction as such. *Figure 3-8* attests to such findings, showing an increase in blowby most notably with load and independent of speed.

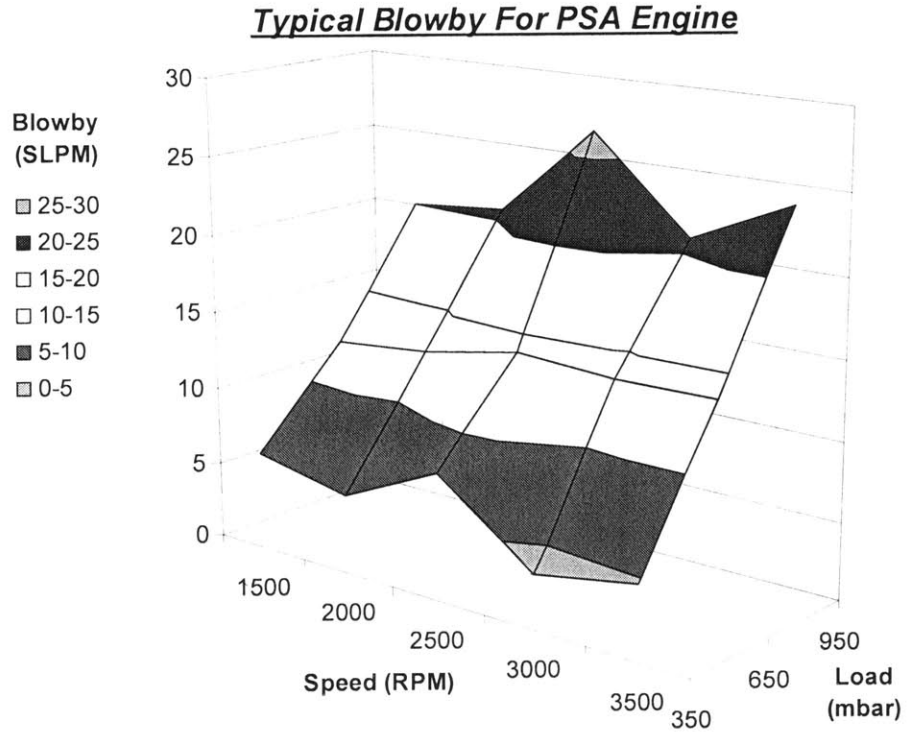

Figure 3-8 – Typical blowby values and trends recorded during the piston designs tested.

3.3.2 Transient Operation

Though most of the concentration of this thesis will be with on the performance of the ring packs during steady-state operating conditions, future research will deal with their performance under transient actions. Therefore, in anticipation for such analysis, the author thought it would be sensible to include one such oil consumption data collection. Prior to the above testing of the pistons of Build 1, this research run tested the LabView code in *Appendix E.* The transient operation was the next research item to execute (as described in *Section 2.3.2.2*), however, calibration and engine configuration took priority, as well as the current temporary position of "Out of Order" of the engine. *Figure 3-9* gives an example of one such test run at 3500RPM going from low load to high load conditions. The peaks in the oil consumption data are quite repeatable and occur after every transition from low to high load. This has been seen in previous research in [7], though the values seen here continue the trend of *Section 3.3.1*: much higher values than what was found by Yilmaz. The measurement soon returns to the engine's steady-state value at high load in approximately one minute. This is true for all three operation intervals. In turn, the return from high to low load is quite stable, with no marked change in the "steady-state" value between the three intervals.

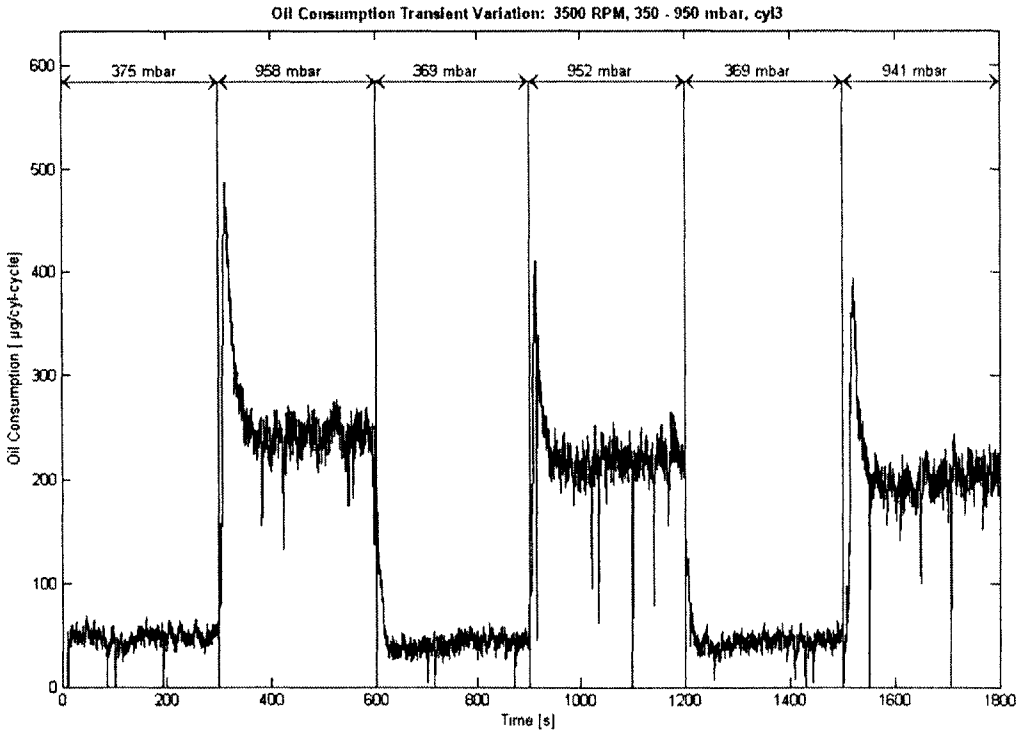

Figure 3-9 – An example of the transient operations performed on the engine during single cylinder analysis. Operating conditions are noted in the graph's title and data set.

The blowby for the testing run shown above is presented in *Figure 3-10*. Here we find that the blowby also shows peaks when going from low to high loading conditions. Likewise, the low load conditions resume steady-state values with no lag time, while the high loading experience peaks that last on the order of 100 seconds, longer than that for the oil consumption lag time seen in *Figure 3-9*. But it too reaches a steady state value much like that in *Figure 3-9*.

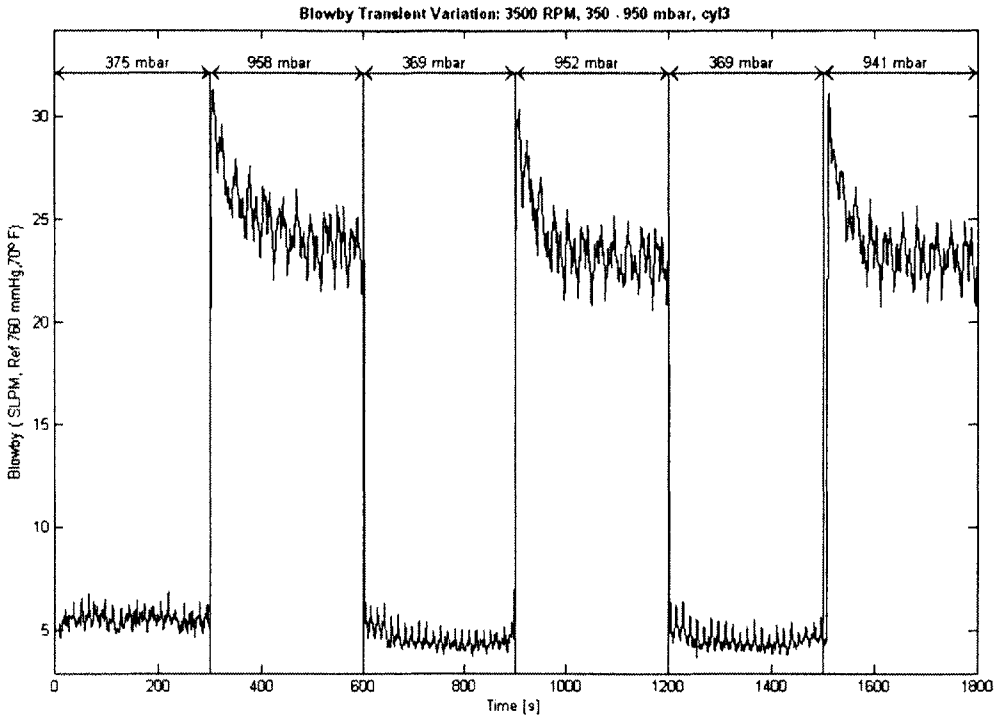

Figure 3-10 – Blowby data for the test run shown in *Figure 3-9*.

Given the limited amount of data for both the steady-state and transient testing of the engine, it was deemed required that computer simulations be run in order to get a better picture of the mechanisms that would cause the trends described above.

3.4 Computer Simulation of the Different Piston Ring Packs

Pressure traces for four speeds and three loading conditions were provided by Steve Przesmitzki from his LIF PSA one-cylinder research engine. These speeds were 1500, 2500, 3500, and 4500 RPM with loading conditions of 300, 500, and 700mbar for each speed. However, no pressure traces were obtained for two points: 500mbar at 1500RPM and 700mbar at 4500RPM. With this broad range of loading and engine speeds, the results from the computer simulations would give a more comprehensive understanding of oil transport and gas flow

through the piston-ring-pack system. With the comparisons presented below of the multiple design considerations considered, it will become possible to make some general conclusions of their effects, whether beneficiary or adverse, to the performance of a given piston-ring-pack in terms of its oil consumption control for this specific engine. This point should be stressed, that these results are more specific to the engine design than anything else. However, the fundamentals of ring dynamics and gas flow, coupled with the design effects, would still give a better clue as to what is actually occurring within the cylinder and provide design recommendations for future development. Unfortunately, due to some of the inherent limitations of the model, the use of OCR groove drain holes cannot be input as a design factor of the pistons. Therefore, the comparison between Piston A and Piston D cannot be accomplished and will be ignored for the remainder of this chapter.

Figures 3-11 through *3-15* show a sample of the graphs generated from the Matlab code reprinted in *Appendix D* for each of the pistons at the aforementioned operating conditions. From these graphs, comparisons were made between the different pistons with regards to their varying performance and effects on gas flow and ring dynamics. Note that the average values obtained for blowby from the model were similar in magnitude to those obtained from experiment.

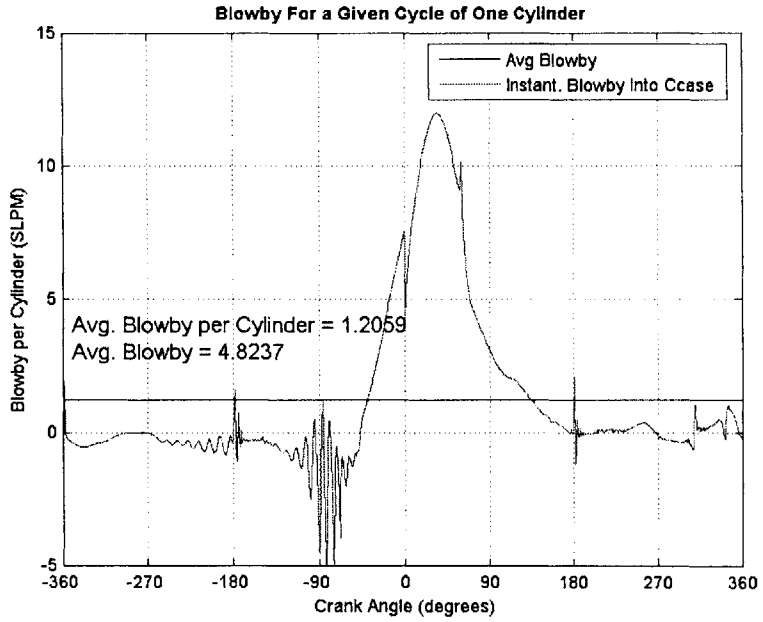

Figure 3-11 – Example of instantaneous blowby taken for two cycles of Piston B's operation. Also calculated are the average blowby on a per cylinder and 4-cylinder basis. For this, the operating conditions were 1500RPM and 300mbar.

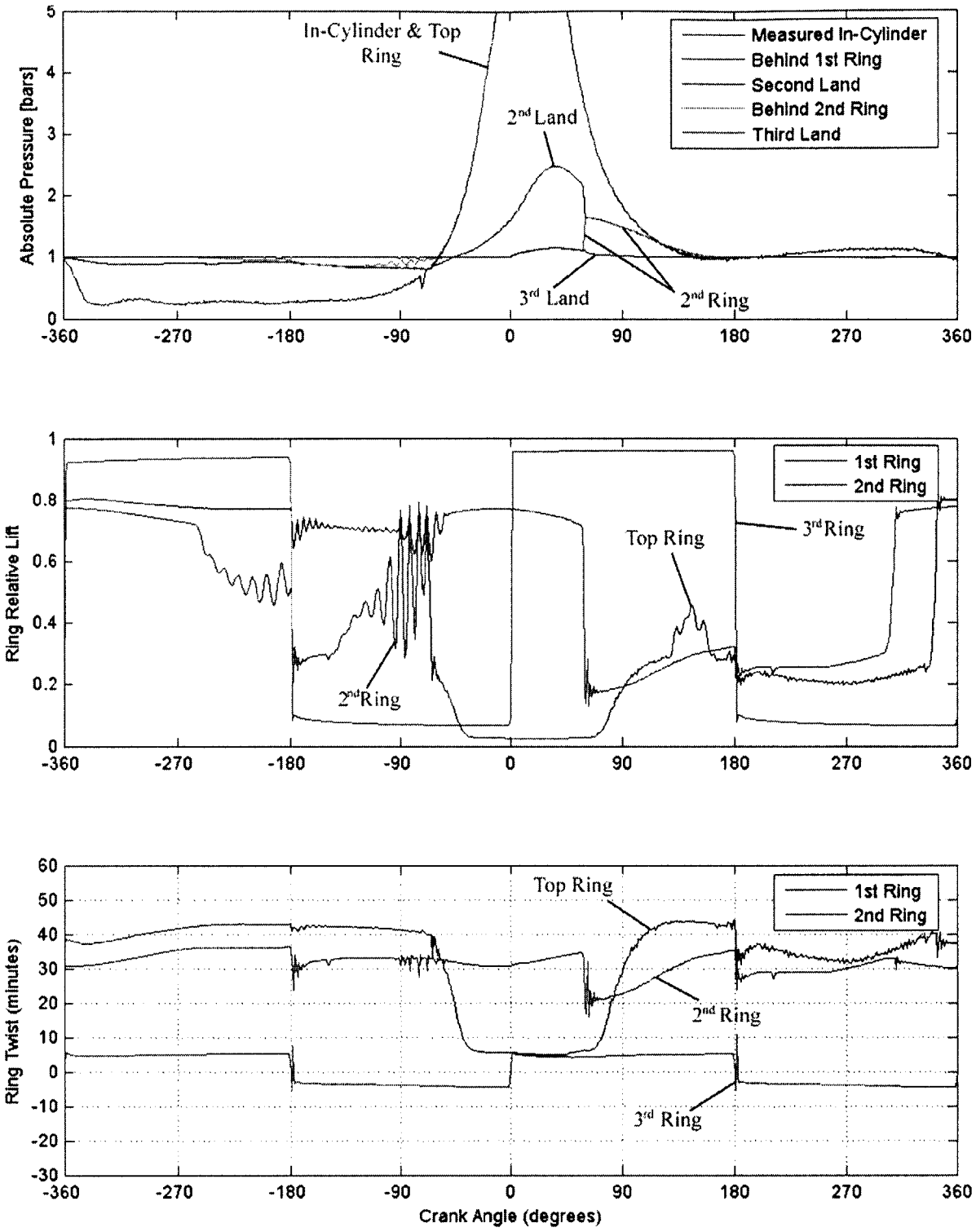

Figure 3-12 – Taken at the same conditions for Piston B as in *Figure 3-11*, 1500RPM and 300mbar, the above illustrates the pressure traces in the annotated areas, the twist of the rings, and the axial position of the rings within their respective grooves over the course of two cycles. Though not labeled, also illustrated is the OCR's position and twist in the bottom two graphs.

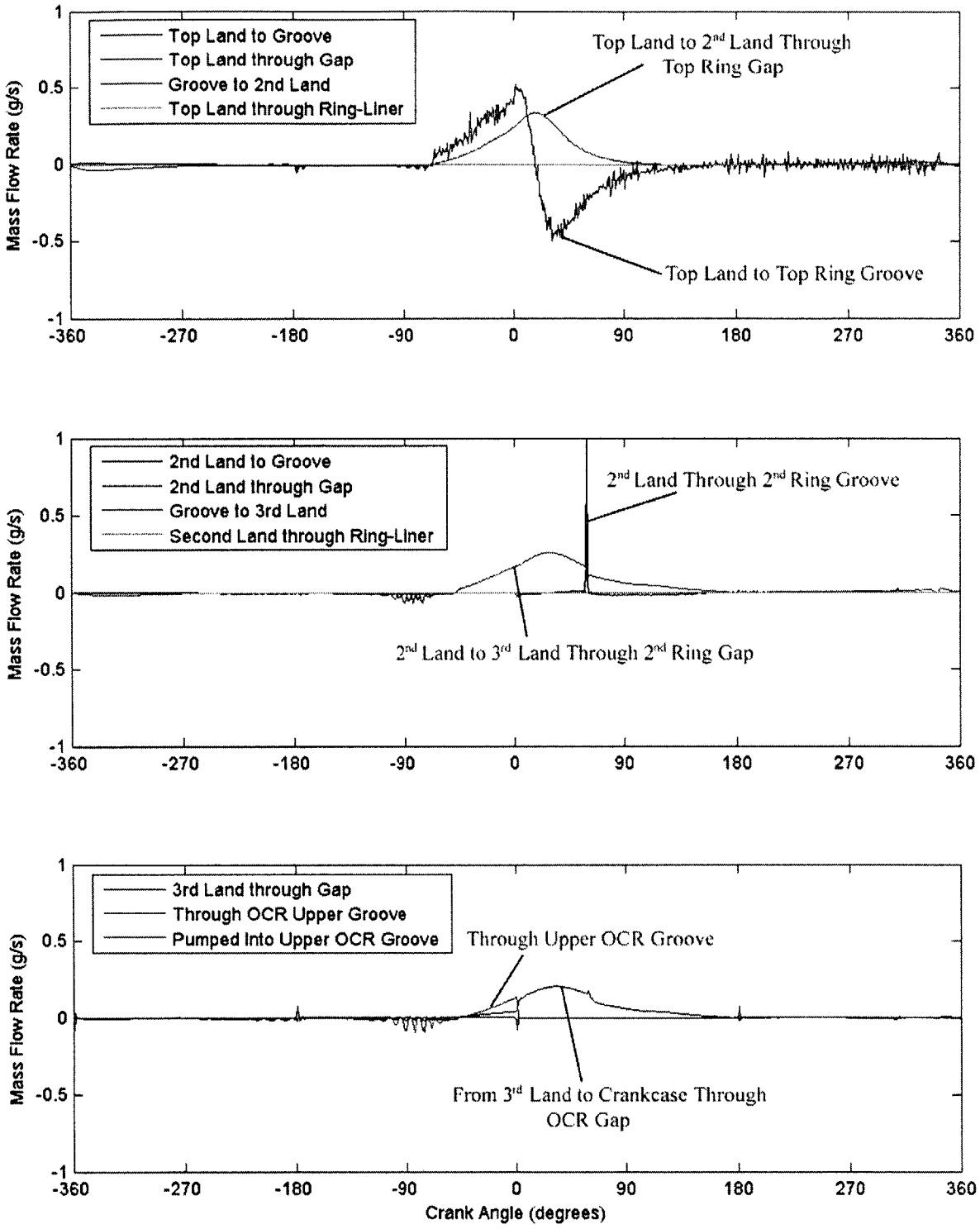

Figure 3-13 – Taken at the same conditions for Piston B as in *Figure 3-11*, 1500RPM and 300mbar, the above illustrates the mass flow rates through the Regions described in *Section 1.3* for the annotated sections of each region considered. Positive values indicate flow advancing downwards towards the crankcase, whether it is into the top of a groove, or out of the bottom of the groove as noted.

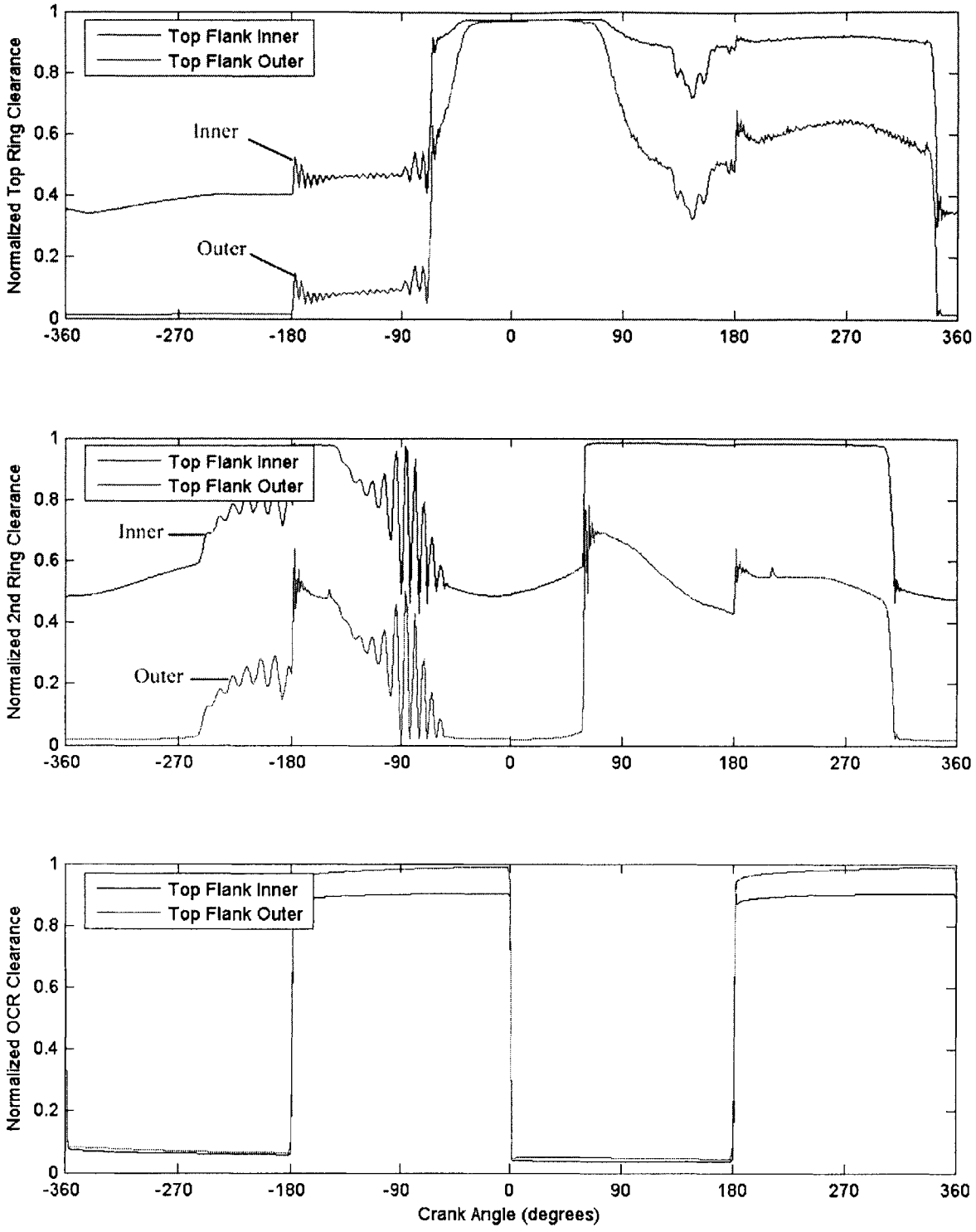

Figure 3-14 – Taken at the same conditions for Piston B as in *Figure 3-11*, 1500RPM and 300mbar, the above illustrates the position of the inner and outer diameter of the upper surfaces of each ring within their respective grooves. This assists in visualizing what is shown in *Figure 3-12* with regards to ring position and ring twist. A value of 1 means the ring edge is on the bottom flank of the groove, and thus the largest distance from the top.

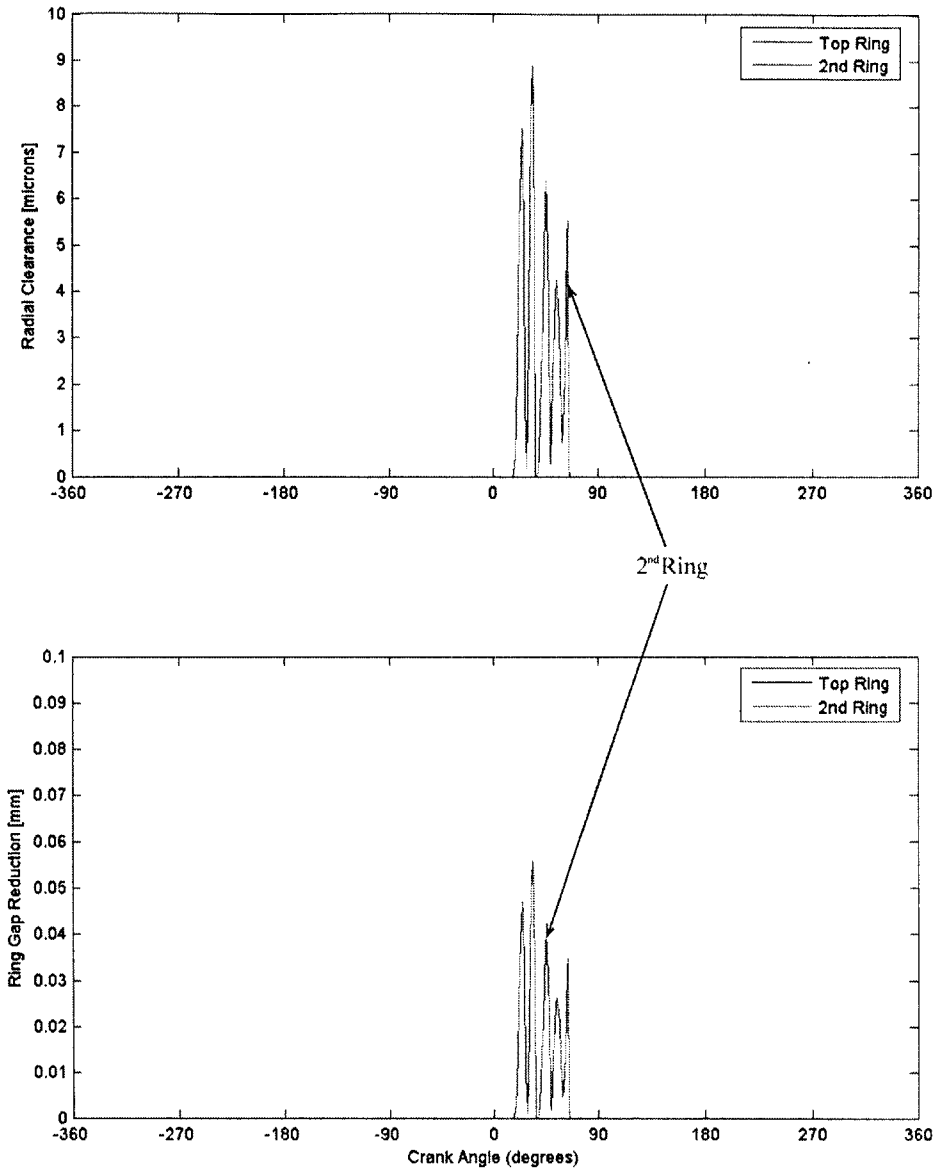

Figure 3-15 - Taken at the 3500RPM and 700mbar, the above illustrates the radial clearance between the top and 2nd ring face and the liner. Additionally shown is the accompanying reduction in the gap width that results from such increases in clearance values. Any positive value signifies radial collapse, if only temporary, for the given ring. Such instances are outlined in *Section 1.4*.

3.4.1 The Use of a V-Cut vs. No V-Cut on the Second Land

Comparisons made between Pistons B and E with the aid of the computer model, RINGPACK-OC, are presented here in the context of the differences in ring dynamics and gas flows between the two designs based upon the existence of a V-Cut, or lack thereof. Conclusions that would amount from these observations will be made in *Chapter 4*.

3.4.1.1 Engine Speed: 1500RPM

At low load (300mbar), Pistons B and E showed markedly similar blowby and ring dynamic traces produced by the model. The mass flow rates through the select regions of study were also similar. The only difference lied in some minor top ring lift for Piston B at the end of the expansion stroke. However, at 700mbar, the two were quite different. While the top and 2nd ring fluttered at the start of the compression stroke for both of them, other aspects were different. First, Piston B's average blowby value (though the traces were similar) was slightly lower. Piston E experienced higher 2nd land pressure and more top ring flutter at the start of the exhaust stroke; however it had less reverse gas flow than Piston B, and thus less gas flow into the combustion chamber. It was also noticed that Piston B's top ring moved more frequently within its groove, pumping more in and out, while Piston E's top ring blocked the groove enough since a majority of the gas flow from the crown land to the 2nd land was through the top ring gap.

3.4.1.2 Engine Speed: 2500RPM

At low loading, the blowby values between the two pistons were similar, as well as their general ring dynamics. The 2nd land pressure drop for Piston B was minor when compared to Piston E, also causing less pressure oscillations for B than E during the compression stroke. As before, top ring and 2nd ring flutter existed at the start of the compression stroke for both. Once the load was increased to 500mbar (mid load range), the differences between the two designs was apparent. The blowby for B was smaller than for E due to the presence of reverse flutter that occurred during the beginning of the exhaust stroke. Also noticed was the presence of 2nd ring radial collapse, which achieved higher peaks (that is, a larger ring gap reduction or larger radial clearance between ring face and liner) in Piston E than in B. This seemed to be rooted in the higher 2nd land pressures achieved by Piston E during the compression and expansion strokes versus B's history. This radial collapse coupled closely with large mass flow rates through the OCR in E versus that through B. Hence this is another source of the blowby disparity. At 700mbar, the blowby and ring dynamics take on similar forms once again. Top ring flutter and reverse blowby are present for both piston designs in the compression and exhaust strokes. Radial collapse also occurs due to the spikes that occurred in the pressure traces of the 2nd and 3rd lands at the start of the expansion stroke as well as the large mass flow rates from the 2nd land to

the 3rd land through the ring face and liner channel. Both experience a gap reduction and radial clearance increase on the same order from the collapse.

3.4.1.3 Engine Speed: 3500RPM

Like at the previous speeds, low loading provided similar graphs between the two pistons. Once again, the blowby was slightly less for B on average, while the top ring groove pressure trace for E was less than that of B, specifically at the end of the compression stroke. At this point, the top ring also experienced flutter, which is attributed to the drop in groove pressure. Increasing to mid-load, not much is new: the average blowby for B is less than for E, reverse gas flow is experienced by the ring pack for B during the exhaust stroke, and E experiences a 2nd ring radial collapse that rivals that of B's. Thanks to the V-Cut's presence, the 2nd land pressure at the start of expansion is less for B than for E. Much like before, the radial collapse for E was caused by a higher pressure on the 2nd land than that for B, hence a greater flow from the 2nd land to the 3rd land. At 700mbar, the top ring's reverse flutter in Piston B is more pronounced. Like at 2500RPM, the reverse blowby that occurs at the start of the exhaust stroke for B and the larger flow due to the radial collapse that occurs at the start of expansion for E causes the greatest difference between the blowby figures obtained (B's average was less than that of E's). Piston E's top ring also flutters, but not at the magnitude seen by Piston B's.

3.4.1.4 Engine Speed: 4500RPM

Low loading produces no change between the two piston ring packs in terms of performance. However, at mid load (500mbar), the 2nd land pressure for B is less than that of E, negating the likelihood for the possibility of radial collapse in Piston B's ring pack. Though they both experience some form of radial collapse, the mass flow rate from the 2nd land to the 3rd through the ring and liner interface is much higher for Piston E than it is for Piston B with more frequent occurrences of such flow than B.

3.4.2 The Use of a Chamfer vs. No Chamfer on the Third Land

Like in *Section 3.4.1*, comparisons will be made between Pistons A/D and E with the aid of the computer model, RINGPACK-OC, noting the differences in ring dynamics and gas flows

caused by the use of a chamfer, or no chamfer, on the 3rd land of the piston. Conclusions that would amount from these observations will be made in *Chapter 4*.

3.4.2.1 Engine Speed: 1500RPM

Running at 300mbar, Pistons D and E exhibited similar blowby behavior and average values. The ring dynamics of the top ring and OCR are similar, however, during the expansion stroke, the 2nd ring is seated at the bottom of its groove later in the cycle (at around 90° into the expansion stroke) for Piston D than for E (which occurs at about 60° into the expansion stroke). At high load operation, the blowby value is greater for D than for E since top ring reverse flutter occurs during the exhaust stroke for E, and thus reverse gas flow. Additionally, the top ring of D experiences less of a positive dynamic twist than E, however its 2nd ring experiences a positive dynamic twist greater than that of E. Towards the end of the expansion stroke, the 2nd land pressure is at a higher value in E's configuration than with D's, adversely affecting the top ring's performance.

3.4.2.2 Engine Speed: 2500RPM

The 2nd land pressure for D continued its trend of being lower than that seen in E, along with D's blowby average value being larger. Due to this lower pressure, the 2nd ring was axially higher within its groove at the end of the expansion stroke for D, assisted by the increased support from the 3rd land chamfer and the 3rd land pressure exposure. At mid load, the blowby is higher for D than E, once again due to the lower 2nd and 3rd land pressure of Piston D. Radial collapse occurs as a result of the higher 2nd land pressures on E, and to a lesser extent on D. However, the mass flow rate through the ring and liner interface is far greater for E than D, much like the comparison of E to B. Note, with the occurrence of radial collapse comes the decrease in the amount of gas flow through the 2nd ring gap. Similar ring physical states such as the 2nd ring positive dynamic twist and the top ring's flutter mimic the trends observed at 1500RPM and 700mbar (where D had more twist and less flutter). During the 700mbar study, E experienced a larger amount of reverse gas flow in comparison to that of D, thus having a lower value of average blowby than D and a higher 2nd land pressure. The higher load brings larger radial collapses for both D and E, though E's are far greater in occasion and intensity.

3.4.2.3 Engine Speed: 3500RPM

The blowby of Piston D went through the roof at low loading, providing and average value that was far greater than seen at the highest speed and load for the design. This upsurge in gas flow seemed to stem from the top and 2nd ring radially collapsing after the 2nd land pressurized above a maximum. As such, the pressure keeps the top ring at the upper part of its groove. After the collapse, the 2nd land depressurizes and the top ring restores to operation on the bottom of the groove and thus mimics the top ring of E. Mass flow rates show spikes where the top and 2nd ring collapsed, causing an upsurge in the amount of gas flow through the ring-liner interface. At mid load, things return to normal: E charts reverse gas flow during the exhaust stroke due to top ring flutter, both have the occurrence of 2nd ring radial collapse on the same order as one another, and the 2nd land pressure trace of D is less than that of E. In the end, the blowby for D is slightly less than that of E. For 700mbar, similar trends ensue. Less 2nd land pressure coupled with less frequent and intense pressure spikes from minor radial collapse separate D's operation from that of E's, where exhaust reverse flutter and large radial clearances from 2nd ring radial collapse catch one's attention.

3.4.2.4 Engine Speed: 4500RPM

At 300mbar, the average blowby value for D is slightly greater than that for E, pairing the added 3rd land volume, the use of a Napier/scraper ring and a comparatively less 2nd land pressure to leave up to *Chapter 4* for discussion. At 500mbar, we have a similar situation with regards to blowby and 2nd land pressure. Additionally, the top ring dynamic twist and axial position within the groove during expansion for D are less than that found in E. As for previous speeds, the occurrence of radial collapse is customary, being much more pronounced for E than for D in frequency.

3.4.3 The Use of Three-Piece, Two-Piece, and U-flex OCRs

As in the two previous sections, observations of the differences in the ring dynamics and gas flows between Pistons C1, C2, and C3 will be noted from figures generated using the computer model, RINGPACK-OC. Thus, in the end, the comparisons between the three types of OCR possibilities, namely three-piece, two-piece, and U-flex, will be realized. Conclusions that would amount from these observations will be made in *Chapter 4*. It seemed the two biggest

factors in the different model behaviors observed for the three different piston-ring-packs were the OCR gap width and the mass of the OCRs. The masses measured and used for the simulations were: 7.816g for the 3-piece (C3), 10.96g for the 2-piece (C2), and 8.115g for the U-flex (C1).

3.4.3.1 Engine Speed: 1500RPM

Blowby was found to be highest for C2, then C1, then C3, with C1 and C3 having similar average blowby values at low loading. The higher flutter of C2 seemed to assist in the pressure drops of the 2nd and 3rd land while facilitating in gas flow. C2 and C3 experienced large OCR flutter, while C1 was mild if at all. The flutter was also facilitated by the larger axial clearances present while the OCR gap widths varied the gas flow from the 2nd land through the 2nd ring gap and in the 3rd land through the OCR gap, causing mass flow rate spikes when the OCR moved up and down within the groove, pumping gases in and out of it. All had lower 2nd land pressure due to the presence of a V-Cut while C2 had the most OCR flutter during the expansion stroke, followed by C3 and virtually none for C1. At high load, the average blowby values were again similar for all the designs, though the OCR flutter from C2 and C3 causes oscillations in the blowby map. This time, even C1 experienced OCR flutter, but the relative magnitudes were the same as before – first C2, then C3, then C1.

3.4.3.2 Engine Speed: 2500RPM

The average blowby values are all on par with each other under low load. C2 and C3 experience the same kind of OCR flutter in the expansion stoke as was seen during 1500RPM, causing similar blowby map oscillation. This caused the 2nd ring to drop down due to the 3rd land pressure drop from the gas release through the OCR. C1 had the lowest 2nd land pressure overall. Like before, judging by the mass flow rates, the OCR acts as a pump for Region I and Region II, while also causing more of a dynamic twist on the 2nd ring due to the pressure changes. Similar trends persist at 500mbar, where the OCR pumping causes more flow through the 2nd ring and OCR grooves rather than through their gaps as seen with C1. At 700mbar, C1 experiences minor flutter, but nothing compared to the level of C2 or C3. Again pressure oscillations are seen on the 2nd and 3rd lands due to the flutter and smaller gaps of the C2 and C3

OCRs. This causes less of a pressure build up on the 2nd land and so the 2nd ring moves to the bottom of the groove later in the cycle for C1 versus C2 or C3.

3.4.3.3 Engine Speed: 3500RPM

At low loading, the blowby is very large for all three designs, mainly due to the top ring flutter (during the compression stroke) from the negative dynamic twist it experiences and the resulting radial collapse of the 2nd ring. Due to a smaller amount of radial collapse of the 2nd ring for C2, the blowby is lower than that of C1 or C3. Like noted earlier, more flow went through the U-flex gaps of C3, while more flowed through the OCR grooves of C1 and C2. When 500mbar was analyzed, the blowby trends for each exhibited those found at 1500 and 2500RPM – the averages for each were similar, with oscillations caused by OCR flutter in the descending order of magnitude like before: C2, C3, and C1. Also repeating were the smaller 2nd and 3rd land pressure traces of C1 versus that of C2 or C3. All of these trends continued at 700mbar.

3.4.3.4 Engine Speed: 4500RPM

Like at 3500RPM, the low load encountered for the three ring packs produced high blowby values due to top ring flutter and 2nd ring radial collapse. In this scenario, the blowby numbers were higher for C2 and C3 versus that of C1, mostly due to the smaller radial collapse experienced by C1, thus decreasing the flow area encountered. At 500mbar, similar trends that were seen at 3500RPM for the same loading are evident. Similar average blowby values with OCR flutter from C2 and C3 and lower 2nd and 3rd land pressures for C1.

Chapter 4: Piston Ring Pack Design Effects

4.1 The Effects of a 2nd Land V-Cut

Judging by the results of *Chapter 3*, the effects of the V-Cut on the 2nd land of the piston are both beneficial and a hindrance. From the data recorded, it is evident that the engine speed has no direct effect on the gas and ring dynamics of the piston-ring-pack when considering the use of the V-Cut. Ring dynamics and gas flow observed at a specific engine load and lower speed were surveyed at the same engine load at a higher speed. The only effect of a V-Cut occurs at 1500RPM, where the residence time and low pressure of the 2nd land for the V-Cut piston caused higher pressure in the 2nd land during the expansion stroke. The combination of lower gas pressure during the expansion stroke and higher gas pressure during exhaust stroke for the 2nd land caused top ring flutter and, thus, is undesirable. This reverse flutter causes some reverse gas flow and, with it, possibly oil consumption due to oil entrainment associated with gas travel through the piston-ring-pack. It is hypothesized that the V-Cut, added to lower the pressure on the 2nd land, would act dually as storage for oil that is thrown up by the piston's inertia. This storage design goal may have been reached by the slight drop in the oil consumption measurements viewed in *Chapter 3* upon operation with increasing speed up to 3500RPM for all loading conditions. However, drawing conclusions solely from the computer simulation shows that no such dependence exists.

Load is a major factor in the ring dynamics and the gas flow when dealing with the presence of a V-Cut on the 2nd land. At low load, 300mbar, the pressure traces and mass flow rates for both piston designs were virtually the same at all speeds. However, increasing to mid-load caused a lot of reverse blowby with the presence of a V-Cut. This is due to a similar scenario as at 1500RPM, however with a twist. Since, with a V-Cut design, the 2nd land pressure is less during most of the cycle with the added volume of the design. As such, the mass flow rate from the 2nd land through the 2nd ring gap to the 3rd land occurs at a slower rate. This causes the 2nd land to be at a higher pressure at the end of the expansion stroke. When placed in combination with the inertia of speeds above 1500RPM, the pressure combats with the inertia much like the flutter during the compression and expansion strokes. Therefore, more oil can be consumed when reverse blowby gases drag the oil up into the combustion chamber. However, the drop in the 2nd land pressure does reduce the intensity and occurrence of 2nd ring radial

collapse, directly inducing high blowby flow into the crankcase. *Figure 4-1* shows an example of how reverse flutter occurs for a piston with a V-Cut, depicting key parts of the graph to focus on in terms of ring position and the land pressures. At the highest load, 700mbar, these trends continue. Without the V-Cut, there's greater 2nd ring radial collapse while with the V-Cut, reverse flutter ensues. *Figure 4-2* shows the differences between the two in terms of the radial collapse of the 2nd ring and the effects the lower pressure has on such an event.

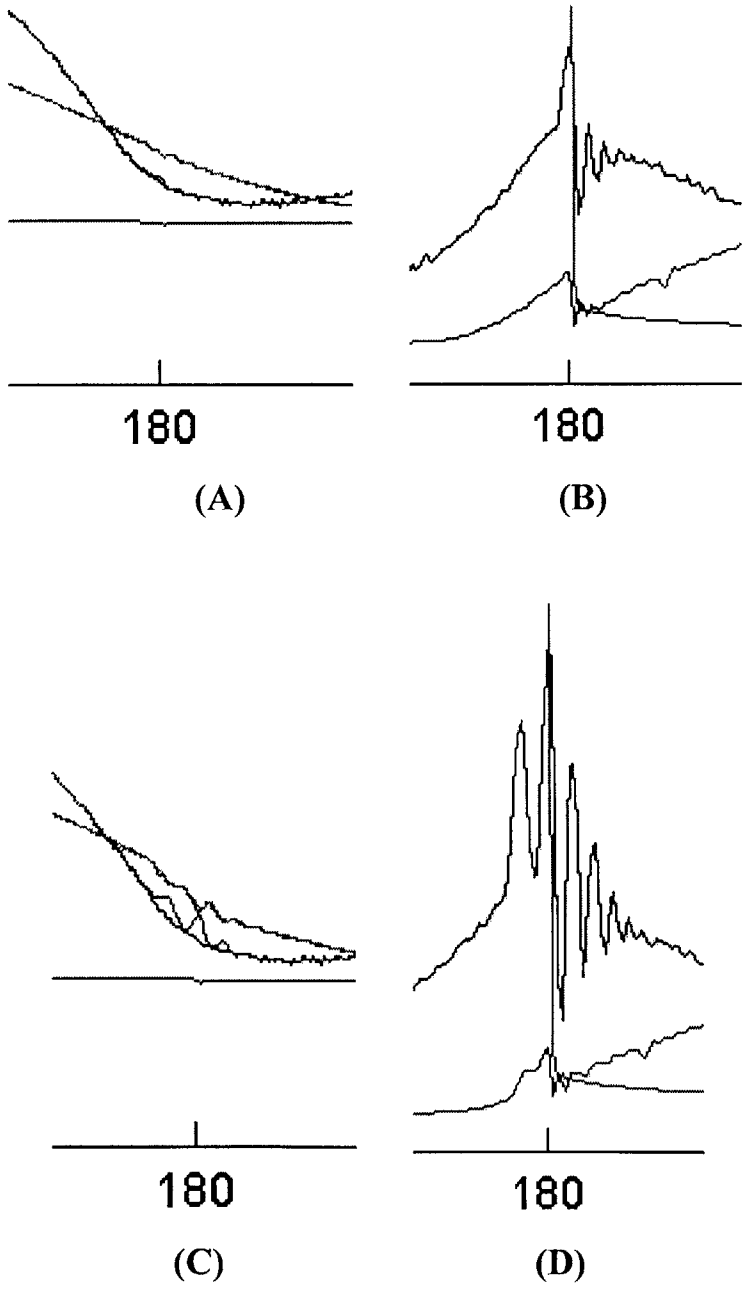

Figure 4-1 – An example of a top ring pressure trace and corresponding ring position within the groove during reverse flutter. Without the V-Cut, **(A)** the pressure trace for the 2nd land and crown land are normal and smooth while **(B)** the top ring experiences modest reverse flutter. As for the piston with the V-Cut, **(C)** the crown land experiences localized pressure peaks at times when the 2nd land pressure experiences valleys, while **(D)** a large amount of reverse flutter occurs for the top ring at the end of the expansion stroke, beginning of the exhaust stroke. The operating conditions shown here are 2500RPM and 500mbar.

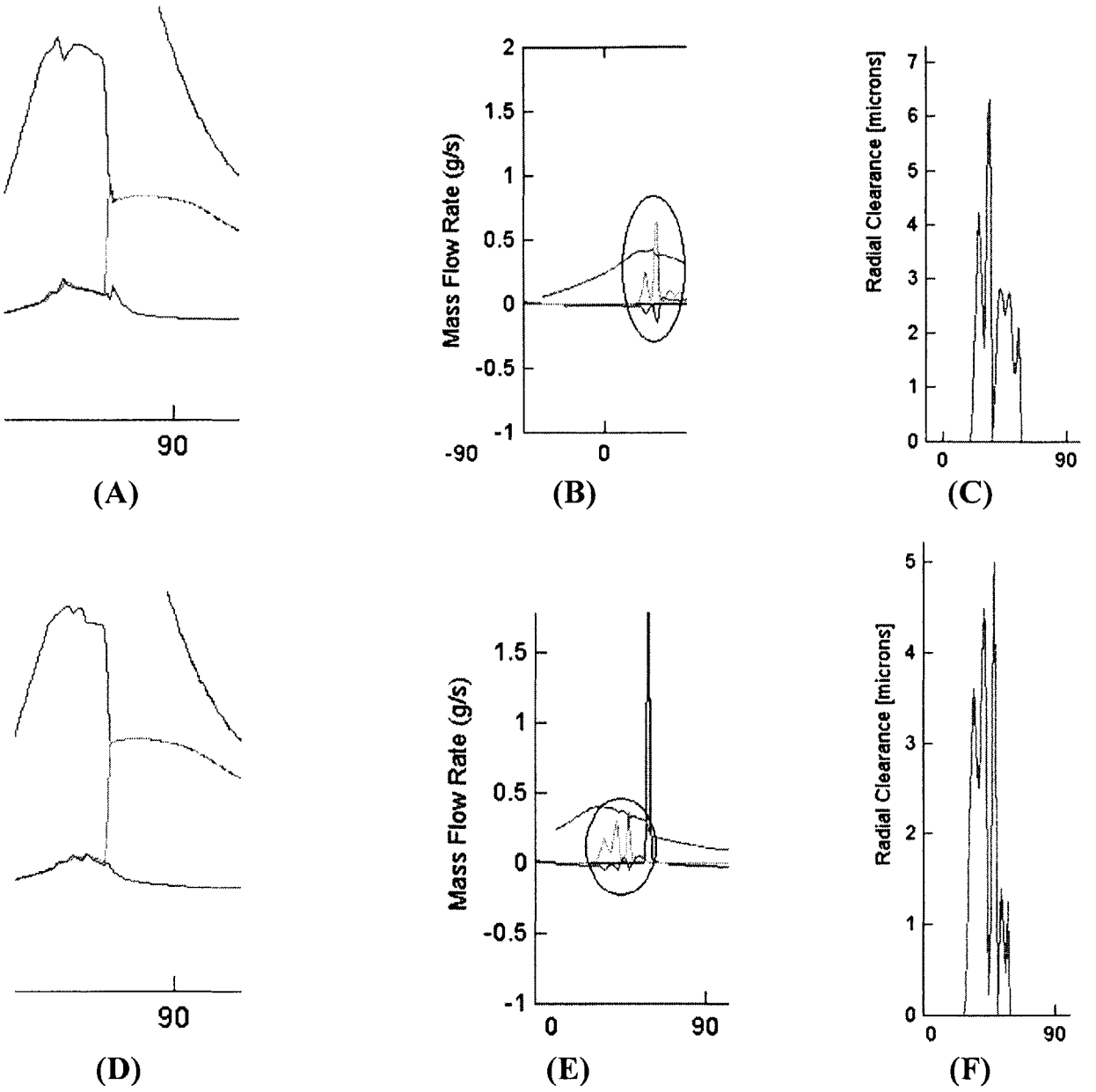

Figure 4-2 - An example of 2nd and 3rd land pressure traces, mass flow rates from the 2nd land to the 3rd land (circled in **(B)** and **(E)**), and the radial clearance of the ring's face from the liner during 2nd ring radial collapse. Without the V-Cut, **(A)** the pressure trace for the 2nd and 3rd land have noticeable spikes while **(B)** the mass flow rate from the 2nd land to the 3rd land by way of the ring-liner interface achieves large fluxes where the 2nd land pressure drops, and **(C)** the radial clearance between the 2nd ring and the liner is intense and frequent causing the 2nd land pressure to drop. For the piston with the V-Cut, **(D)** the 2nd and 3rd land experience milder pressure peaks, **(E)** less intense and frequent mass fluxes occur between the 2nd and 3rd lands, and **(F)** the radial clearance between the 2nd ring and liner doesn't reach the levels of **(C)**. The operating conditions shown here are 2500RPM and 700mbar.

It is unfortunate that Piston E wasn't tested prior to the engine's cessation. Otherwise, more concrete comparisons could be made with the aid of actual oil consumption values. However, we can see some generalization from the data of *Chapter 3*. Namely, at high loading for all speeds recorded, the oil consumption was far greater than at the lower loads, showing the dominance of reverse flutter in the part of the cycle examined. Additionally, at lower loads, the reverse flutter experienced is minimal, coupled with the lack of 2nd ring radial collapse. Depending upon the efficiency of the PCV system, the high blowby values associated with the lack of a V-Cut may increase the oil consumption of the engine versus that of oil entrainment from reverse flutter with V-Cut use.

4.2 The Effects of a 3rd Land Chamfer

In similar fashion with the simulations involving the V-Cut design of the piston, the gas flows and ring dynamics for the pistons invoking the chamfer on the upper region of the 3rd land were not speed dependent. However, the exception to this rule was at 3500RPM and low, 300mbar, loading. Here, the top and 2nd ring both experienced radial collapse towards the end of the expansion stroke in the piston-ring-pack employing the chamfer. As a result, the blowby was immense, though, after the collapse had ceased, the ring dynamics of the two ring pack designs were nearly identical. If such a scenario were to happen in a production engine, the crankcase would become pressurized, as well as the PCV system. The PCV system would become ineffective and thus the oil consumption of the engine would increase drastically. *Figure 4-3* below illustrates the conditions of the pistons as a comparison at these operating conditions.

The addition of the chamfer to the piston-ring-pack employing a Napier/scraper ring is done with two intentions in mind. First, the chamfer would provide an increase in the volume of the upper 3rd land to act as both an oil reservoir in the down-scraping process of the piston's motion. In the process, it is expected that such actions would assist in proper oil control along the liner and lands, leading to a reduction in oil consumption. Of course, the extra amount of oil present on the 3rd land can bridge to the liner, thus negating any oil consumption prevention that the chamfer may have had. The notion of proper oil control and the like isn't realized from the data provided in *Chapter 3*, whose trends are far from apparent with the up and down nature of the oil consumption measurements. From the model, it seems that the biggest factor affecting the chamfer's performance is the engine load at the given speed. This leads to the second

purpose of the chamfer: the decrease in 2nd ring flutter as well as the decrease in 2nd ring radial collapse by exposing more area of the 2nd ring to 3rd land pressure.

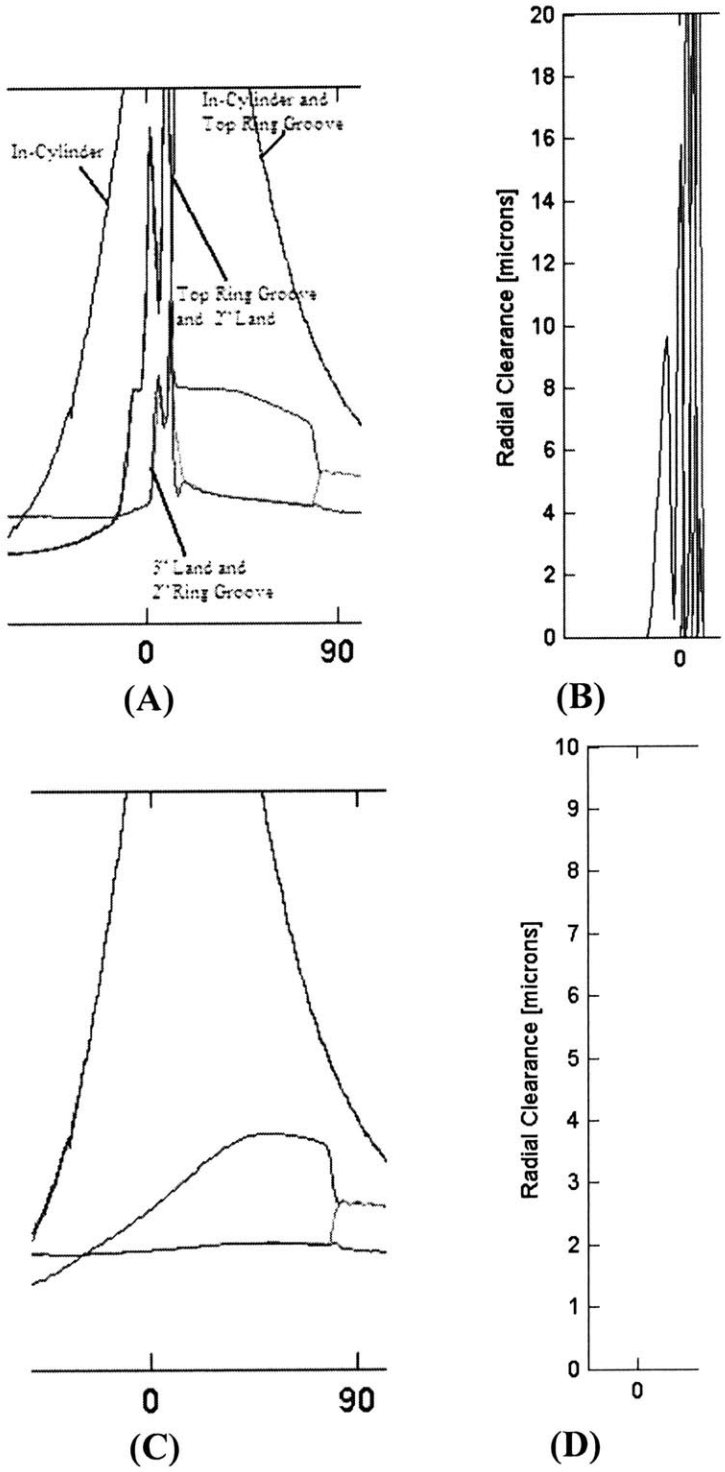

Figure 4-3 – The pressure traces and ring radial clearances from the simulation for the pistons with and without a chamfer. With the chamfer, **(A)** the pressures labeled experience in-cylinder values due to the radial collapse seen in **(B)** for both the top ring and 2nd ring. The piston without the chamfer has **(C)** normal low load pressure traces and **(D)** no radial collapse for either of the rings. The operating conditions shown here are 3500RPM and 300mbar.

At low load, with the exception of 3500RPM as stated, the chamfer effects are noticed fully by the ring dynamics and gas flow. First and foremost, the chamfer accomplishes its job of keeping the 2nd ring seated on the upper part of its groove thanks to the increase in the exposed area. In doing so, two physical phenomena occur: 1) the blowby of the chamfered piston is typically higher than the one without a chamfer, and 2) the 2nd and 3rd land pressures of the piston with a chamfer are less than those without a chamfer. These are interrelated, in that the 3rd land pressure is less due to the added volume the chamfer provides, while the 2nd land pressure decreases because the added pressure differential between the lands facilitates an increase in mass flow down towards the crankcase. The increased mass flow decreases the 2nd land pressure and thus increases the blowby of the piston ring pack. As the load is increased, some trends just mentioned remain the same, while new trends surface. The blowby values for the piston with a chamfer still remained higher and the 2nd and 3rd land pressures were lower than the piston without a chamfer. At the higher loads of course, the increase in 2nd land pressure brings with it 2nd ring radial collapse and reverse flutter of the top ring during the exhaust stroke. The chamfered piston experienced similar events on a much smaller scale, much like the V-Cut assisted in such occurrences. It is apparent from such data that the chamfer accomplishes its purpose of improving 2nd ring stability during the piston's normal operation, though not fully preventing radial collapse. However, unlike the V-Cut piston, the reverse flutter experienced by the chamfered piston was negligible if at all, while the piston without a chamfer had notable reverse flutter, owing to the higher 2nd land pressures. *Figure 4-4* presents the differences between the top ring's movement within the groove and the accompanying pressure traces.

Similarly to the testing of the V-Cut, it is unfortunate that Piston E wasn't tested prior to the engine's temporary shut down. Otherwise, more concrete comparisons could be made with the aid of actual oil consumption values. As such, no concluding generalizations can be made from the data of *Chapter 3*. The oil consumption measurements experienced up-and-down readings for all the loads measured, though the lower load seemed to experience higher oil consumption than the mid load. But, such conclusions as to why can't be formulated without the testing of Piston E and its lack of a chamfer.

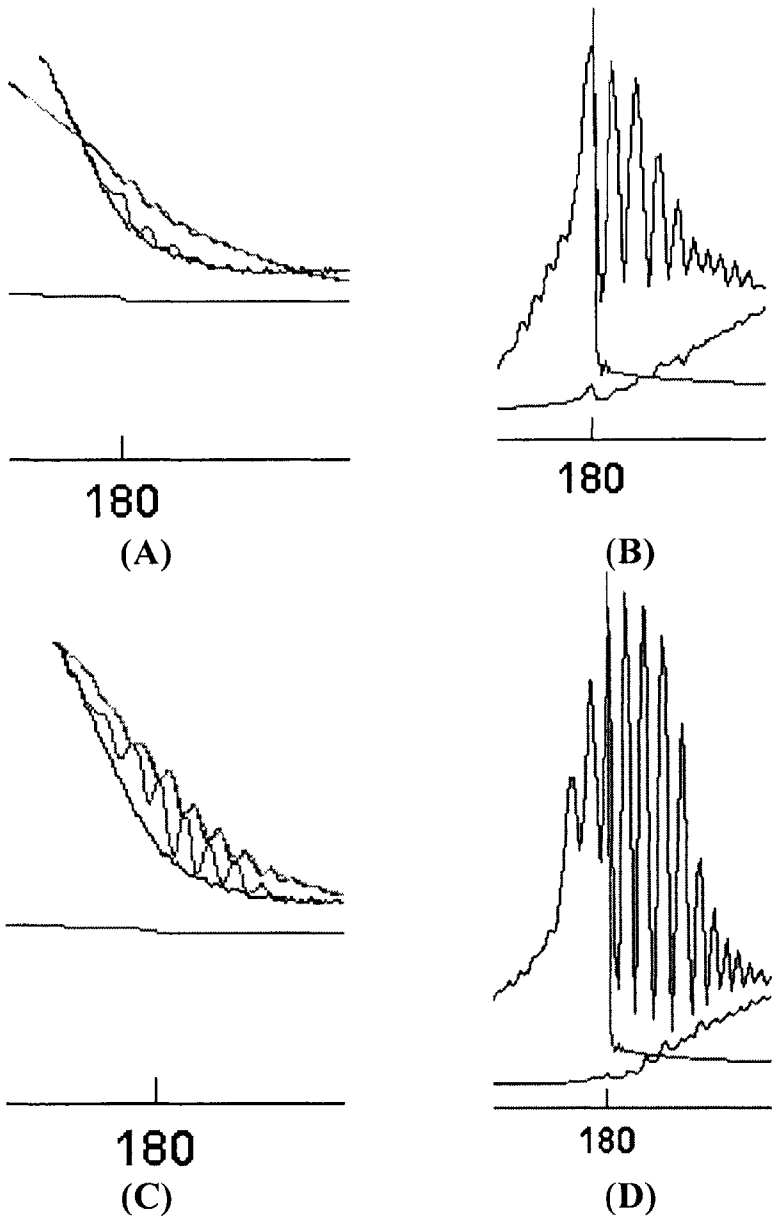

Figure 4-4 – An example of top ring pressure traces and corresponding ring positions within the groove during reverse flutter. With the chamfer, **(A)** the pressure trace for the 2nd land and crown land have some minor pressure oscillations due to **(B)** the top ring experiencing modest reverse flutter. As for the piston without the chamfer, **(C)** the crown land experiences large localized pressure peaks at times when the 2nd land pressure experiences deep valleys. This is attributed to **(D)** a large amount of reverse flutter occurs for the top ring at the end of the expansion stroke, beginning of the exhaust stroke. The operating conditions shown here are 2500RPM and 700mbar.

4.3 The Effects of the Oil Control Ring Design

The use of different oil control rings is very important from a cost perspective. If similar performance characteristics can be reproduced with use of a 3-piece or 2-piece design that a U-flex one has, the 3-piece or 2-piece oil control ring would be used due to their cheaper manufacturing cost. However, performance differences do exist, and it's inopportune that the comparisons weren't performed experimentally. The only data available is that of the piston-ring-pack that makes use of the U-flex oil control ring. From the recorded data, the only trend that stands out that will be made note of later on is the dependency of the oil consumption on

load more so than speed. At wide-open-throttle, the oil consumption of the ring pack is many times greater than that of the low loads tested. The speed dependency isn't fully realized, and without other tests, conclusions cannot be made.

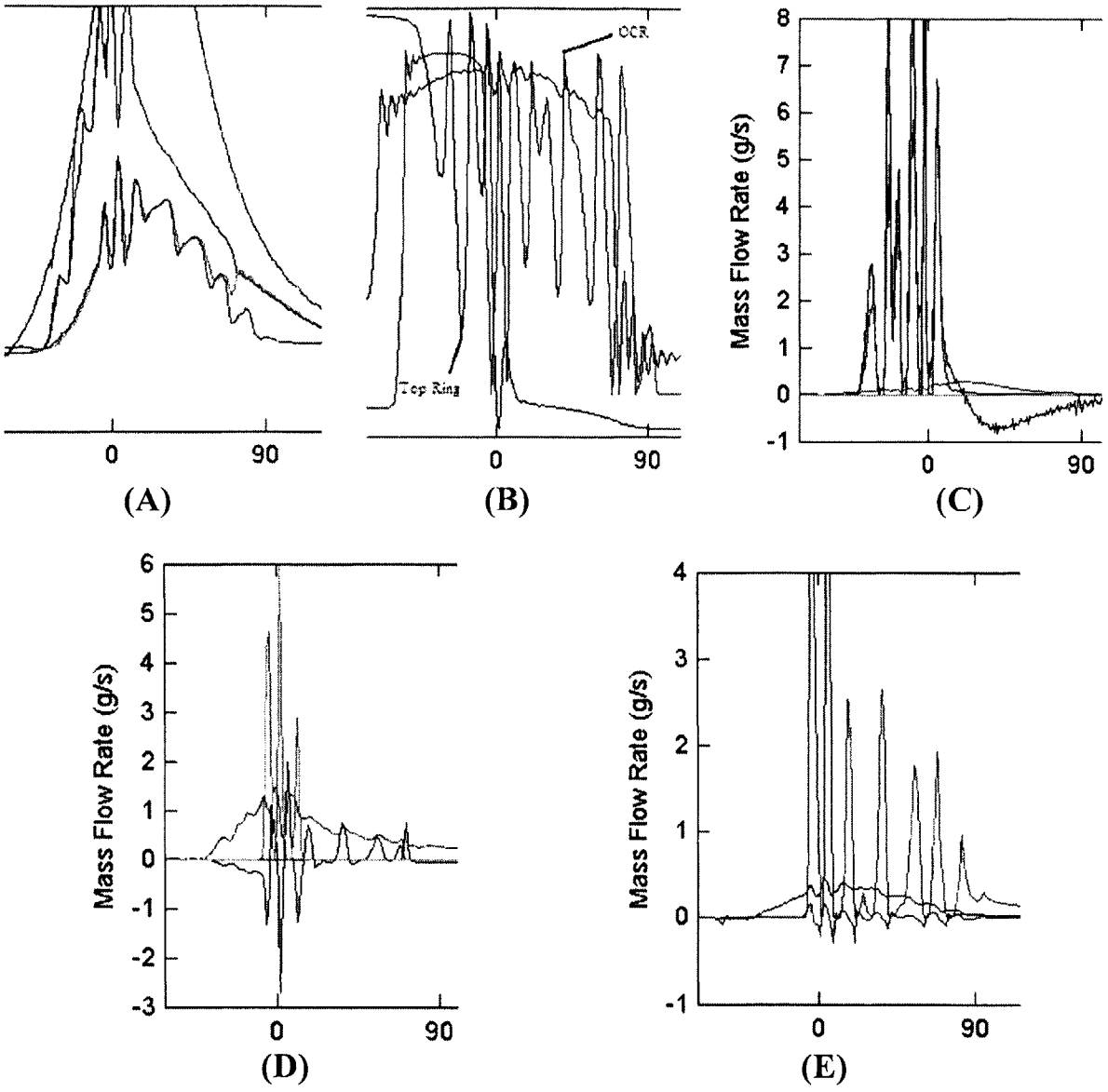

Figure 4-5 – The pressure traces, ring positions, and mass flow rates through select regions for the piston-ring-pack employing the 2-piece oil control ring. **(A)** Large pressure oscillations fill the 2nd and 3rd lands in addition to all of the ring grooves due to the **(B)** top ring's flutter and the OCR flutter. As a result of the top ring flutter, **(C)** a large amount of gas flows through the top ring groove to the 2nd land, while **(D)** the 2nd ring's radial collapse causes high mass flow rates through the ring-liner interface to the 3rd land. Finally, the high pressures and the OCR oscillation **(E)** cause gas flow through the OCR groove down towards the crankcase. Operating conditions shown are 3500RPM and 300mbar.

However, the computer simulations show that speed does play a factor in the ring pack's control, though not necessarily on the use of the oil control ring. To be mentioned here solely in passing, the ring packs tested employed a barrel-faced top ring with no static twist. As discussed in *Chapter 1*, such a design experiences extreme flutter conditions at higher speeds (3500RPM and up for this specific design) and low loads (300mbar). *Figure 4-5* shows how this looks with the given pressure traces, ring radial clearance, and the mass flow rates through select areas. This phenomenon of top ring flutter aside, the engine speed, as far as the models are concerned, is not a major factor in the performance of the oil control ring design. Rather, the loading conditions that the piston-ring-pack is subjected to play a larger, more definite role in the OCR's performance characteristics.

No matter the loading conditions, the 2-piece and 3-piece oil control rings experienced a much greater amount of flutter than the U-flex. As a result, the blowby maps reflected the oscillations in gas flow to the crankcase accordingly. At low loading, 300mbar, the U-flex had no flutter, more than likely attributed to similar reason discussed in [7]. Namely, the U-flex has a larger number of gaps, distributed evenly around its circumference. The increase in the total gap area releases the gas pressure of the 3rd land more effectively. Further, judging by the mass flow plots produced by the computer program, more goes through the "gap" than through the OCR groove. As with the 3rd land chamfer discussed earlier, the drop in the 3rd land pressure also facilitates a drop in the 2nd land pressure by way of mass flow. The other rings' gap areas are far less, forcing the gases to flow through their respective groove and case the oscillations seen in *Figure 4-6*. Another design variable that may have caused the increase in OCR flutter is the increase in the axial distance from the OCR flank of the 2-piece or 3-piece to the ring groove surface. The increase in this dimension makes it possible for the ring to experience more axial movement within its respective groove and allow more gases to enter/exit during operation. This increased gas flow area plays an additional role in the ring's dynamics.

As the load is increased for all speeds examined, the amount of flutter viewed for each ring design increases as well as the pumping of gases down towards the crankcase. In summation, the U-flex has the best stability and pumping characteristics of the three tested, decreasing blowby while not increasing the notion of reverse gas flow. The decrease in blowby, depending upon the efficiency of the PCV system, would have a favorable effect on the engine's total oil consumption. Cost really does follow function and performance.

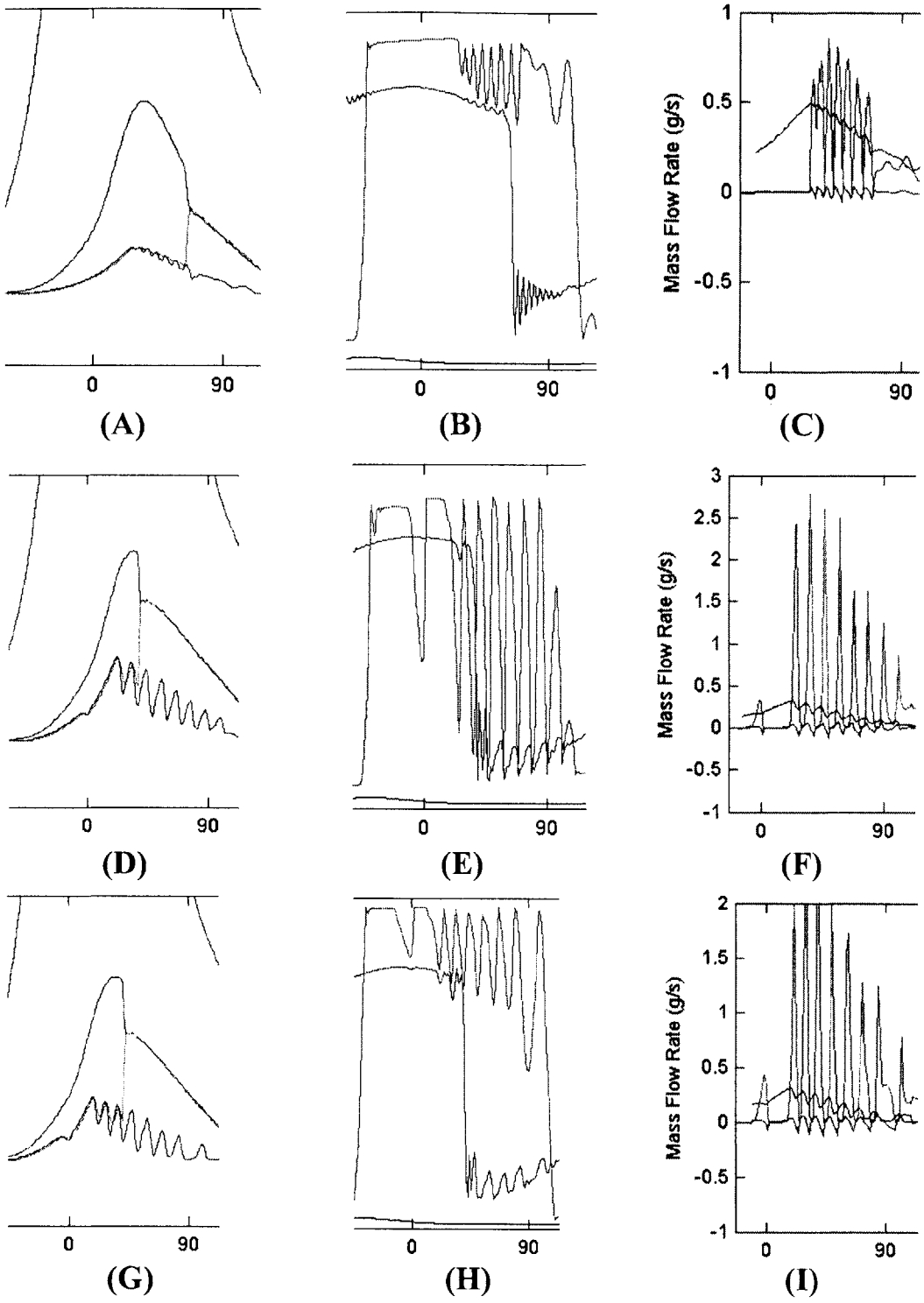

Figure 4-6 – The pressure traces of the 3rd and 2nd lands, the ring position of the OCR within its groove, and the amount of mass flowing through the OCR groove are illustrated above. The U-flex **(A)** 3rd land pressure is rather stable with **(B)** minor OCR flutter and corresponding **(C)** small groove gas flow. Similar graphs for the 2-piece **(D)**, **(E)**, and **(F)**, and the 3-piece **(G)**, **(H)**, and **(I)** show more oscillations with greater peaks all at 2500RPM and 700mbar.

4.4 The Effects of Oil Control Ring Groove Drain Holes: Limited Analysis

Regrettably, the data accrued from the experimental tests was cut short when studying the piston that lacked OCR groove drainage holes. Therefore, it wasn't possible to make direct comparisons to the oil consumption measurements recorded for the piston with OCR groove drainage holes. Even if the data was completed, reasonable conclusions would not have been able to be drawn properly without the "musical chairs" of the pistons between the cylinders in order to account for the bore distortion. Additionally, the computer simulation models used do not account for the presence of groove drainage holes. However, some hypotheses can still be made. First, the accumulation of oil on the 3rd land is traditionally drained through, with the aid of the pumping action of the oil control ring, the drainage holes present on the back of the groove. This was discussed earlier in *Chapter 1*. As such, at lower loads, the oil isn't able to pump the OCR effectively for proper oil transport to the crankcase. The oil pools on the 3rd land, not being able to drain through the groove, and can bridge to the liner, causing a marked increase in oil consumption. This was viewed in *Chapter 3*. At higher loads, such mechanisms aren't as important since most of the flow goes through the gaps of the U-flex rather than around the OCR and through the groove. Future experiment should test this with other OCR designs.

(This page was intentionally left blank)

Chapter 5: Conclusions

The thesis was intended to be an experimental study on the effects of piston-ring-pack design changes on the steady-state and transient oil consumption of a spark ignition engine. However, after some minor measurements for a given engine configuration at steady-state, the engine experienced a major malfunction that cause it to cease operation. As such, the focus of the study shifted to a more theoretical, computer-simulated concentration of the aforementioned design changes to be examined. Different speeds and loads were analyzed along with some general observations made with regards to the different piston-ring-packs used. In the end, the direct effect of the design modifications on ring dynamics and gas flow were qualified, while indirect assumptions were made as to the effects this would have on oil consumption. Namely, the effects of a V-Cut on the 2nd land, a chamfer on the 3rd land, OCR groove drain holes, and the design of the OCR were examined.

As previously intended, a robust and effective measurement system was setup on a four-cylinder 2.0L spark ignition engine. External control of oil temperature, coolant temperature, and the recording of in-cylinder variables led to a more complete understanding of the environment with which the oil was transporting through. Such variables included the liner temperature at two different axial locations, the land pressures at two locations, and the combustion chamber pressure. These measurements, along with the real-time oil consumption values of individual cylinders, were collected by a data acquisition system. The real-time oil consumption values were generated with the aide of a sulfur-trace method, a sulfur-dioxide analyzer, and the use of exhaust taps placed on each exhaust manifold runner. Additionally, the blowby of the engine was also recorded to confer with previous research done on the same engine.

Before the engine ceased operation, oil consumption measurements were recorded during steady-state operation for three different piston designs and partially of fourth design. The operating conditions of the engine at steady-state tallied a total of fifteen points: five different speed (1500 to 3500RPM in 500RPM intervals) and three different load (350, 650, and 950mbar). Unfortunately, no transient traces were created, though some examples of preliminary tests were included. Thus, with the operation of the engine put into question and requiring months of down time before it would become fully functional, computer simulation

codes were utilized. The models required the in-cylinder measurements as input as well as the dimensions of the piston-ring-packs to be tested. Unfortunately, the engine loads used for the simulations were 300, 500, and 700mbar, while the speeds were 1500, 2500, 3500 and 4500RPM. Regardless, the ring dynamics and gas flow were illustrated and qualities of each design were deduced.

The presence of a V-Cut on the 2nd land of the piston had beneficial and adverse effects on the general performance of the ring pack. The added volume decreased the 2nd land pressure enough to avoid 2nd ring radial collapse. This decreased the amount of blowby experienced by the engine and, thus, would assist in the PCV system's performance. However, the added volume also caused reverse flutter to occur at lower loads, which is a direct pathway to increased oil consumption due to oil's entrainment by the gasses. Speed dependence wasn't realized, though load dependence is apparent. At higher loads, the V-Cut's role is minimal. Depending upon the efficiency of the PCV system, the high blowby values associated with the lack of a V-Cut may increase the oil consumption of the engine versus that of oil entrainment from reverse flutter with V-Cut use.

Using a chamfer on the upper portion of the 3rd land also has mixed results. By exposing more of the 2nd ring to the 3rd land pressure, stability of the ring is greatly improved. At lower loads, blowby of the chamfered piston is typically higher than the one without a chamfer since the 2nd and 3rd land pressures of the piston with a chamfer are less than those without a chamfer. Much like the V-Cut, the chamfer diminishes radial collapse at most speeds, though not fully preventing it. However, unlike the V-Cut piston, the chamfered piston experiences negligible reverse flutter. As such, the 3rd land chamfer seems to be better suited towards oil consumption prevention, with the corollary that the PCV system is effective for higher values of blowby flow.

Aside from the weight differences between the oil control rings tested during for the simulation, the biggest design issues were their clearance within the grooves and their gap width. The U-flex, with the larger overall "gap" width, fluttered less and produced less blowby fluctuation than the 2-piece or 3-piece rings OCRs. This added stability in the 3rd land and eased the overall pressure distribution throughout the ring pack. Additionally, the larger gap area of the U-flex provided areas for leakage to the crankcase. With the addition of larger groove clearances for the 2-piece and 3-piece rings came the increase in mass flow into and out of the grooves. With smaller gaps widths through which the gases were able to pass through, the mass

flux into the OCR grooves for the 2-piece and 3-piece was far greater than for the U-flex. Furthermore, the added pumping that occurs with increasing engine speed increased mass flow towards the crankcase for the 2- and 3-piece. As such, these large spikes in the blowby flow through the PCV system would render it ineffective at times, increasing oil flow to the fresh charge for combustion. Thus, for proper oil control, the U-flex ring is the OCR of choice. It shouldn't be neglected that the U-flex is priced accordingly, being more expensive than the other two. The final note can be made with regards to the existence of OCR drainage holes. Their use is imperative for proper oil control at any operating condition, especially low loads, in order to drain the excess oil from the 3rd land. Without their employment, bridging and high oil consumption can occur. Both have been observed in previous studies.

This research, though theoretical in nature, brings together many ideas that offer solutions to common problems. Radial collapse, reverse flutter, OCR cost, and the use of drainage holes all are part of the attempts to improve the piston-ring-pack performance while driving down the cost of production. By using oil consumption and friction as benchmarks for performance, a better ring pack can be designed and put to use in production engines. It is with hopes that future experiments will test these theoretical conclusions with the continuation of the pistons not installed in the engine due to the events previously explained.

(This page was intentionally left blank)

References

[1] Brown, M. A.; McCann, H.; Thomspon, D. M.: "Characterization of the Oil Film Behaviour Between the Liner and Piston of a Heavy-Duty Diesel Engine," SAE Paper 932784, 1993.

[2] Heywood, J.B., Internal Combustion Engine Fundamentals, McGraw-Hill, 1988.

[3] Yoshida, H.; Yamada, M.; Kobayashi, H.: "Diesel Engine Oil Consumption Depending on Piston Ring Motion and Design," SAE Paper 930995, 1993.

[4] Burnett, P.J.: "Relationship Between Oil Consumption, Deposit Formation and Piston Ring Motion for Single-Cylinder Diesel Engines," SAE Paper 920089, 1992.

[5] Wilkins, A., J., J.; Hannington, N., A.; Matthey, J.: "The Effect of Fuel and Oil Additives on Automobile Catalyst Performance: The Suitability of Platinum Metals Confirmed," Platinum Metals Rev., Vol. 34, Issue 1, pp. 16-24, 1990.

[6] Froelund, K.: "Real-Time Steady-State Measurement of PCV-Contribution to Oil Consumption on Ford 4.6L SI-Engine," SAE Paper 2000-01-2876, 2000.

[7] Yilmaz, E.: "Sources and Characteristics of Oil Consumption in a Spark-Ignition Engine," Ph.D. Thesis, Department of Mechanical Engineering, MIT, September 2003.

[8] Furuhama, S.; Hiruma, M.; Tsuzita, M.: "Piston Ring Motion and Its Influence on Engine Tribology," SAE Paper 790860, 1979.

[9] Stecher, F.: "Analysis of Piston Ring Packs for Combustion Engines," SAE Paper 790863, 1979.

[10] McGeehan, J. A.: "A Survey of the Mechanical Design Factors Affecting Engine Oil Consumption," SAE Paper 790864, 1979.

[11] Hill, S. H.: "Cylinder Bore Finishes and Their Effect on Oil Consumption," SAE Paper 2001-01-3550, 2001.

[12] Hitosugi, H.; Nagoshi, K.; Komada, M.; Furuhama, S.: "Study on Mechanism of Lubricating Oil Consumption Caused by Cylinder Bore Deformation," SAE Paper 960305, 1996.

[13] Orrin, D. S.; Coles, B. W.: "Effects of Engine Oil Composition on Oil Consumption," SAE Paper 710141, 1971.

[14] Yilmaz, E.; Tian, T.; Wong, V. W.; Heywood, J. B.: "The Contribution of Different Oil Consumption Sources to Total Oil Consumption in a Spark Ignition Engine," SAE Paper 2004-01-2909, 2004.

[15] Yilmaz, E.; Tian, T.; Wong, V. W.; Heywood, J. B.: "An Experimental and Theoretical Study of the Contribution of Oil Evaporation to Oil Consumption," SAE Paper 2002-01-2684, 2002.

[16] Thirouard, B.; Tian, T.: "Oil Transport in the Piston Ring Pack (Part I): Identification and Characterization of the Main Oil Transport Routes and Mechanisms," SAE Paper 2003-01-1952. 2003.

[17] Thirouard, B.; Tian, T.: "Oil Transport in the Piston Ring Pack (Part II): Zone Analysis and Macro Oil Transport Model," SAE Paper 2003-01-1953. 2003.

[18] Thirouard, B.; Tian, T.; Hart, D. P.: "Investigation of Oil Transport Mechanisms in the Piston Ring Pack of a Single Cylinder Diesel Engine, Using Two Dimensional Laser Induced Fluorescence," SAE Paper 982658. 1998.

[19] Przesmitzki, S.; Vokac, A.; Tian, T.: "An Experimental Study of Oil Transport between the Piston Ring Pack and Cylinder Liner," SAE Paper 2005-01-3823, 2005.

[20] Yilmaz, E.; Thirouard, B.; Tian, T.; Wong, V. W.; Heywood, J. B.; Lee, N.: "Analysis of Oil Consumption Behavior during Ramp Transients in a Production Spark Ignition Engine," SAE Paper 2001-01-3544, 2001.

[21] Vokac, A.; Tian, T.: "An Experimental Study of Oil Transport on the Piston Third Land and the Effects of Piston and Ring Designs," SAE Paper 2004-01-1934, 2004.

[22] Nakashima, K.; Ishihara, S.; Urano, K.; Murata, K.: "A Study on Lubricating Oil Flow into the Combustion Chamber for the Top Ring with a Special Joint," SAI Paper 982441, 1998.

[23] Min, B.S.; Kim, J. S.; Oh, D. Y.; Choi, J. K.: "Dynamic Characteristics of Oil Consumption – Relationship Between the Instantaneous Oil Consumption and the Location of Piston Ring Gap," SAE Paper 982442, 1998.

[24] Tian, T.: "Modeling the performance of the Piston Ring-Pack in Internal Combustion Engines," Ph.D. Thesis , Department of Mechanical Engineering, MIT, June 1997.

[25] Tian, T.; Wong, V. W.; Heywood, J.B.: "A Piston Ring-Pack Film Thickness and Friction Model for Multigrade Oils and Rough Surfaces," SAE Paper 962032, 1996.

[26] Tian, T.: "Dynamic behaviours of piston rings and their practical impact. Part 1: ring flutter and ring collapse and their effects on gas flow and oil transport," Proc. Instn Mech Engrs, Vol. 216, Part J, Journal of Engineering Tribology, pp. 209-228, 2002.

[27] Tian, T.; Wong, V. W.; Heywood, J.B.: "Modeling the Dynamics and Lubrication of Three Piece Oil Control Rings in Internal Combustion Engines," SAE Paper 982657, 1998.

[28] Liu, L.; Tian, T.: "Modeling Piston Ring-Pack Lubrication With Consideration of Ring Structural Response," SAE Paper 2005-01-1641, 2005.

[29] Cho, Y.; Tian, T.: "Modeling Engine Oil Vaporization and Transport of the Oil Vapor in the Piston Ring Pack of Internal Combustion Engines," SAE Paper 2004-01-2912, 2004.

[30] Jocsak, J; Li, Y.; Tian, T.; Won, V. W.: "Modeling and Optimizing Honing Texture for Reduced Friction in Internal Combustion Engines," SAE Paper 2006-01-0647, 2006.

[31] Thirouard, B.: "Characterization and Modeling of the Fundamental Aspects of Oil transport in the Piston-Ring Pack of Internal Combustion Engines," Ph.D. Thesis, Department of Mechanical Engineering, MIT, May 2001

[32] Yost, D. M.; Frame, E. A.: "Evaluation of High-Temperature Diesel Engine Liquid Lubricants," SAE Paper 952544, 1995.

[33] De Petris, C.; Giglio, V.; Police, G.: "A Mathematical Model of the Evaporation of the Oil Film Deposed on the Cylinder Surface of IC Engines," SAE Paper 972920. 1997.

[34] Warrick, F.; Dykehouse, R., "An Advanced Radiotracer Technique for Assessing and Plotting Oil Consumption in Diesel and Gasoline Engines," SAI Paper 700052, 1970.

[35] Ariga, S.: "Observation of Transient Oil Consumption with In-Cylinder Variables," SAE Paper 961910, 1996.

[36] Iijima, N.; Miyamoto, T.; Takiguchi, M.; Kai, R.; Sato, M.: "An Experimental Study on Phenomena of Piston Ring Collapse," SAE Paper 2002-01-0483, 2002.

[37] Automobiles Citroën: Direction Export Europe, Documentation Après Vente. January 1998. Moteur: Moteurs XU – Révision, Réf. BRE0384F. Société Anonyme, Inc.

[38] Weng, W.; Richardson, D. E.: "Cummins Smart Oil Consumption Measuring System," SAE Paper 2000-01-0927, 2000.

[39] Meriam Instrument. March 1993. Laminar Flow Elements: Installation & Operation Instructions. Cleveland, Ohio.

[40] Antek Instruments, Inc. August 1997. Operating Manual: Model R 6000 SE Sulfur in Exhaust Gas. Houston, TX.

(This page was intentionally left blank)

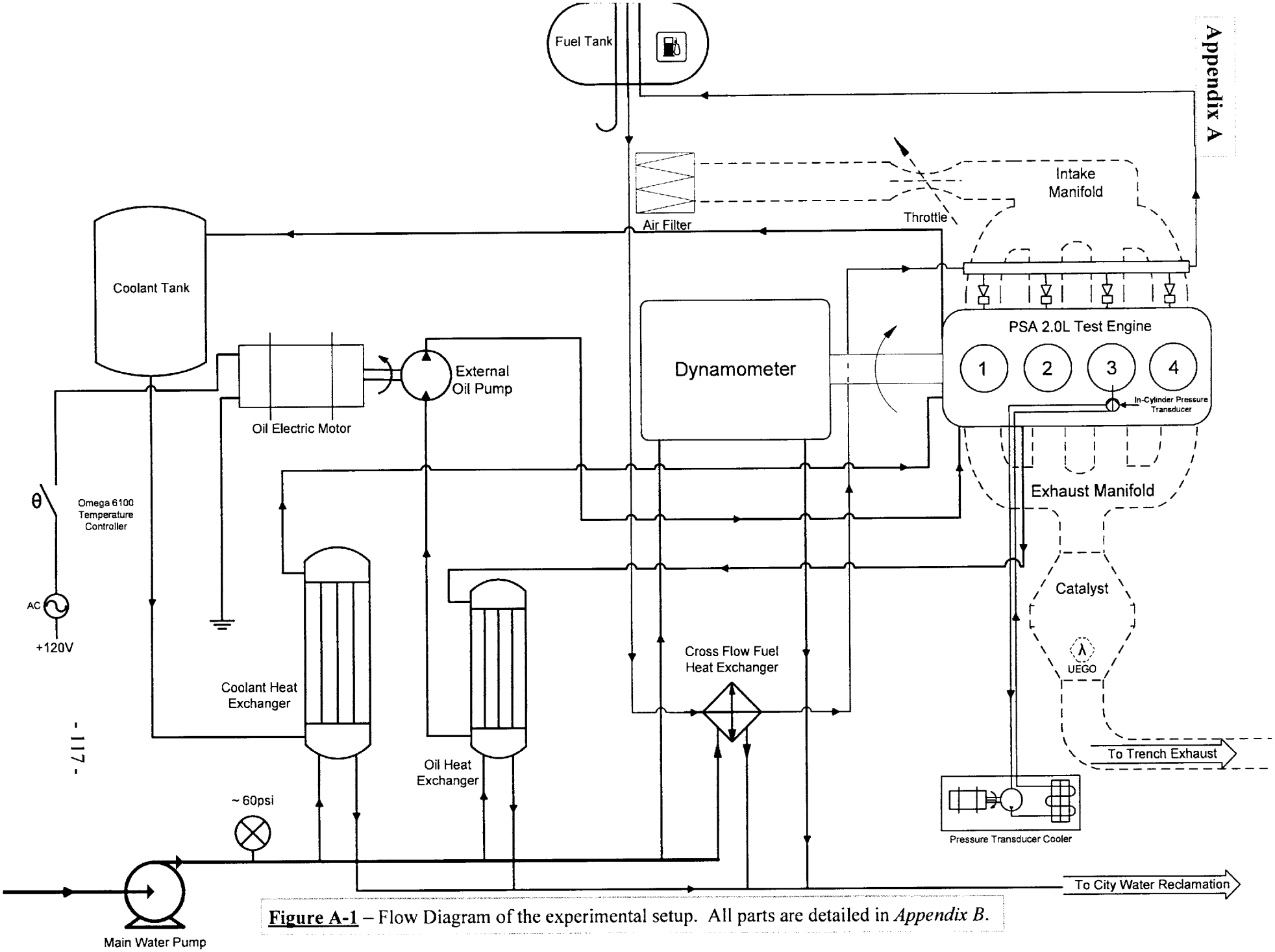

Figure A-1 – Flow Diagram of the experimental setup. All parts are detailed in *Appendix B*.

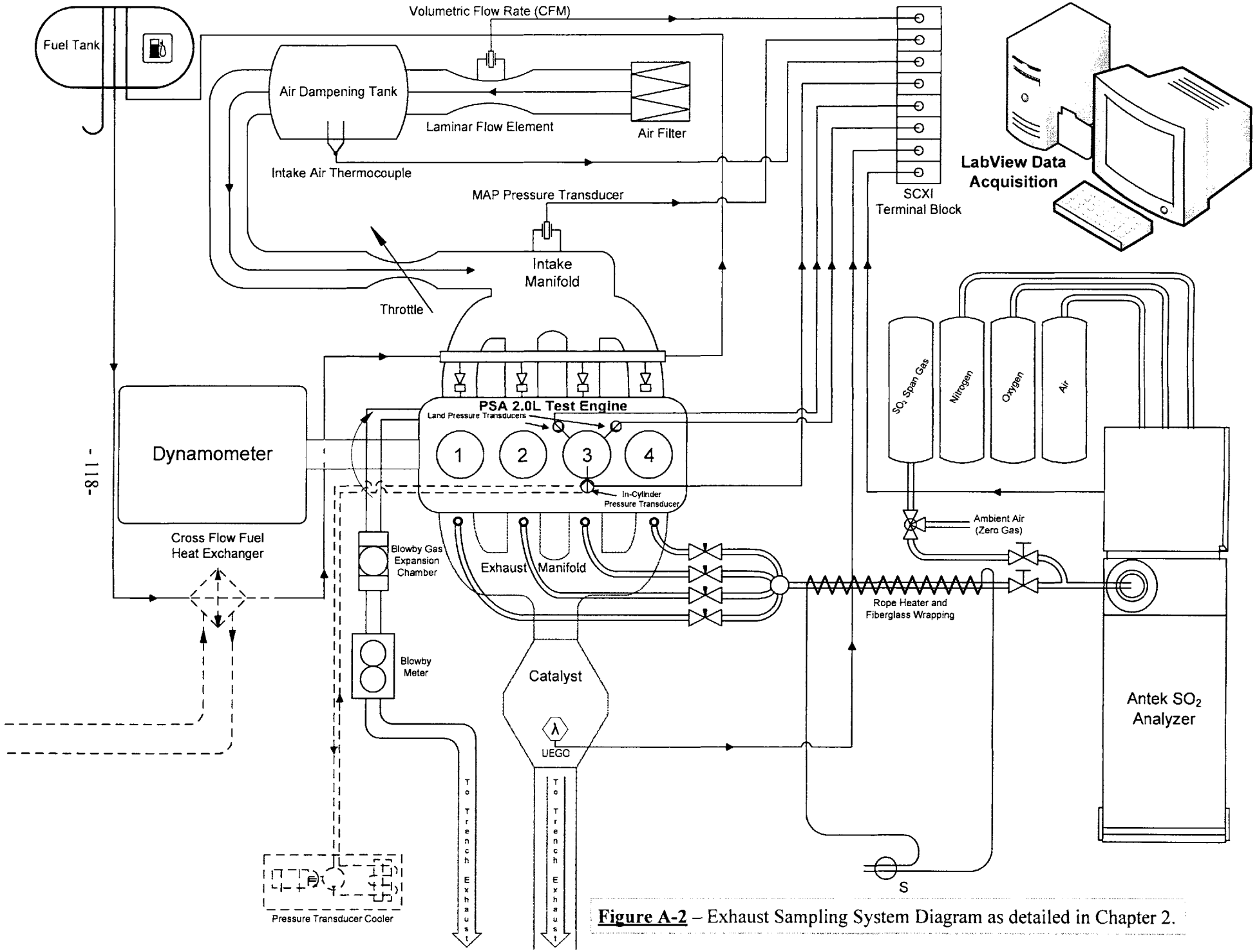

Figure A-2 – Exhaust Sampling System Diagram as detailed in Chapter 2.

Appendix B

Coolant Heat Exchanger	
Manufacturer	American Industrial Heat Transfer Inc.
Model No.	AB-703-C4-EP-TP 1194
Serial No.	42687
Shell Pressure	250psi (max)
Tube Pressure	150psi (max)
Temperature	350°F (max)

Table B-1 – Specifications of the heat exchanger used on the engine coolant.

Coolant Regulator Valve for Heat Exchanger	
Manufacturer	Sterlco, Inc.
Type	56T
Range	140°F - 240°F
Pipe Size	5/8" NPT

Table B-2 – Specifications of the regulator valve for the heat exchanger in *Table B-1*.

Oil Heat Exchanger	
Manufacturer	American Industrial Heat Transfer Inc.
Model No.	AA-624-4-4-TP 694
Serial No.	36907
Shell Pressure	250psi (max)
Tube Pressure	150psi (max)
Temperature	350°F (max)

Table B-3 – Specifications of the heat exchanger used to cool the engine oil in the pan.

Oil Heat Exchanger Pump	
Manufacturer	Viking Pump, Inc.
Model No.	F432
Serial No.	10450609

Table B-4 – Specifications of the pump that pushes the oil through the heat exchanger in *Table B-3*.

Oil Heat Exchanger Universal Electric Motor	
Manufacturer	MagneTek
Part No.	HG2P021
Serial No.	36F 73477A
Stock No.	934
Power	$^1/_3$ HP
Speed	1725RPM
Voltage	115V
Frequency	60Hz
Amps	6A

Table B-5 – Specifications of the electric motor that drove the oil pump described in *Table B-4*.

Rope Heater	
Manufacturer	Omega Engineering, Inc.
Model No.	HSK-11572A
Length	10ft.
Power	1200W
Input Voltage	120VAC

Table B-6 – Specifications of the rope heater used on the exhaust sample line illustrated in *Appendix A*.

Laminar Flow Element	
Manufacturer	Meriam Instrument
Model	50MH10-4
Serial No.	740211-G1
Gas	Air
Flow	162.66CFM@8"H2O
Calibration Conditions	70°F & 29.92" Hg Abs.

Table B-7 – Specifications of the flow restriction used to measure the mass air flow rate into the engine.

Air Flow Meter Pressure Transducer	
Manufacturer	Data Instruments, Inc.
Type	Model SA
Range (psia)	0 - 25
Part No.	9301202
Serial No.	2394-0023

Table B-8 – Specifications of the pressure transducer that measures the pressure drop across the flow element of *Table B-7*.

Intake Manifold Pressure Transducer	
Manufacturer	Data Instruments, Inc.
Type	Model SA
Range (psia)	0 - 25
Part No.	9301202
Serial No.	2394-0023

Table B-9 – Specifications on the pressure transducer used to calculate the load of the engine at a given operating condition.

In-Cylinder Pressure Transducer	
Manufacturer	Kistler
Type	6061B
Serial No.	1111151
Measurement Range	1: 0-250bar
	2: 0-50bar
Sensitivity	1: 26.3 $^{pC}/_{bar}$
	2: 26.6 $^{pC}/_{bar}$
Calibrated At:	50°C

Table B-10 – Specifications of the water-cooled pressure transducer to be used to obtain the pressure tracers within the cylinder for a given operating condition.

In-Cylinder Pressure Transducer Cooler	
Manufacturer	ITW Cooling Systems
Model No.	2500SS
Serial No.	WC37345-1201
Reservoir Capacity	2 gallons distilled water
Max Pump Operating Conditions	100psi; 1.7GPM (6.4LPM)
Water Connection Type	1/4 NPT

Table B-11 – Specifications of the cooling system for the pressure transducer described in *Table B-10.*

Left Hand Side Pressure Transducer	
Manufacturer	Kistler
Type	6051B
Serial No.	557991
Measurement Range	1: 0-250bar
	2: 0-50bar
Sensitivity	1: 7.29 $^{pC}/_{bar}$
	2: 7.31 $^{pC}/_{bar}$
Calibrated At:	200°C

Table B-12 – The upper-land pressure transducer that measures the 2nd land pressure as described by *Figure 2-4* as Transducer 1.

Right Hand Side Pressure Transducer	
Manufacturer	Kistler
Type	6051B
Serial No.	557992
Measurement Range	1: 0-250bar
	2: 0-50bar
Sensitivity	1: 7.14 $^{pC}/_{bar}$
	2: 7.17 $^{pC}/_{bar}$
Calibrated At:	200°C

Table B-13 - The lower-land pressure transducer that measures the 2nd and 3rd land pressure as described by *Figure 2-4* as Transducer 2.

Charge Amplifier	
Manufacturer	Kistler
Type	5010
Model	Dual Mode
Operating Temperature	32-122°F
Current Limit	5mA
Output Voltage	± 10V
Accuracy	≤ ± 0.5%
Measurement Range	± 10 - 999000pC
Sensor Sensitivity	0.01-9990 $^{pC}/_{MU}$
	0.01-9990 $^{mV}/_{MU}$

Table B-14 – Specifications of the charge amplifier that converted the transducer signal for the data acquisition system in *Appendix A.*

Blowby Meter Pressure Transducer	
Manufacturer	Omega Engineering, Inc.
Range (psia)	0 - 25
Part No.	PX176-025A5V
Serial No.	06104-00YNRG

Table B-15 – Specifications of the pressure transducer used to correct the blowby volumetric flow rate for STP conditions.

Dynamometer	
Manufacturer	Dynamatic
Type	Force Absorbing - Water Cooled
Part No.	0M0-067151-1000
Model No.	AD-S063
Serial No.	000012450A
Rated Capacity	220HP @ 750 - 8000RPM
Torque Arm	12"
DC Excitation	45V, 5.4A, 5.35Ω @ 20°C
Water Requirements	22GPM(max), 45psi(min) - 100psi(max)
Controller	Digalog Dynamometer Controller

Table B-16 – Specifications of the dynamometer that was coupled to the engine for the duration of and future experiment.

Stepper Motor	
Manufacturer	Pacific Scientific
Model	PowerMax II: Bipolar Series
Model No.	M22NRXA-LNF-N3-00
Rated Current Per Winding	3.3A (DC)
Max Power	56W
Max Angular Speed	1500RPM
Full Step Angle	1.8°
Holding Torque	1.8N-m
Supply Voltage	± 5V
Operating Temp. Range	90°C (Max)
Ambient Operating Temp.	40°C

Table B-17 – Specifications of the stepper motor used to open and close the throttle plate of the engine and thus control the load during operation.

Stepper Motor Indexer Driver	
Manufacturer	Pacific Scientific
Model	5240
Serial No.	0000159894
Date Code	9506
Input Voltage	115 VAC (60Hz)
Input Current	1A
Output Voltage	± 5V
Output Speed Options	Hi and Lo

Table B-18 – Specifications of the driver that controlled the stepper motor described in *Table B-17.*

Digital Encoder	
Manufacturer	BEI Sensor & Systems Company: Industrial Encoder Division
Model No.	XH25E-F1-SS-2000-T5-ABZC-8830-LED-SM13
Part No.	924-01005-950
Serial No.	T0054767
Voltage Input	5V DC

Table B-19 – Specifications of the digital encoder that would have provided the signal for the start of the cylinder traces in the data acquisition system.

Lambda Meter	
Manufacturer	ECM
Model	Lambda Pro
Lambda Range	0.55-1.75 (8-25AFR)
Accuracy	$\pm$ 1% @ λ = 1.0; $\pm$ 2% elsewhere
Response Time	< 150ms
Calculation Time	1ms
Fuels Supported	Gasoline, Methanol, etc.
Voltage Input Required	11-28 VDC
Analog Output Voltage	0-5V, linearized

Table B-20 – Specifications for the lambda meter that provided the data on how far the engine deviated from stoichiometric at any one point in time.

Data Acquisition Computer	
Manufacturer	Dell
Model	Dimension 4550
Processor	P4 - 2.39GHz
RAM	1GB, PC 2700
Hard Drive	60GB
DAQ-MX	PCI-6221

Table B-21 – The data acquisition system used to accrue most, if not all, of the data from the instruments described in this section.

Data Acquisition Box	
SCXI - 1000 Breakout Box	
Manufacturer	National Instruments
Part No.	181445M-01
Serial No.	1188383
SCXI 1303-1101: Voltage Acquisition	
Manufacturer	National Instruments
Part No.	185164A-01
Serial No.	114D2E3
SCXI 1303-1103: Thermocouple Acquisition	
Manufacturer	National Instruments
Part No.	185164A-01
Serial No.	1155DBA

Table B-22 – The data acquisition devices purchased from National Instruments to be used during the experimental phase of the research.

Temperature Solenoid Controller	
Manufacturer	Omega Technologies
Model	6100
Type	6102K-0-500F
Range (°F)	0 - 500
Thermocouple	K

Table B-23 – Temperature controller use to activate oil pump in oil cooling operations during the experimental run.

Appendix C

CHEVRON PHILLIPS CHEMICAL CO. LP
Box 4910, The Woodlands, TX 77387
10001 Six Pines Dr, The Woodlands, TX 77380

Packing List

Delivery Number/Date:
87194292 / 07/26/2006
Employee Responsible:
Kelly Amengual
Customer P.O./Date:
CREDIT CARD / 07/23/2006
Sales Order no./Date:
6302538 / 07/23/2006
Ship-From:
X301/ABAT / PTX PHILTEX BORGER TX
Via:
LTL Carrier-Road /
Transportation Charges:
PPD FOB Dest./Prepaid & Added
Route:
YFSY
YELLOW FREIGHT SYSTEMS INC

Sold-To customer number: 10007907
Bill-To customer number: 40001549
MASSACHUSETTS INSTITUTE OF TECHNOLO
PO Box 9169
CAMBRIDGE MA 02139
Ship-To customer number: 20004379
MASSACHUSETTS INSTITUTE OF TECHNOLO
BLDG 31-063
60 VASSAR ST
CAMBRIDGE MA 02139

TERMS: Net Upon Receipt FROM DATE OF INVOICE
REQUESTED SHIP DATE: 07/26/2006
LOAD DATE: 07/26/2006

Item	Material Description	Qty
000010		1.00 EA

NO SULFUR GASOLINE, 54 GAL DRUM
1020433
NW: 338.002 LB 153.315 KG
GW: 397.990 LB 180.525 KG
HM: X
GASOLINE
3
UN1203
II
-37°C
FREIGHT NAME: GASOLINE
API GRAVITY: 57.17 Density: 6.26
R&D GASOLINE - NO SULFUR GASOLINE
EPA RFG ID 4404
FOR USE IN RESEARCH, DEVELOPMENT, AND TEST PROGRAMS ONLY
USERS MUST HAVE AN R&D EXEMPTION GRANTED BY THE US EPA ADMINISTRATOR
BASE GASOLINE - NOT FOR SALE TO THE ULTIMATE CONSUMER
QTY SHIP: 1.00 EA
QTY SHIP: 53.994 UG6
LOTS: 6GPNSG01

Figure C-1 – Page 1 of a sample data sheet given along with every barrel of no-sulfur gasoline purchase to run the experiments. Reprinted from Chevron-Phillips hardcopy.

Chevron Phillips Chemical Company LP

CoA Date: 07/26/2006

Certificate of Analysis

Shipped To: MASSACHUSETTS INSTITUTE OF TECHNOLO
BLDG 31-063
60 VASSAR ST
CAMBRIDGE MA 02139
USA
Recipient:
Fax:

PO #: CREDIT CARD
CPC Delivery #: 87194292
Ship Date: 07/26/2006
Package/Mode: 54 GAL DRUM
Quantity: 1 EA
Certification Date: 07/20/2006
Transportation ID:
Shelf Life: Undetermined

Product: NO SULFUR GASOLINE, 54 GAL DRUM

Material Code:1020433

Lot Number: 6GPNSG01

Property	Test Method	Specification	Value	Unit
Specific Gravity 60/60	ASTM D-4052		0.7397	
API Gravity	ASTM D-1250		59.8	
Sulfur	ASTM D-5453	<= 2.0	0.9	ppm
Reid Vapor Pressure	ASTM D-5191	7.0 - 9.0	8.3	PSI
Hydrogen	ASTM D-5291		13.9	WT%
Carbon	ASTM D-5291		86.1	WT%
Net Heat of Combustion	ASTM D-240		18502	BTU/LB
Distillation - IBP	ASTM D-86		101	FAH
Distillation - 5%	ASTM D-86		108	FAH
Distillation - 10%	ASTM D-86		130	FAH
Distillation - 20%	ASTM D-86		157	FAH
Distillation - 30%	ASTM D-86		178	FAH
Distillation - 40%	ASTM D-86		198	FAH
Distillation - 50%	ASTM D-86		217	FAH
Distillation - 60%	ASTM D-86		238	FAH
Distillation - 70%	ASTM D-86		257	FAH
Distillation - 80%	ASTM D-86		280	FAH
Distillation - 90%	ASTM D-86		309	FAH
Distillation - 95%	ASTM D-86		383	FAH
Distillation - EP	ASTM D-86		383	FAH
Distillation - Loss	ASTM D-86		1.8	ML
Distillation - Residue	ASTM D-86		1.0	ML
Aromatics	ASTM D-1319		27.1	LV%
Olefins	ASTM D-1319		1.4	LV%
Saturates	ASTM D-1319		71.5	LV%
Research Octane Number	ASTM D-2699		90.4	
Motor Octane Number	ASTM D-2700		84.6	
Benzene	Chromatography		0.00	LV%

Figure C-2 – Page 2 of a sample data sheet given along with every barrel of no-sulfur gasoline purchase to run the experiments. Reprinted from Chevron-Phillips hardcopy.

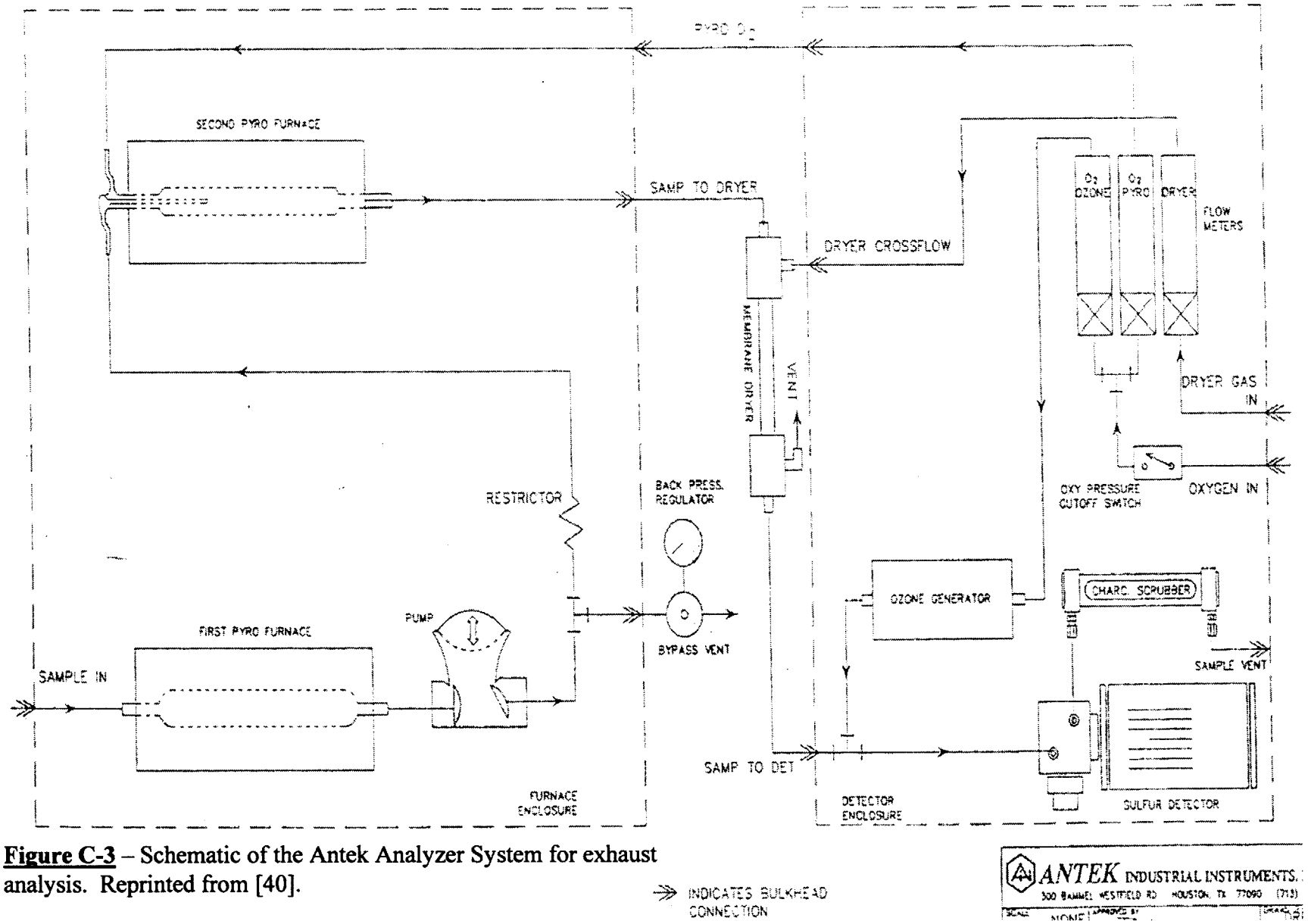

Figure C-3 – Schematic of the Antek Analyzer System for exhaust analysis. Reprinted from [40].

(This page was intentionally left blank)

Appendix D

```
clf
clear
load 'press.out'
load 'lift.out'
n=length(press);
for i=1:n
 ca(i)=press(i,1);
 p1(i)=press(i,2);
 p2(i)=press(i,3);
 p3(i)=press(i,4);
 p4(i)=press(i,5);
 p5(i)=press(i,6);
 h1(i)=lift(i,2);
 h2(i)=lift(i,3);
 tw1(i)=lift(i,4);
 tw2(i)=lift(i,5);
end

subplot(311)
plot(ca,p1,ca,p2,ca,p3,ca,p4,ca,p5,'linewidth',0.2)
set(gca,'fontsize',7)
legend('Measured In-Cylinder','Behind 1st
Ring','Second Land','Behind 2nd Ring','Third
Land')
axis([-360 360 0 5])
xax=[-360 -270 -180 -90 0 90 180 270 360];
set(gca,'Xtick',xax)
ylabel('Absolute Pressure [bars]','fontsize',9)
set(gca,'fontsize',9)

subplot(312)
plot(ca,h1,ca,h2,'r',ca,lift(:,6),'linewidth',0.2)
axis([-360 360 0 1])
xax=[-360 -270 -180 -90 0 90 180 270 360];
set(gca,'Xtick',xax)
set(gca,'fontsize',7)
legend('1st Ring','2nd Ring')
ylabel('Ring Relative Lift','fontsize',9)
set(gca,'fontsize',9)

subplot(313)
plot(ca,tw1,ca,tw2,'r',ca,lift(:,7),'linewidth',0.2)
axis([-360 360 -30 60])
xax=[-360 -270 -180 -90 0 90 180 270 360];
set(gca,'Xtick',xax)
set(gca,'fontsize',7)
legend('1st Ring','2nd Ring')
xlabel('Crank Angle (degrees)','fontsize',9)
ylabel('Ring Twist (minutes)','fontsize',9)
set(gca,'fontsize',9)
grid
 set(gcf,'paperposition',[0.05 0.45 7.5 9.45])
saveas(gcf, ['lift'], 'tiff')
```

```
clf
clear
load 'edget.out'
n=length(edget);
for i=1:n
 ca(i)=edget(i,1);
 liftt1i(i)=edget(i,2);
 liftt1o(i)=edget(i,3);
 liftt2i(i)=edget(i,4);
 liftt2o(i)=edget(i,5);
 liftt3i(i)=edget(i,6);
 liftt3o(i)=edget(i,7);
end
subplot(311)
plot(ca,liftt1i,ca,liftt1o,'linewidth',0.2)
set(gca,'fontsize',7)
legend('Top Flank Inner','Top Flank
Outer','Location','NorthWest')
axis([-360 360 0 1])
xax=[-360 -270 -180 -90 0 90 180 270 360];
set(gca,'Xtick',xax)
ylabel('Normalized Top Ring
Clearance','fontsize',9)
set(gca,'fontsize',9)

subplot(312)
plot(ca,liftt2i,ca,liftt2o,'linewidth',0.2)
axis([-360 360 0 1])
xax=[-360 -270 -180 -90 0 90 180 270 360];
set(gca,'Xtick',xax)
set(gca,'fontsize',7)
legend('Top Flank Inner','Top Flank
Outer','Location','NorthWest')
ylabel('Normalized 2nd Ring
Clearance','fontsize',9)
set(gca,'fontsize',9)

subplot(313)
plot(ca,liftt3i,ca,liftt3o,'linewidth',0.2)
axis([-360 360 0 1])
xax=[-360 -270 -180 -90 0 90 180 270 360];
set(gca,'Xtick',xax)
set(gca,'fontsize',7)
legend('Top Flank Inner','Top Flank
Outer','Location','NorthWest')
xlabel('Crank Angle (degrees)','fontsize',9)
ylabel('Normalized OCR Clearance','fontsize',9)
set(gca,'fontsize',9)

set(gcf,'paperposition',[0.05 0.45 7.5 9.45])
saveas(gcf, ['RingPos'], 'tiff')
```

Figure D-1 – Matlab code for ring pack pressures & dynamics(Left) and ring position(Right).

```
clf
clear
load 'blowio.out'
slpmconvert=.00002155;
n=length(blowio);
for i=1:n
 ca(i)=blowio(i,1);
 blowcv(i)=blowio(i,2)/slpmconvert;
 blowcc(i)=blowio(i,3)/slpmconvert;
end

avgblowby(1,1:n)=mean(blowcc);
avgblowby_engine(1,1:n)=4*mean(blowcc);
subplot(111)
plot(ca,avgblowby,ca,blowcc,'linewidth',0.2)
set(gca,'fontsize',7)
legend('Avg Blowby','Instant. Blowby into
Ccase')
axis([-360 360 -5 15]);
xax=[-360 -270 -180 -90 0 90 180 270 360];
set(gca,'Xtick',xax)
xlabel('Crank Angle (degrees)','fontsize',9)
ylabel('Blowby per Cylinder (SLPM)','fontsize',9)
set(gca,'fontsize',9)
title ({'Blowby For a Given Cycle of One
Cylinder'},'FontWeight','bold')
grid

   text(-350,4,['Avg. Blowby per Cylinder = '
num2str(avgblowby(1:1))]);
   text(-350,3,['Avg. Blowby = '
num2str(avgblowby_engine(1:1))]);


set(gcf, 'PaperPositionMode', 'auto');
saveas(gcf, ['Blowby'], 'tiff')
```

```
clf
clear
load 'lift_rl.out'
n=length(lift_rl);
for i=1:n
 ca(i)=lift_rl(i,1);
 rl1(i)=lift_rl(i,2);
 rl2(i)=lift_rl(i,3);
 gap1_reduction(i)=lift_rl(i,4);
 gap2_reduction(i)=lift_rl(i,5);
end
subplot(211)
plot(ca,rl1,ca,rl2,'linewidth',0.2)
set(gca,'fontsize',7)
legend('Top Ring','2nd Ring')
axis([-360 360 0 10])
xax=[-360 -270 -180 -90 0 90 180 270 360];
set(gca,'Xtick',xax)
ylabel('Radial Clearance [microns]','fontsize',9)
set(gca,'fontsize',9)

subplot(212)
plot(ca,gap1_reduction,ca,gap2_reduction,'linew
idth',0.2)
axis([-360 360 0 .1])
xax=[-360 -270 -180 -90 0 90 180 270 360];
set(gca,'Xtick',xax)
set(gca,'fontsize',7)
legend('Top Ring','2nd Ring')
xlabel('Crank Angle (degrees)','fontsize',9)
ylabel('Ring Gap Reduction [mm]','fontsize',9)
set(gca,'fontsize',9)

set(gcf,'paperposition',[0.05 0.45 7.5 9.45])
saveas(gcf, ['RadCollapse'], 'tiff')
```

Figure D-2 – Matlab code for instantaneous (crank angle degree) blowby(Left) and the distance of the ring face profile from the cylinder wall(Right).

Note that in *Figures D-1* and *D-2*, the programs for blowby and ring dynamics were modified from those provided by Steve Przesmitzki. The other two programs, and the one reprinted below in *Figure D-3*, take advantage of the output files created by running the ring pack executable provided by Tian Tian and referenced in [24].

```
clf
clear
load 'mdot.out'
n=length(mdot);
for i=1:n
 ca(i)=mdot(i,1);
 mdot12(i)=1000*mdot(i,2);
 mdot13(i)=1000*mdot(i,3);
 mdot23(i)=1000*mdot(i,4);
 mdot34(i)=1000*mdot(i,5);
 mdot35(i)=1000*mdot(i,6);
 mdot45(i)=1000*mdot(i,7);
 mdot56(i)=1000*mdot(i,8);
 mdot_rl1(i)=1000*mdot(i,9);
 mdot_rl2(i)=1000*mdot(i,10);
 mdotocrt(i)=1000*mdot(i,11);
 pumpocrt(i)=1000*mdot(i,12);
end
 subplot(311)
plot(ca,mdot12,ca,mdot13,ca,mdot23,ca,mdot_rl1,'linewidth',0.2)
set(gca,'fontsize',7)
legend('Top Land to Groove','Top Land through Gap', 'Groove to 2nd Land','Top Land through Ring-
Liner','Location','NorthWest')
axis([-360 360 -1 1])
xax=[-360 -270 -180 -90 0 90 180 270 360];
set(gca,'Xtick',xax)
ylabel('Mass Flow Rate (g/s)','fontsize',9)
set(gca,'fontsize',9)
 subplot(312)
plot(ca,mdot34,ca,mdot35,ca,mdot45,ca,mdot_rl2,'linewidth',0.2)
axis([-360 360 -1 1])
xax=[-360 -270 -180 -90 0 90 180 270 360];
set(gca,'Xtick',xax)
set(gca,'fontsize',7)
legend('2nd Land to Groove','2nd Land through Gap', 'Groove to 3rd Land','Second Land through Ring-
Liner','Location','NorthWest')
ylabel('Mass Flow Rate (g/s)','fontsize',9)
set(gca,'fontsize',9)
 subplot(313)
plot(ca,mdot56,ca,mdotocrt,ca,pumpocrt,'linewidth',0.2)
axis([-360 360 -1 1])
xax=[-360 -270 -180 -90 0 90 180 270 360];
set(gca,'Xtick',xax)
set(gca,'fontsize',7)
legend('3rd Land through Gap','Through OCR Upper Groove','Pumped Into Upper OCR
Groove','Location','NorthWest')
xlabel('Crank Angle (degrees)','fontsize',9)
ylabel('Mass Flow Rate (g/s)','fontsize',9)
set(gca,'fontsize',9)
 set(gcf,'paperposition',[0.05 0.45 7.5 9.45])
saveas(gcf, ['MassFlows'], 'tiff')
```

Figure D-3 – Matlab code for instantaneous (crank angle degree) mass flow rate in $^{g}/_{s}$ for various regions along the piston ring pack.

```
%%% Using Lab Pro files to Create Plots For STEADY STATE PLOTS

clear all
%%%%% Type file name
%function A='input';
%Example
%A='2_17_07_2500_cyl3.lvm';
%5_04_07_1500_430_cyl3
A = input('[Steady State] Please Insert the File Name: ','s');

if isempty(A)
   disp('No File Name Selected')
   A = input('[Steady State] Please Insert the File Name: ','s');
elseif isempty(A)
   disp('No File Name Selected')
   A = input('Please Insert the File Name: ','s');
     end

%%%%Size of Running Average
size = 10;
%%%% Select Time Range of Plot (in seconds)
t_min=0;
t_max=1200;

%IMPORT Text Data
fid=fopen(A,'r');

%Textscan importing function with omitted headerlines set to 23

B= textscan(fid, ' %f32 %f32 %f32 %f32 %f32 %f32 %f32 %f32 %f32 %f32 %f32 %f32 %f32 %f32 %f32 %f32
%f32 %f32 %f32 %f32 %f32 %f32 %f32 %f32 %f32 %f32 %f32 %f32 %f32 %f32 %f32 %f32
%f32','headerLines', 23); % Reads row 1 of col 1-4

% {} give values, () give size
B{:};

fclose(fid);
%%Get Values for each Parameter

%Parameters to be imported, B{n} n refers to the column number

time= B{1};
ug_cyl=B{28};
blowby=B{29};
pressure=B{7};
rpm=B{22};
g_hr=B{27};

%% Set the time range of the values
time_range=(t_min<time & time<t_max);

%%% Calculate Running Averages
g_hr_avg=filter(ones(1,size)/size,1,g_hr);
```

```
ug_cyl_avg=filter(ones(1,size)/size,1,ug_cyl);
 blowby_avg=filter(ones(1,size)/size,1,blowby);
pressure_avg=filter(ones(1,size)/size,1,pressure);
rpm_avg=filter(ones(1,size)/size,1,rpm);

%Creates and Saves plot
%%format of saved plots
F='bmp';
scrsz = get(0,'ScreenSize'); %%Find Screen Size

%figure(1)
 figure('Position',[0 0 scrsz(3) .9*scrsz(4)])
plot(time(time_range),g_hr_avg(time_range))
ylabel('Oil Consumption [g/hr]')
 if  min(g_hr_avg(time_range))> 0
    ylim([.8*min(g_hr_avg(time_range)) 1.2*max(g_hr_avg(time_range))]);
else
    ylim([0 1.2*max(g_hr_avg(time_range))]);
end;
 xlabel('Time [s]')
title (['Oil Consumption: ' A(9:12) ' RPM, ' A(14:16) ' mbar, Cylinder ' A(21)],'FontWeight','bold')
fig=gcf
G=[A(1:7) '_Oil_g_hr_' A(9:12) '_RPM_' A(14:16) '_mbar_cyl' A(21) ]
saveas (gcf,G,F)

%figure(2)
figure('Position',[0 0 scrsz(3) .9*scrsz(4)])
plot(time(time_range),ug_cyl_avg(time_range))
ylabel('Oil Consumption [ µg/cyl-cycle]')
xlabel('Time [s]')
if min(ug_cyl_avg(time_range))> 0
    ylim([.8*min(ug_cyl_avg(time_range)) 1.2*max(ug_cyl_avg(time_range))]);
 else
   ylim([0 1.2*max(ug_cyl_avg(time_range))]);
 end;
 itle (['Oil Consumption: ' A(9:12) ' RPM, ' A(14:16) ' mbar, Cylinder ' A(21)],'FontWeight','bold')
 G=[A(1:7) '_Oil_ug_cyl-cycle_' A(9:12) '_RPM_' A(14:16) '_mbar_cyl' A(21) ]
saveas (gcf,G,F)

%figure(3)
figure('Position',[0 0 scrsz(3) .9*scrsz(4)])
plot(time(time_range),blowby_avg(time_range))
ylabel('Blowby ( SLPM, Ref 760 mmHg,70° F)')
ylim([.7*mean(blowby_avg(time_range)) 1.3*mean(blowby_avg(time_range))])
xlabel('Time [s]')
title (['Blowby: ' A(9:12) ' RPM, ' A(14:16) ' mbar, Cylinder ' A(21)],'FontWeight','bold' )
 G=[A(1:7) '_Blowby_' A(9:12) '_RPM_' A(14:16) '_mbar_cyl' A(21) ]
saveas (gcf,G,F)

%figure(4)
figure('Position',[0 0 scrsz(3) .9*scrsz(4)])
plot(time(time_range),pressure_avg(time_range))
ylabel('Intake Manifold Pressure [mbar]')
ylim([.7*mean(pressure_avg(time_range)) 1.3*mean(pressure_avg(time_range))])
xlabel('Time [s]')
```

```
title (['Intake Manifold Pressure: ' A(9:12) ' RPM, ' A(14:16) ' mbar, Cylinder ' A(21)],'FontWeight','bold')
G=[A(1:7) '_Pressure_' A(9:12) '_RPM_' A(14:16) '_mbar_cyl' A(21) ]
saveas (gcf,G,F)

%figure(5)
figure('Position',[0 0 scrsz(3) .9*scrsz(4)])
plot(time(time_range),rpm_avg(time_range))
ylabel('Speed [RPM]')
ylim([(mean(rpm_avg(time_range))-100) (mean(rpm_avg(time_range))+100)])
xlabel('Time [s]')
title (['Speed: '  A(9:12) ' RPM, ' A(14:16) ' mbar, Cylinder ' A(21)],'FontWeight','bold')
G=[A(1:7) '_Speed_' A(9:12) '_RPM_' A(14:16) '_mbar_cyl' A(21) ]
saveas (gcf,G,F)

%%%Code Developed by Diego A. Melani Spring 2007
```

Figure D-4 – Matlab code used to create oil consumption trace graphs (in terms of $^{g}/_{cyl\text{-}hr}$ and $^{\mu g}/_{cyl\text{-}cycle}$), a blowby graph, a load graph, and speed graph, all as a function of time during steady-state operation. This was described in *Section 2.3.2.1*. Code developed by Diego Melani of MIT.

```
%%% Using Lab View files to Create Plots For TRANSIENT LOADS PLOTS
clear all

%%%%% Insert file name Write the filename with the extension lvm, without
%%%%% the extension the input will not work
A = input('[Transient Loads] Please Insert the File Name: ','s');
if isempty(A)
   disp('No File Name Selected')
   A = input('[Transient Loads] Please Insert the File Name: ','s');
elseif isempty(A)
   disp('No File Name Selected')
   A = input('Please Insert the File Name: ','s');
end

%%%%Size of Running Average
size = 10;
%%%% Select Time Range of Plot (in seconds)
t_min=10;
t_max=1800;

%IMPORT Text Data
fid=fopen(A,'r'); %Command for data acquisition

%Textscan importing function with omitted headerlines set to 23: this will
%start reading for values after that line

B= textscan(fid, ' %f32 %f32 %f32 %f32 %f32 %f32 %f32 %f32 %f32 %f32 %f32 %f32 %f32 %f32 %f32 %f32
%f32 %f32 %f32 %f32 %f32 %f32 %f32 %f32 %f32 %f32 %f32 %f32 %f32 %f32 %f32 %f32
%f32','headerLines', 23); % Reads row 1 of col 1-4

% {} give values, () give size
B{:};
```

```
 fclose(fid);
%%Get Values for each Parameter

%Parameters to be imported, B{n} n refers to the column number
 time= B{1};
ug_cyl=B{28};
blowby=B{29};
pressure=B{7};
rpm=B{22};
g_hr=B{27};

%% Set the time range of the values
time_range=(t_min<time & time<t_max);

%%% Calculate Running Averages
g_hr_avg=filter(ones(1,size)/size,1,g_hr);
ug_cyl_avg=filter(ones(1,size)/size,1,ug_cyl);
 blowby_avg=filter(ones(1,size)/size,1,blowby);
pressure_avg=filter(ones(1,size)/size,1,pressure);
rpm_avg=filter(ones(1,size)/size,1,rpm);

%Creates and Saves plot
%%format of saved plots
F='bmp';
scrsz = get(0,'ScreenSize'); %%Find Screen Size

%Get Maximum Line Value and Vertical lines
%Modify the M multiplier to lower or increase the Y values for all the
%lines/arrows/text

M=max(g_hr_avg(time_range));
y=1.2*M;
lineheight=[0:.1:y];
line1=300;
line2=600;
line3=900;
line4=1200;
line5=1500;
line6=1800;
if pressure_avg(t_max)==NaN
stop;
disp('Missing Values of Parameters for Time Range')
end

%%%Text Insert Location and Pressure Values
t1=(0<time & time<301);
t2=(301<time & time<601);
t3=(601<time & time<901);
t4=(901<time & time<1201);
t5=(1201<time & time<1501);
t6=(1501<time & time<1801);

p1=pressure_avg(t1);
```

```
p2=pressure_avg(t2);
p3=pressure_avg(t3);
p4=pressure_avg(t4);
p5=pressure_avg(t5);
p6=pressure_avg(t6);

p1_avg=mean(p1);
p2_avg=mean(p2);
p3_avg=mean(p3);
p4_avg=mean(p4);
p5_avg=mean(p5);
p6_avg=mean(p6);

%figure(1)
figure('Position',[0 0 scrsz(3) .9*scrsz(4)])

%%Vertical Lines
plot(line1,lineheight,'k');
hold on
plot(line2,lineheight,'k');
plot(line3,lineheight,'k');
plot(line4,lineheight,'k');
plot(line5,lineheight,'k');

%%%%Doubleheaded Arrows and Text Labels
y1=1.0056*y;
%Y position of text/side arrows

yt=1.22*M;

x1=[0:300];
x2=[300:600];
x3=[600:900];
x4=[900:1200];
x5=[1200:1500];
x6=[1500:1800];

%%%Horizontal Arrow Lines
plot(x1,y,'k-');
plot(x2,y,'k-');
plot(x3,y,'k-');
plot(x4,y,'k-');
plot(x5,y,'k-');
plot(x6,y,'k-');

plot(time(time_range),g_hr_avg(time_range))
ylabel('Oil Consumption [g/hr]')

%setting the limit for graph's Y boundary
if min(g_hr_avg(time_range))>0
   ylim([.8*min(g_hr_avg(time_range)) 1.3*M]);
else
    ylim([0 1.3*M]);
end;
```

```
xlabel('Time [s]')
title (['Oil Consumption Transient Variation:  ' A(9:12) ' RPM, ' A(20:22) ' - ' A(24:26) ' mbar, cyl'
A(31)],'FontWeight','bold')
 hold off

 %% Determining the number of digits for the pressure value
z=[p1_avg p2_avg p3_avg p4_avg p5_avg p6_avg];
maximum_pressure=max(z)
if maximum_pressure>=1000
   x=4
else
   x=3
end

p1_s=num2str(p1_avg,x);
p1_ss=[p1_s(1,:) ' mbar'];

text('position',[100,yt],'string',p1_ss,'FontSize',10);

%%% Creates line & Side Arrows with reference from data not figure
text('position',[0,y1],'string','\leftarrow','FontSize',18);
text('position',[250,y1],'string','\rightarrow','FontSize',18);

text('position',[300,y1],'string','\leftarrow','FontSize',18);
text('position',[550,y1],'string','\rightarrow','FontSize',18);

text('position',[600,y1],'string','\leftarrow','FontSize',18);
text('position',[850,y1],'string','\rightarrow','FontSize',18);

text('position',[900,y1],'string','\leftarrow','FontSize',18);
text('position',[1150,y1],'string','\rightarrow','FontSize',18);

text('position',[1200,y1],'string','\leftarrow','FontSize',18);
text('position',[1450,y1],'string','\rightarrow','FontSize',18);

text('position',[1500,y1],'string','\leftarrow','FontSize',18);
text('position',[1750,y1],'string','\rightarrow','FontSize',18);

p2_s=num2str(p2_avg,x);
p2_ss=[p2_s(1,:) ' mbar'];
text('position',[375,yt],'string',p2_ss,'FontSize',10);

p3_s=num2str(p3_avg,x);
p3_ss=[p3_s(1,:) ' mbar'];
text('position',[680,yt],'string',p3_ss,'FontSize',10);

p4_s=num2str(p4_avg,x);
p4_ss=[p4_s(1,:) ' mbar'];
text('position',[980,yt],'string',p4_ss,'FontSize',10);

p5_s=num2str(p5_avg,x);
p5_ss=[p5_s(1,:) ' mbar'];
```

```
text('position',[1280,yt],'string',p5_ss,'FontSize',10);
 p6_s=num2str(p6_avg,x);
p6_ss=[p6_s(1,:) ' mbar'];

text('position',[1580,yt],'string',p6_ss,'FontSize',10);

fig=gcf
G=[A(1:7) '_transloadOil_g_hr_' A(9:12) '_RPM_' A(20:22) '_' A(24:26) '_mbar_cyl' A(31) '.bmp']
saveas (gcf,G)

%%%%%%%%%%%%%%%%%%%%%%%%%%%%%%%%%%%%%%%%%%%%%%%%%%%%%%%%%
%%%%%%%%%%%%%%%%%%%%%%%%%%%%%%%%%
%figure(2)
M2=max(ug_cyl_avg(time_range));
y22=1.2*M2
lineheight2=[0:.1:y22];

figure('Position',[0 0 scrsz(3) .9*scrsz(4)])

%%Vertical Lines
plot(line1,lineheight2,'k');
hold on
plot(line2,lineheight2,'k');
plot(line3,lineheight2,'k');
plot(line4,lineheight2,'k');
plot(line5,lineheight2,'k');
%Y position of text/side arrows
y2=1.2067*M2; %Arrow position
yt2=1.22*M2;
%x values are the same for both

%Horizontal Arrow Lines
 plot(x1,y22,'k-');
plot(x2,y22,'k-');
plot(x3,y22,'k-');
plot(x4,y22,'k-');
plot(x5,y22,'k-');
plot(x6,y22,'k-');

plot(time(time_range),ug_cyl_avg(time_range))
ylabel('Oil Consumption [ µg/cyl-cycle]')
if min(ug_cyl_avg(time_range))>0
   ylim([.8*min(ug_cyl_avg(time_range)) 1.3*M2]);
else
      ylim([0 1.3*M2]);
end;

xlabel('Time [s]')
title (['Oil Consumption Transient Variation:  ' A(9:12) ' RPM, ' A(20:22) ' - ' A(24:26) ' mbar, cyl'
A(31)],'FontWeight','bold')
 hold off
 text('position',[100,yt2],'string',p1_ss,'FontSize',10);

%%% Creates  Side Arrows with reference from data not figure
```

```
text('position',[0,y2],'string','\leftarrow','FontSize',18);
text('position',[250,y2],'string','\rightarrow','FontSize',18);

text('position',[300,y2],'string','\leftarrow','FontSize',18);
text('position',[550,y2],'string','\rightarrow','FontSize',18);

text('position',[600,y2],'string','\leftarrow','FontSize',18);
text('position',[850,y2],'string','\rightarrow','FontSize',18);

text('position',[900,y2],'string','\leftarrow','FontSize',18);
text('position',[1150,y2],'string','\rightarrow','FontSize',18);

text('position',[1200,y2],'string','\leftarrow','FontSize',18);
text('position',[1450,y2],'string','\rightarrow','FontSize',18);

text('position',[1500,y2],'string','\leftarrow','FontSize',18);
text('position',[1750,y2],'string','\rightarrow','FontSize',18);

%p2_s=num2str(p2_avg,x);
p2_ss=[p2_s(1,:) ' mbar'];
text('position',[375,yt2],'string',p2_ss,'FontSize',10);

%p3_s=num2str(p3_avg,x);
p3_ss=[p3_s(1,:) ' mbar'];
text('position',[680,yt2],'string',p3_ss,'FontSize',10);

%p4_s=num2str(p4_avg,x);
p4_ss=[p4_s(1,:) ' mbar'];
text('position',[980,yt2],'string',p4_ss,'FontSize',10);

%p5_s=num2str(p5_avg,x);
p5_ss=[p5_s(1,:) ' mbar'];
 text('position',[1280,yt2],'string',p5_ss,'FontSize',10);

%p6_s=num2str(p6_avg,x);
p6_ss=[p6_s(1,:) ' mbar'];
 text('position',[1580,yt2],'string',p6_ss,'FontSize',10);
 G=[A(1:7) '_transloadOil_ug_cyl-cycle_' A(9:12)  '_RPM_' A(20:22) '_' A(24:26) '_mbar_cyl' A(31) '.bmp']
 saveas (gcf,G)

%figure(3)
%Change the multiplier in M3 to scale the graph

M3=.95*max(blowby_avg(time_range));
y4=1.08*M3;
lineheight3=[0:.01:y4];
figure('Position',[0 0 scrsz(3) .9*scrsz(4)])

%%%vertical lines
plot(line1,lineheight3,'k');
hold on
plot(line2,lineheight3,'k');
plot(line3,lineheight3,'k');
```

```
plot(line4,lineheight3,'k');
plot(line5,lineheight3,'k');
%Y position of text/side arrows
y3=1.085*M3;
yt3=1.097*M3;

%x values are the same for both
 plot(x1,y4,'k','LineWidth',1);
plot(x2,y4,'k','LineWidth',1);
plot(x3,y4,'k','LineWidth',1);
plot(x4,y4,'k','LineWidth',1);
plot(x5,y4,'k','LineWidth',1);
plot(x6,y4,'k','LineWidth',1);

%p1_s=num2str(p1_avg,x);
p1_ss=[p1_s(1,:) ' mbar'];

plot(time(time_range),blowby_avg(time_range))
ylabel('Blowby ( SLPM, Ref 760 mmHg,70° F)')
xlabel('Time [s]')

if min(blowby_avg(time_range))>0
   ylim([.8*min(blowby_avg(time_range)) 1.15*M3])
else
       ylim([0 1.15*M3])
 end

title (['Blowby Transient Variation: '  A(9:12)  ' RPM, ' A(20:22) ' - ' A(24:26) ' mbar, cyl'
A(31)],'FontWeight','bold')
hold off
 text('position',[100,yt3],'string',p1_ss,'FontSize',10);

%%% Creates line & Side Arrows with reference from data not figure
text('position',[0,y3],'string','\leftarrow','FontSize',18);
text('position',[250,y3],'string','\rightarrow','FontSize',18);

text('position',[300,y3],'string','\leftarrow','FontSize',18);
text('position',[550,y3],'string','\rightarrow','FontSize',18);

text('position',[600,y3],'string','\leftarrow','FontSize',18);
text('position',[850,y3],'string','\rightarrow','FontSize',18);

text('position',[900,y3],'string','\leftarrow','FontSize',18);
text('position',[1150,y3],'string','\rightarrow','FontSize',18);

text('position',[1200,y3],'string','\leftarrow','FontSize',18);
text('position',[1450,y3],'string','\rightarrow','FontSize',18);

text('position',[1500,y3],'string','\leftarrow','FontSize',18);
text('position',[1750,y3],'string','\rightarrow','FontSize',18);

%p2_s=num2str(p2_avg,x);
p2_ss=[p2_s(1,:) ' mbar'];
text('position',[375,yt3],'string',p2_ss,'FontSize',10);
```

```
%p3_s=num2str(p3_avg,x);
p3_ss=[p3_s(1,:) ' mbar'];
text('position',[680,yt3],'string',p3_ss,'FontSize',10);

%p4_s=num2str(p4_avg,x);
p4_ss=[p4_s(1,:) ' mbar'];
text('position',[980,yt3],'string',p4_ss,'FontSize',10);

%p5_s=num2str(p5_avg,x);
p5_ss=[p5_s(1,:) ' mbar'];
 text('position',[1280,yt3],'string',p5_ss,'FontSize',10);

%p6_s=num2str(p6_avg,x);
p6_ss=[p6_s(1,:) ' mbar'];
 text('position',[1580,yt3],'string',p6_ss,'FontSize',10);
G=[A(1:7) '_transloadBlowby_' A(9:12) '_RPM_' A(20:22) '_' A(24:26) '_mbar_cyl' A(31) '.bmp']
 saveas (gcf,G)

%figure(4)
figure('Position',[0 0 scrsz(3) .9*scrsz(4)])
plot(time(time_range),pressure_avg(time_range))
ylabel('Intake Manifold Pressure [mbar]')
xlabel('Time [s]')
title (['Intake Manifold Pressure Transient Variation: ' A(9:12) ' RPM, ' A(20:22) ' - ' A(24:26) ' mbar, cyl'
A(31)],'FontWeight','bold')
G=[A(1:7) '_transloadPressure_' A(9:12) '_RPM_' A(20:22) '_' A(24:26) '_mbar_cyl' A(31) '.bmp']
saveas (gcf,G)

%figure(5)
figure('Position',[0 0 scrsz(3) .9*scrsz(4)])
plot(time(time_range),rpm_avg(time_range))
ylabel('Speed [RPM]')
xlabel('Time [s]')
title (['Speed Transient Variation:  ' A(9:12)  ' RPM, ' A(20:22) ' - ' A(24:26) ' mbar, cyl'
A(31)],'FontWeight','bold')
G=[A(1:7) '_transloadSpeed_' A(9:12) '_RPM_' A(20:22) '_' A(24:26) '_mbar_cyl' A(31) '.bmp']
 saveas (gcf,G)

%%%Code Developed by Diego A. Melani Spring 2007
```

Figure D-5 – Matlab code used to create oil consumption trace graphs (in terms of $^{g}/_{cyl\text{-}hr}$ and $^{\mu g}/_{cyl\text{-}cycle}$), a blowby graph, a load graph, and speed graph, all as a function of time during transient load operation. This was described in *Section 2.3.2*. Code developed by Diego Melani of MIT.

```
%%% transspeed code
%%% Using Lab Pro files to Create Plots For TRANSIENT LOADS PLOTS
 clear all

%%%%% Insert file name
A = input(' [Transient Speeds] Please Insert the File Name: ','s');
if isempty(A)
```

```
   disp('No File Name Selected')
   A = input('[Transient Speeds] Please Insert the File Name: ','s');
elseif isempty(A)
   disp('No File Name Selected')
   A = input('Please Insert the File Name: ','s');
end

%%%%Size of Running Average
size = 10;
%%%% Select Time Range of Plot (in seconds)
t_min=10;
t_max=1800;

%IMPORT Text Data
fid=fopen(A,'r');

%Textscan importing function with omitted headerlines set to 23
 B= textscan(fid, ' %f32 %f32 %f32 %f32 %f32 %f32 %f32 %f32 %f32 %f32 %f32 %f32 %f32 %f32 %f32 %f32
%f32 %f32 %f32 %f32 %f32 %f32 %f32 %f32 %f32 %f32 %f32 %f32 %f32 %f32 %f32 %f32
%f32','headerLines', 23); % Reads row 1 of col 1-4

% {} give values, () give size
B{:};
fclose(fid);
%%Get Values for each Parameter

%Parameters to be imported, B{n} n refers to the column number
 time= B{1};
ug_cyl=B{28};
blowby=B{29};
pressure=B{7};
rpm=B{22};
g_hr=B{27};

 %% Set the time range of the values
time_range=(t_min<time & time<t_max);

%%% Calculate Running Averages
g_hr_avg=filter(ones(1,size)/size,1,g_hr);
ug_cyl_avg=filter(ones(1,size)/size,1,ug_cyl);

blowby_avg=filter(ones(1,size)/size,1,blowby);
pressure_avg=filter(ones(1,size)/size,1,pressure);
rpm_avg=filter(ones(1,size)/size,1,rpm);

%Creates and Saves plot
%%format of saved plots
F='bmp';
scrsz = get(0,'ScreenSize'); %%Find Screen Size

%Get Maximum Line Value and Vertical lines
%Modify the M multiplier to lower or increase the Y values for all
M=.9*max(g_hr_avg(time_range));
y=1.2*M;
```

```
lineheight=[0:.1:y];
line1=300;%305
line2=600;%607
line3=900;%907
line4=1200;%1207
line5=1500;%1507
line6=1800;

%figure(1)
figure('Position',[0 0 scrsz(3) .9*scrsz(4)])

%%Vertical Lines
plot(line1,lineheight,'k');
hold on
plot(line2,lineheight,'k');
plot(line3,lineheight,'k');
plot(line4,lineheight,'k');
plot(line5,lineheight,'k');

%%%Insert Text for RPM values
t1=(0<time & time<301);
t2=(301<time & time<601);
t3=(601<time & time<901);
t4=(901<time & time<1201);
t5=(1201<time & time<1501);
t6=(1501<time & time<1801);
p1=rpm_avg(t1);
p2=rpm_avg(t2);
p3=rpm_avg(t3);
p4=rpm_avg(t4);
p5=rpm_avg(t5);
p6=rpm_avg(t6);
 p1_avg=mean(p1);
p2_avg=mean(p2);
p3_avg=mean(p3);
p4_avg=mean(p4);
p5_avg=mean(p5);
p6_avg=mean(p6);
%Average Pressure throughout Run
avgpr=mean(pressure_avg);
avge_pr=num2str(avgpr,3);
avg_pr=[avge_pr(1,:) ' mbar'];

%%%%Doubleheaded Arrows and Text Labels

%Y position of text/side arrows
 yt=1.225*M;
x1=[0:300];
x2=[300:600];
x3=[600:900];
x4=[900:1200];
x5=[1200:1500];
x6=[1500:1800];
y1=1.005*y;%for arrow heads
```

```
%%%Horizontal Arrow Lines
plot(x1,y,'k-');
plot(x2,y,'k-');
plot(x3,y,'k-');
plot(x4,y,'k-');
plot(x5,y,'k-');
plot(x6,y,'k-');
 plot(time(time_range),g_hr_avg(time_range))
if min(g_hr_avg(time_range))>0
   ylim([.8*min(g_hr_avg(time_range)) 1.3*M]);
else
   ylim([0 1.3*M]);
end;
ylabel('Oil Consumption [g/hr]')
xlabel('Time [s]')

title (['Transient Oil Consumption: ' avg_pr ', ' A(19:22) '-' A(24:27) ' RPM, Cylinder '
A(32)],'FontWeight','bold')
hold off
p1_s=num2str(p1_avg,4);
p1_ss=[p1_s(1,:) ' RPM'];
text('position',[80,yt],'string',p1_ss,'FontSize',10);

%%% Creates line & Side Arrows with reference from data not figure
text('position',[0,y1],'string','\leftarrow','FontSize',18);
text('position',[250,y1],'string','\rightarrow','FontSize',18);
 text('position',[300,y1],'string','\leftarrow','FontSize',18);
text('position',[550,y1],'string','\rightarrow','FontSize',18);
 text('position',[600,y1],'string','\leftarrow','FontSize',18);
text('position',[850,y1],'string','\rightarrow','FontSize',18);
text('position',[900,y1],'string','\leftarrow','FontSize',18);
text('position',[1150,y1],'string','\rightarrow','FontSize',18);
 text('position',[1200,y1],'string','\leftarrow','FontSize',18);
text('position',[1450,y1],'string','\rightarrow','FontSize',18);
 text('position',[1500,y1],'string','\leftarrow','FontSize',18);
text('position',[1750,y1],'string','\rightarrow','FontSize',18);
 p2_s=num2str(p2_avg,4);
p2_ss=[p2_s(1,:) ' RPM'];
text('position',[375,yt],'string',p2_ss,'FontSize',10);
p3_s=num2str(p3_avg,4);
p3_ss=[p3_s(1,:) ' RPM'];
text('position',[680,yt],'string',p3_ss,'FontSize',10);
 p4_s=num2str(p4_avg,4);
p4_ss=[p4_s(1,:) ' RPM'];
text('position',[980,yt],'string',p4_ss,'FontSize',10);
p5_s=num2str(p5_avg,4);
p5_ss=[p5_s(1,:) ' RPM'];
 text('position',[1280,yt],'string',p5_ss,'FontSize',10);
p6_s=num2str(p6_avg,4);
p6_ss=[p6_s(1,:) ' RPM'];
 text('position',[1580,yt],'string',p6_ss,'FontSize',10);
 fig=gcf
G=['transspeedOil_g_hr_' A(19:22) '_' A(24:27) '_RPM_cyl' A(32) '.bmp']
saveas (gcf,G)
```

```
 %figure(2)
M2=.88*max(ug_cyl_avg(time_range));
y22=1.2*M2;
lineheight2=[0:.1:y22];
figure('Position',[0 0 scrsz(3) .9*scrsz(4)])

%%Vertical Lines
plot(line1,lineheight2,'k');
hold on
plot(line2,lineheight2,'k');
plot(line3,lineheight2,'k');
plot(line4,lineheight2,'k');
plot(line5,lineheight2,'k');
%Y position of text/side arrows
y2=1.206*M2;
yt2=1.22*M2;
%x values are the same for both

%Horizontal Arrow Lines
plot(x1,y22,'k-');
plot(x2,y22,'k-');
plot(x3,y22,'k-');
plot(x4,y22,'k-');
plot(x5,y22,'k-');
plot(x6,y22,'k-');
plot(time(time_range),ug_cyl_avg(time_range))
ylabel('Oil Consumption [ µg/cyl-cycle]')
if min(ug_cyl_avg(time_range))>0
   ylim([.8*min(ug_cyl_avg(time_range)) 1.3*M2]);
else
      ylim([0 1.3*M2]);
end;
title (['Transient Oil Consumption: ' avg_pr  ', ' A(19:22) '-' A(24:27) ' RPM, Cylinder '
A(32)],'FontWeight','bold')
hold off
text('position',[100,yt2],'string',p1_ss,'FontSize',10);

%%% Creates  Side Arrows with reference from data not figure
text('position',[0,y2],'string','\leftarrow','FontSize',18);
text('position',[250,y2],'string','\rightarrow','FontSize',18);
text('position',[300,y2],'string','\leftarrow','FontSize',18);
text('position',[550,y2],'string','\rightarrow','FontSize',18);
text('position',[600,y2],'string','\leftarrow','FontSize',18);
text('position',[850,y2],'string','\rightarrow','FontSize',18);
 text('position',[900,y2],'string','\leftarrow','FontSize',18);
text('position',[1150,y2],'string','\rightarrow','FontSize',18);
 text('position',[1200,y2],'string','\leftarrow','FontSize',18);
text('position',[1450,y2],'string','\rightarrow','FontSize',18);
 text('position',[1500,y2],'string','\leftarrow','FontSize',18);
text('position',[1750,y2],'string','\rightarrow','FontSize',18);
 p2_s=num2str(p2_avg,4);
p2_ss=[p2_s(1,:) ' RPM'];
text('position',[375,yt2],'string',p2_ss,'FontSize',10);
p3_s=num2str(p3_avg,4);
p3_ss=[p3_s(1,:) ' RPM'];
```

```
text('position',[680,yt2],'string',p3_ss,'FontSize',10);
 p4_s=num2str(p4_avg,4);
p4_ss=[p4_s(1,:) ' RPM'];
text('position',[980,yt2],'string',p4_ss,'FontSize',10);
 p5_s=num2str(p5_avg,4);
p5_ss=[p5_s(1,:) ' RPM'];
 text('position',[1280,yt2],'string',p5_ss,'FontSize',10);
 p6_s=num2str(p6_avg,4);
p6_ss=[p6_s(1,:) ' RPM'];
text('position',[1580,yt2],'string',p6_ss,'FontSize',10);
G=['transspeedOil_ug_cyl-cycle_' A(19:22) '-' A(24:27) '_RPM_cyl' A(32) '.bmp']
 saveas (gcf,G)

%figure(3)
M3=.95*max(blowby_avg(time_range));
 y4=1.07*M3;
lineheight3=[0:.01:y4];
 figure('Position',[0 0 scrsz(3) .9*scrsz(4)])

%%%vertical lines
plot(line1,lineheight3,'k');
hold on
plot(line2,lineheight3,'k');
plot(line3,lineheight3,'k');
plot(line4,lineheight3,'k');
plot(line5,lineheight3,'k');

%Y position of text/side arrows
y3=1.074*M3;
yt3=1.087*M3;

%x values are the same for both
 plot(x1,y4,'k','LineWidth',1);
plot(x2,y4,'k','LineWidth',1);
plot(x3,y4,'k','LineWidth',1);
plot(x4,y4,'k','LineWidth',1);
plot(x5,y4,'k','LineWidth',1);
plot(x6,y4,'k','LineWidth',1);
p1_s=num2str(p1_avg,4);
p1_ss=[p1_s(1,:) ' RPM'];
plot(time(time_range),blowby_avg(time_range))
ylabel('Blowby ( SLPM, Ref 760 mmHg,70° F)')
xlabel('Time [s]')
 if min(blowby_avg(time_range))>0
   ylim([.8*min(blowby_avg(time_range)) 1.15*M3])
else
       % min(g_hr_avg(time_range))<0
       ylim([0 1.15*M3])
end
 title (['Transient Blowby: ' avg_pr ', ' A(19:22) '-' A(24:27) ' RPM, Cylinder ' A(32)],'FontWeight','bold' )
hold off
 text('position',[100,yt3],'string',p1_ss,'FontSize',10);

%%% Creates line & Side Arrows with reference from data not figure
text('position',[0,y3],'string','\leftarrow','FontSize',18);
```

```
text('position',[250,y3],'string','\rightarrow','FontSize',18);
text('position',[300,y3],'string','\leftarrow','FontSize',18);
text('position',[550,y3],'string','\rightarrow','FontSize',18);
 text('position',[600,y3],'string','\leftarrow','FontSize',18);
text('position',[850,y3],'string','\rightarrow','FontSize',18);
text('position',[900,y3],'string','\leftarrow','FontSize',18);
text('position',[1150,y3],'string','\rightarrow','FontSize',18);
 text('position',[1200,y3],'string','\leftarrow','FontSize',18);
text('position',[1450,y3],'string','\rightarrow','FontSize',18);
 text('position',[1500,y3],'string','\leftarrow','FontSize',18);
text('position',[1750,y3],'string','\rightarrow','FontSize',18);
p2_s=num2str(p2_avg,4);
p2_ss=[p2_s(1,:) ' RPM'];
text('position',[375,yt3],'string',p2_ss,'FontSize',10);
p3_s=num2str(p3_avg,4);
p3_ss=[p3_s(1,:) ' RPM'];
text('position',[680,yt3],'string',p3_ss,'FontSize',10);
  p4_s=num2str(p4_avg,4);
p4_ss=[p4_s(1,:) ' RPM'];
text('position',[980,yt3],'string',p4_ss,'FontSize',10);
p5_s=num2str(p5_avg,4);
p5_ss=[p5_s(1,:) ' RPM'];
 text('position',[1280,yt3],'string',p5_ss,'FontSize',10);
 p6_s=num2str(p6_avg,4);
p6_ss=[p6_s(1,:) ' RPM'];
text('position',[1580,yt3],'string',p6_ss,'FontSize',10);
 G=['transspeedblowby_' A(19:22) '_' A(24:27) '_RPM_cyl' A(32) '.bmp']
saveas (gcf,G)

%figure(4)
figure('Position',[0 0 scrsz(3) .9*scrsz(4)])
plot(time(time_range),pressure_avg(time_range))
ylabel('Intake Manifold Pressure [mbar]')
xlabel('Time [s]')
title (['Transient Intake Manifold Pressure: ' avg_pr ', ' A(19:22) '-' A(24:27) ' - ' A(24:27) ' RPM, Cylinder '
A(32)],'FontWeight','bold')
G=['transspeedPressure_' A(19:22) '_' A(24:27) '_RPM_cyl' A(33) '.bmp']
saveas (gcf,G)

%figure(5)
figure('Position',[0 0 scrsz(3) .9*scrsz(4)])
plot(time(time_range),rpm_avg(time_range))
ylabel('Speed [RPM]')
xlabel('Time [s]')
 title (['Transient Speed: ' avg_pr ', ' A(19:22) '-' A(24:27) ' RPM, Cylinder ' A(32)],'FontWeight','bold')
G=['transspeedSpeed_' A(19:22) '_' A(24:27) '_RPM_cyl' A(32) '.bmp']
 saveas (gcf,G)

%%%Code Developed by Diego A. Melani Spring 2007
```

Figure D-6 – Matlab code used to create oil consumption trace graphs (in terms of $^{g}/_{cyl\text{-}hr}$ and $^{\mu g}/_{cyl\text{-}cycle}$), a blowby graph, a load graph, and speed graph, all as a function of time during transient speed operation. This was described in *Section 2.3.2.* Code developed by Diego Melani of MIT.

```
%%% Calculate Average Oil Consumption
 clear all
%%%%% Type file name
%function A='input';
%Example
%A='2_17_07_2500_cyl3.lvm';
%5_04_07_1500_430_cyl3
A = input('[Steady State] Please Insert the File Name: ','s');

if isempty(A)
   disp('No File Name Selected')
   A = input('[Steady State] Please Insert the File Name: ','s');
elseif isempty(A)
   disp('No File Name Selected')
   A = input('Please Insert the File Name: ','s');
     end

 %%%%Size of Running Average
size = 10;
%%%% Select Time Range of Plot (in seconds)
t_min = str2num(input('[Steady State] Minimum Time Range: ','s'));
 if isempty(t_min)
   disp('No value selected')
   A = input('[Steady State] Minimum Time Range: ','s');
elseif isempty(t_min)
   disp('No value')
   A = input('[Steady State] Minimum Time Range: ','s');
end
 t_max = str2num(input('[Steady State] Maximum Time Range: ','s'));
if isempty(t_max)
   disp('No value selected')
   A = input('[Steady State] Maximum Time Range: ','s');
elseif isempty(t_max)
   disp('No value')
   A = input('[Steady State] Maximum Time Range: ','s');
     end
%t_min=0;
%t_max=1800;

%IMPORT Text Data
fid=fopen(A,'r');

%Textscan importing function with omitted headerlines set to 23
 B= textscan(fid, ' %f32 %f32 %f32 %f32 %f32 %f32 %f32 %f32 %f32 %f32 %f32 %f32 %f32 %f32 %f32 %f32
%f32 %f32 %f32 %f32 %f32 %f32 %f32 %f32 %f32 %f32 %f32 %f32 %f32 %f32 %f32 %f32
%f32','headerLines', 23); % Reads row 1 of col 1-4

% {} give values, () give size
B{:};
fclose(fid);
%%Get Values for each Parameter

%Parameters to be imported, B{n} n refers to the column number
 time= B{1};
ug_cyl_old=B{28};
```

```
blowby=B{29};
pressure=B{7};
rpm=B{22};
g_hr_old=B{27};
% Added from Diego's Code
lambda=B{6};
air_flow=B{4};
SO_Voltage=B{5};
g_hr=g_hr_old+(0.113154448*(g_hr_old./SO_Voltage));
ug_cyl=ug_cyl_old+(0.113154448*(ug_cyl_old./SO_Voltage));

%% Set the time range of the values
time_range=(t_min<time & time<t_max);

%%% Calculate Running Averages
g_hr_avg=filter(ones(1,size)/size,1,g_hr);
ug_cyl_avg=filter(ones(1,size)/size,1,ug_cyl);
blowby_avg=filter(ones(1,size)/size,1,blowby);

%blowby_avg=filter(ones(1,size)/size,1,blowby);
%pressure_avg=filter(ones(1,size)/size,1,pressure);
%rpm_avg=filter(ones(1,size)/size,1,rpm);
Avg_Oil_Consumption_g_hr=0;
Avg_Oil_Consumption_ug_cyl=0;
Area_g_hr=0;
Area_ug_cyl_cycle=0;
Transient_Number=0;
trans6=t_max*10;
t_new=(t_max*10)+1;
for j = 3001:3000:t_new
   i_low=j-2999;
   Transient_Number=Transient_Number+1
   for i = i_low:1:j
      Area_g_hr=(g_hr_avg(i,:)+g_hr_avg(i-1,:))/6000;
      Area_ug_cyl_cycle=(ug_cyl_avg(i,:)+ug_cyl_avg(i-1,:))/6000;
      Avg_Oil_Consumption_g_hr=Avg_Oil_Consumption_g_hr+Area_g_hr;
      Avg_Oil_Consumption_ug_cyl=Avg_Oil_Consumption_ug_cyl+Area_ug_cyl_cycle;
   end
   Avg_Oil_Consumption_g_hr
   Avg_Oil_Consumption_ug_cyl
   Avg_Oil_Consumption_g_hr=0;
   Avg_Oil_Consumption_ug_cyl=0;
   Area_g_hr=0;
   Area_ug_cyl_cycle=0;
end
```

Figure D-7 – Matlab code used to calculate the average oil consumption for a given, user-input time frame in both $^{g}/_{cyl\text{-}hr}$ and $^{\mu g}/_{cyl\text{-}cycle}$ as well as provide the average blowby for that time frame. This was described in *Section 2.3.2*. Code developed by Diego Melani of MIT.

(This page was intentionally left blank)

Appendix E

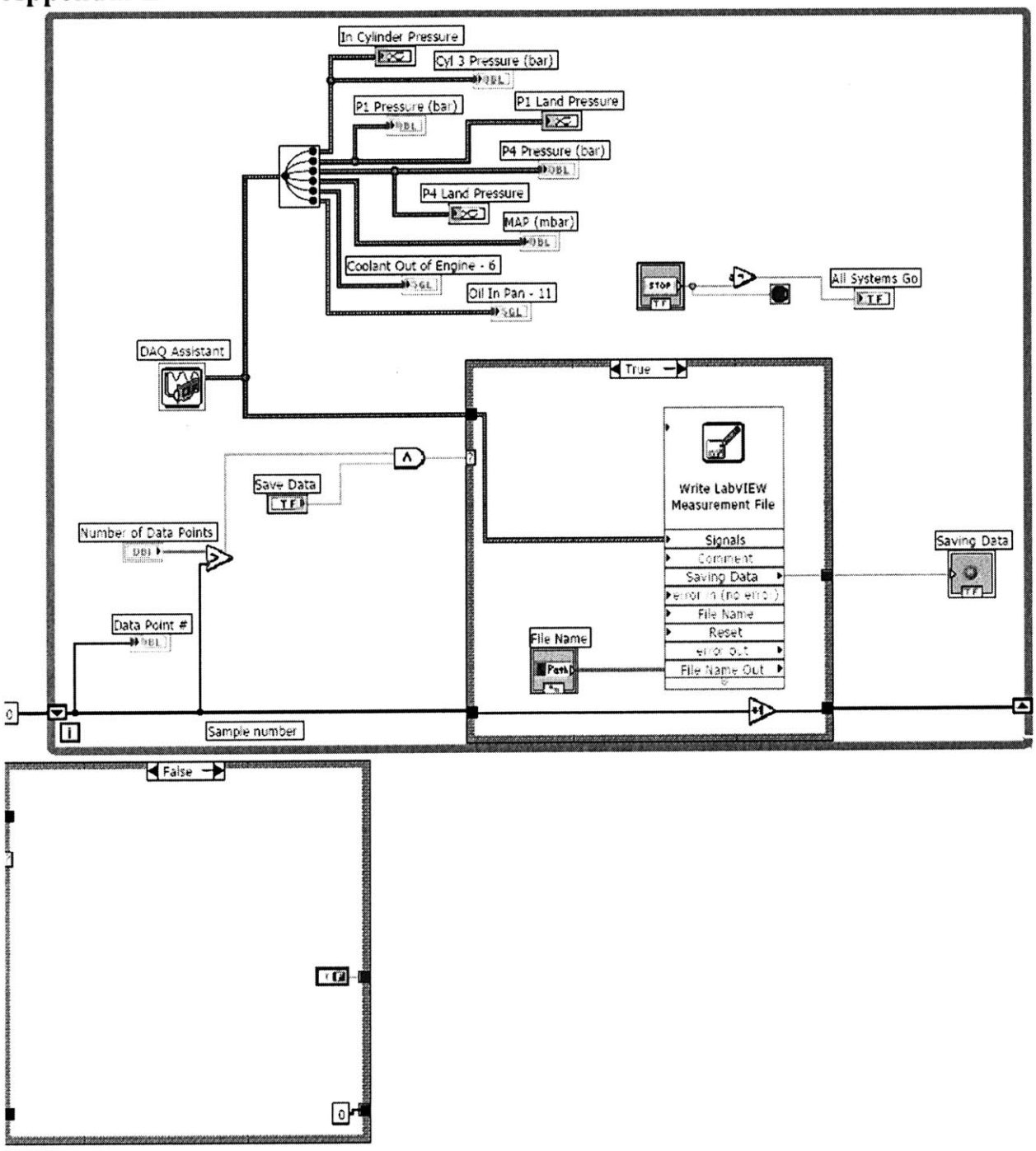

Figure E-1 – Block diagram of the LabView program used to record the pressure traces of the measured cylinder.

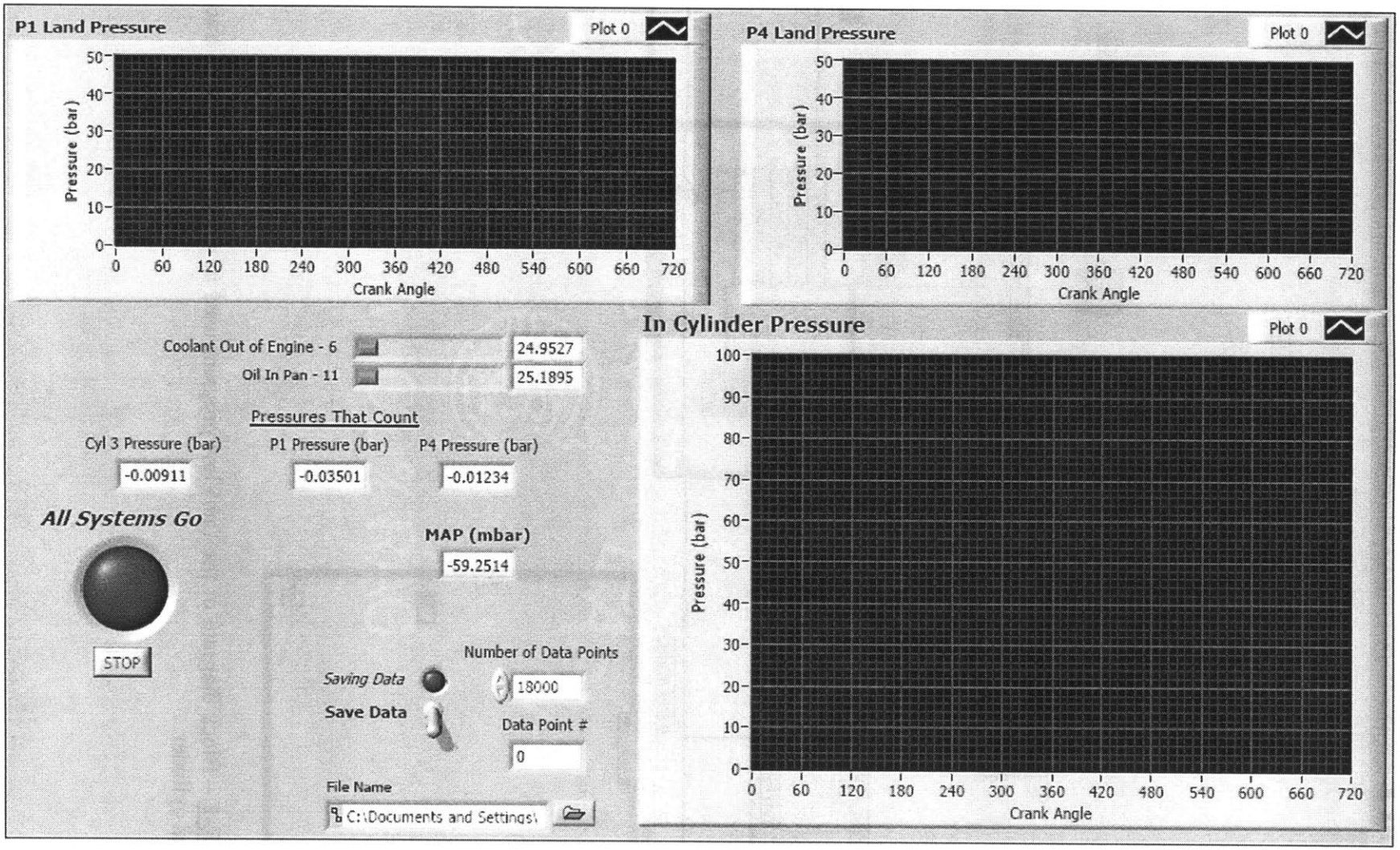

Figure E-2 – Front panel display for the pressure trace program, whose block diagram is illustrated in *Figure E-1* above.

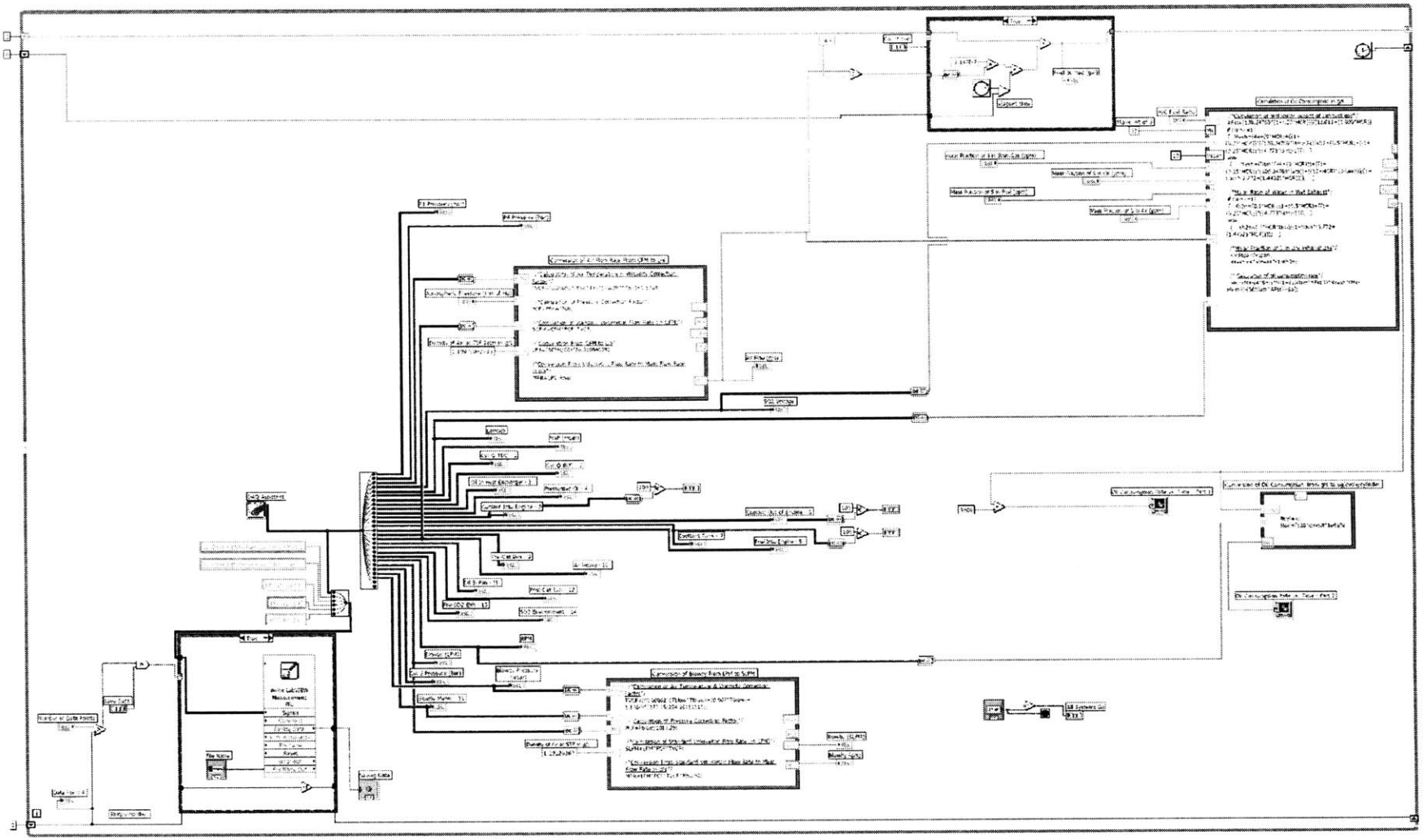

Figure E-3 – Block diagram of the LabView program used to record the steady-state oil consumption measurements.

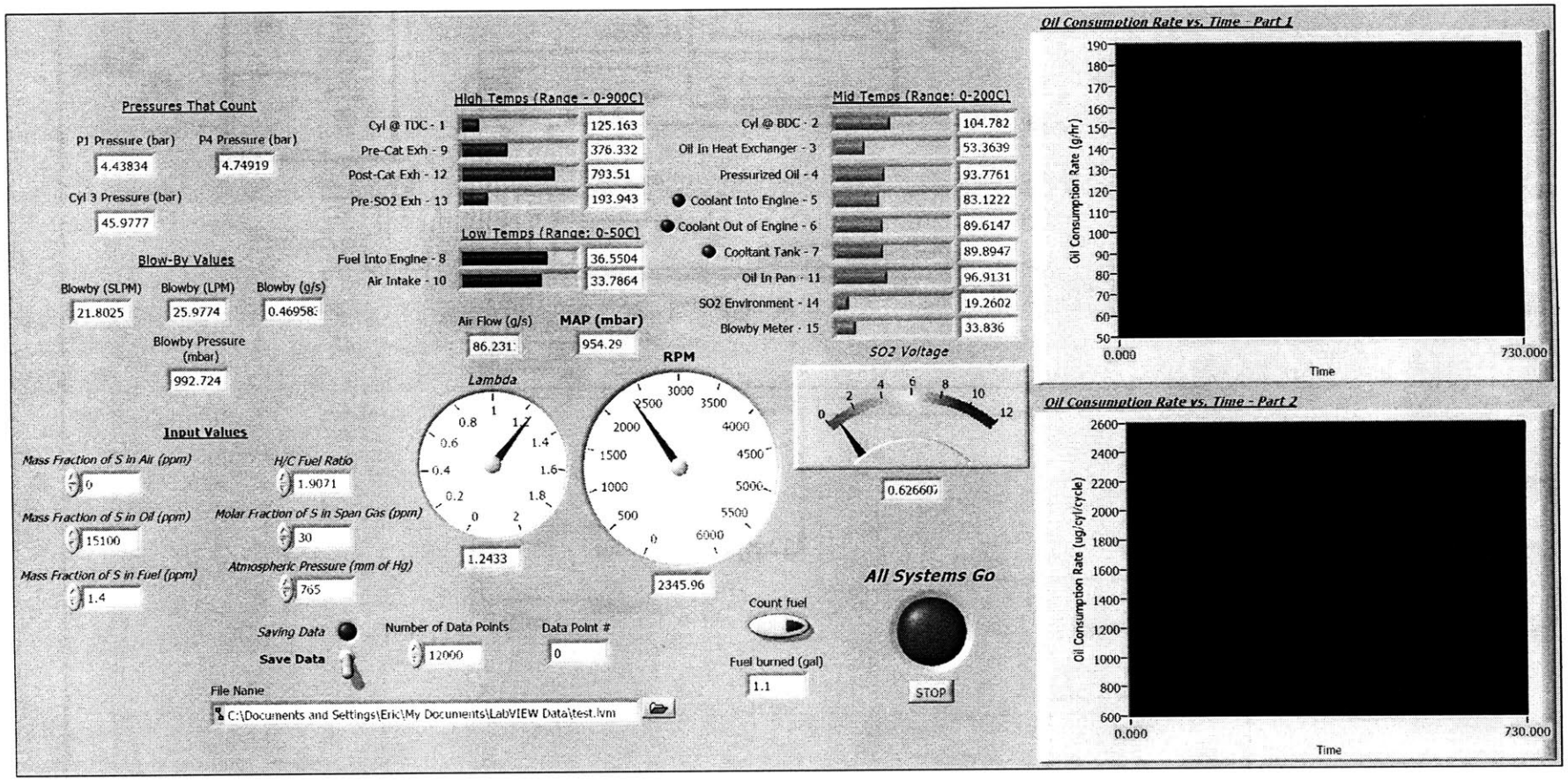

Figure E-4 – Front panel display for the steady-state oil consumption program, whose block diagram is illustrated in *Figure E-3*.

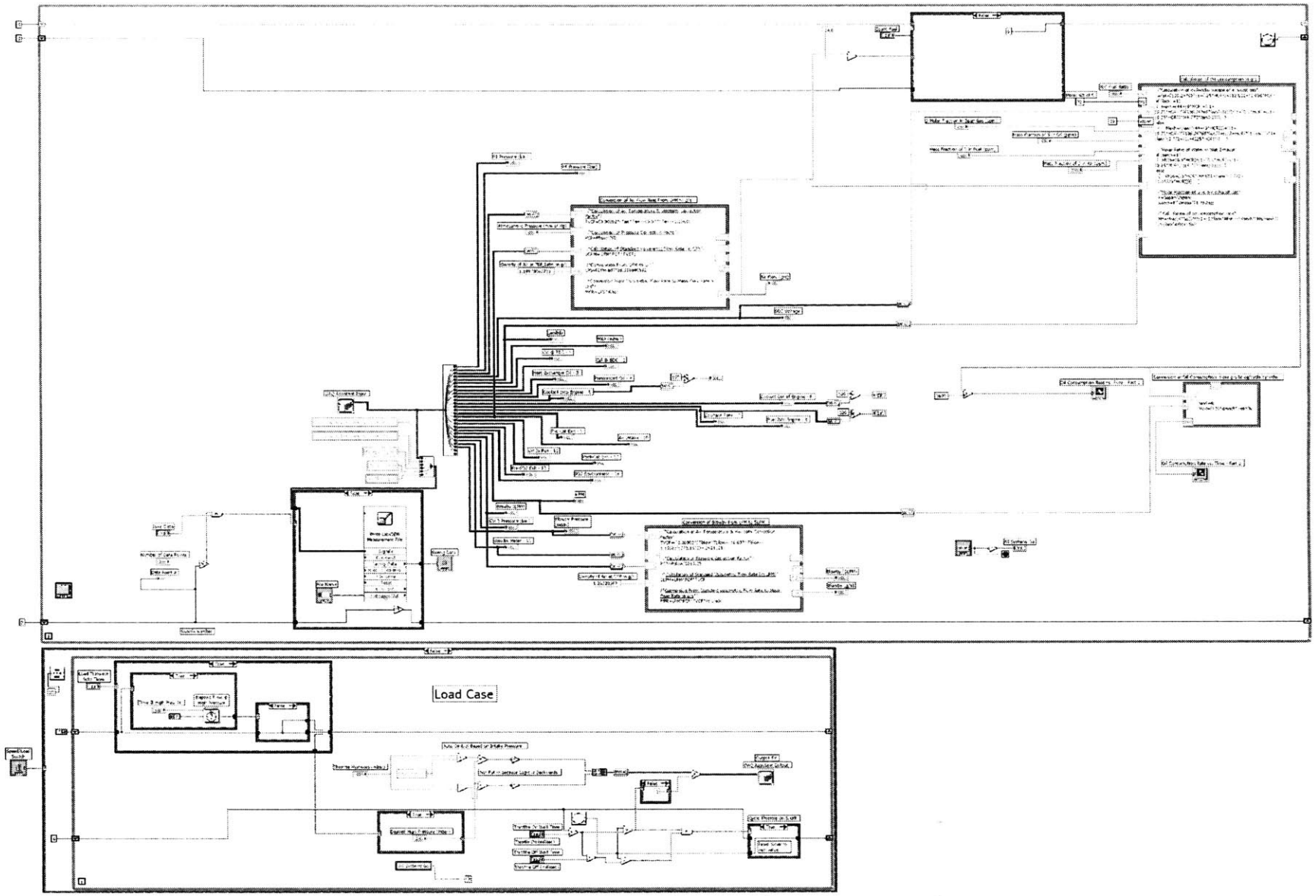

Figure E-5 – Block diagram of the LabView program used to record the transient oil consumption measurements.

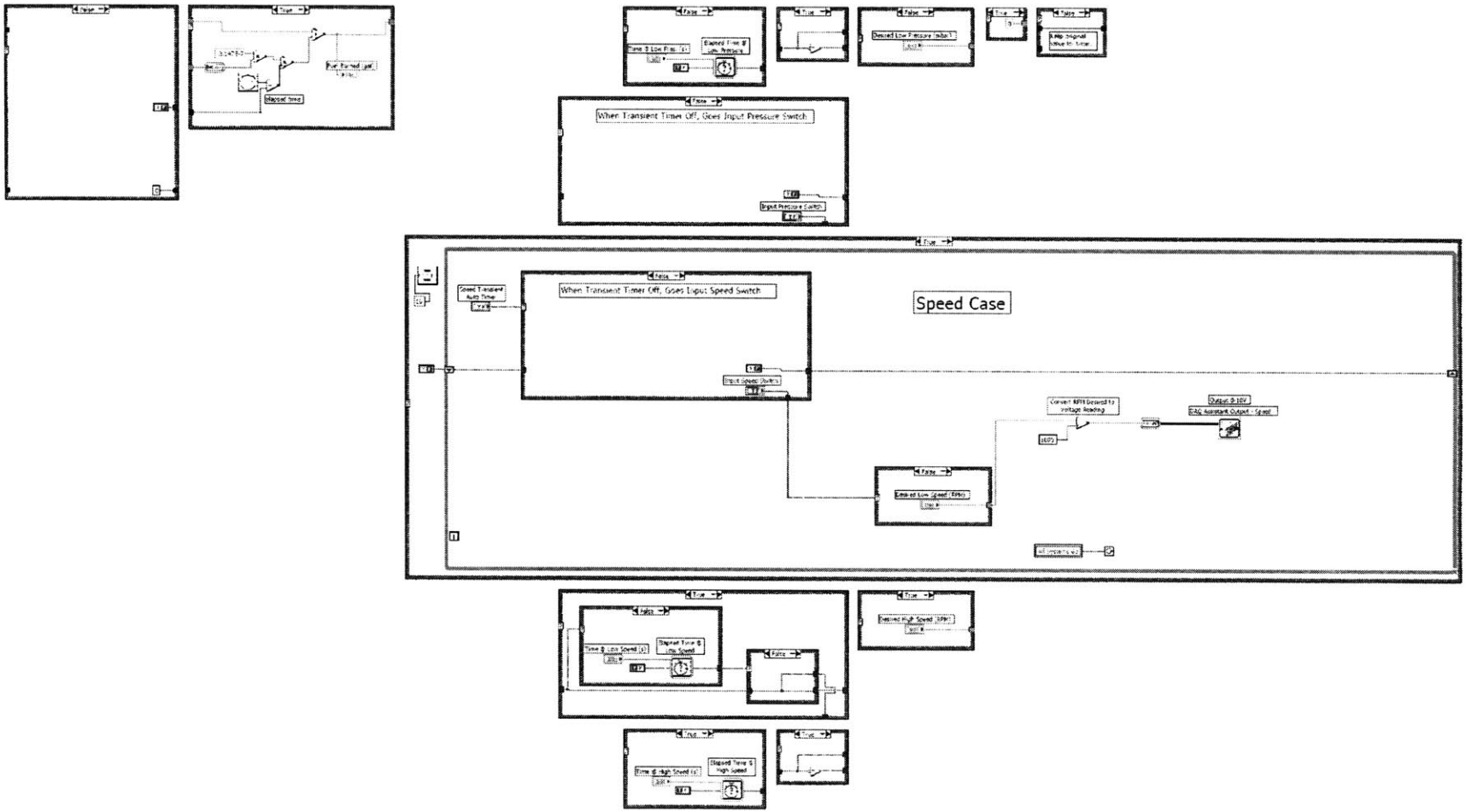

Figure E-6 – Conditional block diagram from *Figure E-5*.

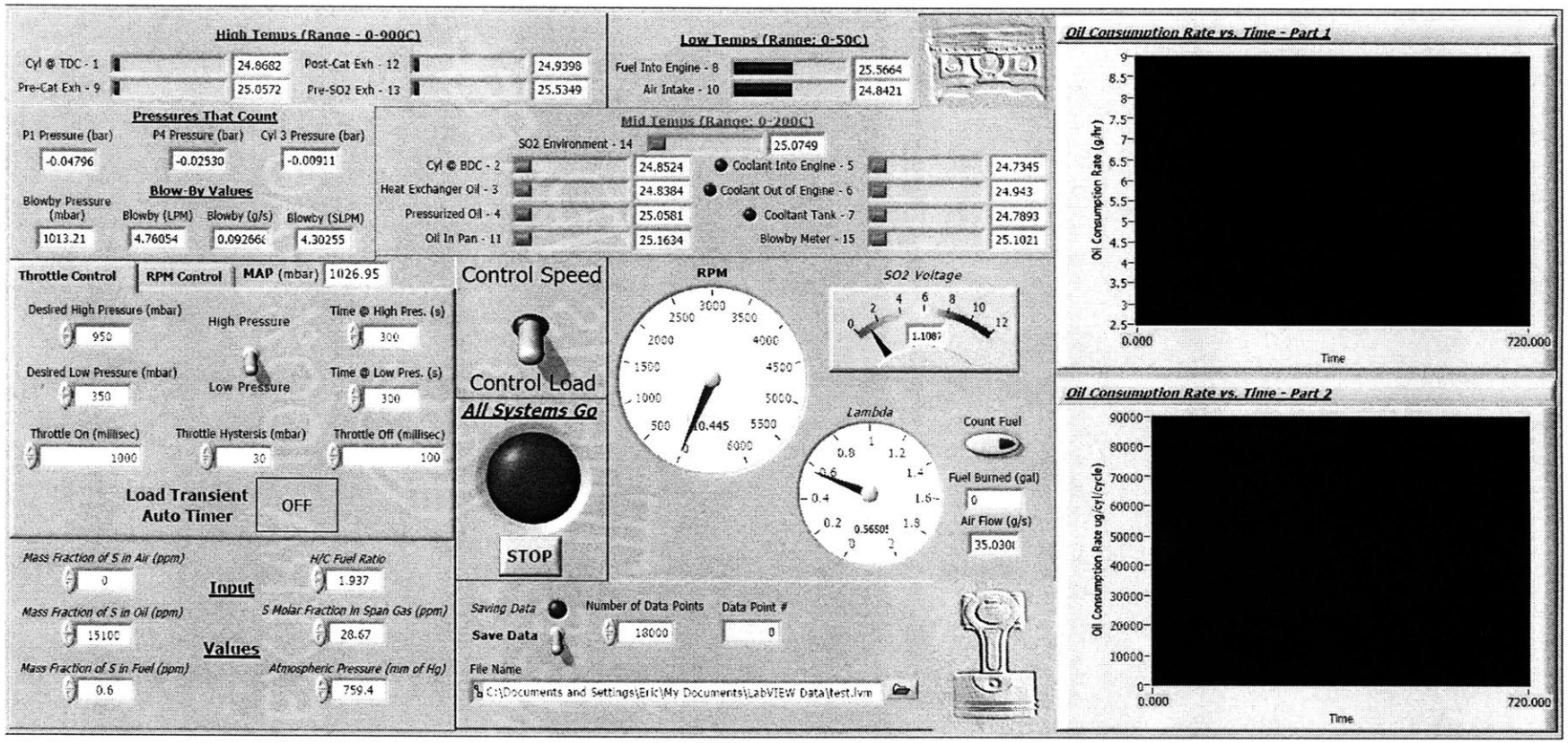

Figure E-7 – Front panel display for the transient oil consumption program, whose block diagram is illustrated in *Figures E-5* and *E-6*.